

REPORT NO.
UCB/EERC-79/01
APRIL 1979

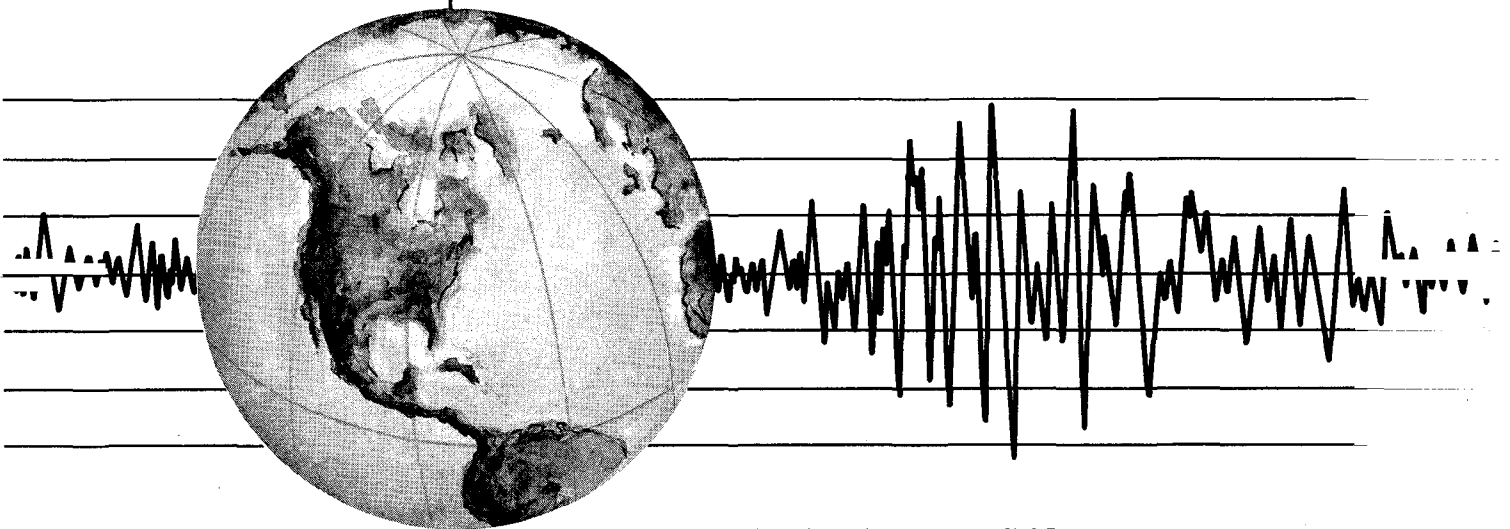
EARTHQUAKE ENGINEERING RESEARCH CENTER

HYSTERETIC BEHAVIOR OF LIGHTWEIGHT REINFORCED CONCRETE BEAM-COLUMN SUBASSEMBLAGES

by

BRIAN FORZANI
EGOR P. POPOV
VITELMO V. BERTERO

Report to Sponsor:
National Science Foundation



COLLEGE OF ENGINEERING

UNIVERSITY OF CALIFORNIA · Berkeley, California

REPRODUCED BY
**NATIONAL TECHNICAL
INFORMATION SERVICE**
U. S. DEPARTMENT OF COMMERCE
SPRINGFIELD, VA. 22161



BIBLIOGRAPHIC DATA SHEET	1. Report No. NSF/RA-790121	2.	3. Recipient's Accession No. PB298267	
4. Title and Subtitle Hysteretic Behavior of Lightweight Reinforced Concrete Beam-Column Subassemblages			5. Report Date April 1979	
7. Author(s) Brian Forzani, Egor P. Popov and Vitelmo V. Bertero			6.	
9. Performing Organization Name and Address Earthquake Engineering Research Center University of California, Richmond Field Station 47th and Hoffman Blvd. Richmond, California, 94804			8. Performing Organization Rept. No. UCB/EERC-79/01	
12. Sponsoring Organization Name and Address National Science Foundation 1800 G. Street, N.W. Washington, D.C. 20550			10. Project/Task/Work Unit No.	
15. Supplementary Notes			11. Contract/Grant No. ENV76-04263	
16. Abstracts This paper describes an experimental investigation into the behavior of interior beam-column joints of a ductile moment-resisting frame constructed of lightweight aggregate concrete. Emphasis is placed on the effects of bond deterioration in the joint region. Results of experiments carried out on two lightweight R/C specimens are compared with similar experiments on specimens constructed of normal weight concrete. Comparison reveals a similar performance when the specimens are subjected to monotonically increasing lateral loads, but a considerably poorer performance of the lightweight specimens when subjected to cyclic loading similar to that which can be expected from severe seismic excitations. Recommendations are given for improving observed behavior and for further research.			13. Type of Report & Period Covered	
17b. Identifiers/Open-Ended Terms			14.	
17c. COSATI Field/Group			15. Supplementary Notes	
18. Availability Statement Release Unlimited		19. Security Class (This Report) UNCLASSIFIED	21. No. of Pages 110	
		20. Security Class (This Page) UNCLASSIFIED	22. Price AD6-A01	



HYSTERETIC BEHAVIOR OF LIGHTWEIGHT
REINFORCED CONCRETE BEAM-COLUMN SUBASSEMBLAGES

by

Brian Forzani
Research Assistant
University of California, Berkeley

Egor P. Popov
Professor of Civil Engineering
University of California, Berkeley

Vitelmo V. Bertero
Professor of Civil Engineering
University of California, Berkeley

A report on research sponsored by
the National Science Foundation

Report No. UCB/EERC-79/01
Earthquake Engineering Research Center
College of Engineering
University of California
Berkeley, California

April 1979

ABSTRACT

This paper describes an experimental investigation into the behavior of interior beam-column joints of a ductile moment-resisting frame constructed of lightweight aggregate concrete. Emphasis is placed on the effects of bond deterioration in the joint region. Results of experiments carried out on two lightweight R/C specimens are compared with similar experiments on specimens constructed of normal weight concrete. Comparison reveals a similar performance when the specimens are subjected to monotonically increasing lateral loads, but a considerably poorer performance of the lightweight specimens when subjected to cyclic loading similar to that which can be expected from severe seismic excitations. Recommendations are given for improving observed behavior and for further research.

ACKNOWLEDGEMENTS

The authors most gratefully acknowledge the support provided by the National Science Foundation under Grant No. ENV 76-04263, subproject No. 0-21201. D. Clyde, B. Lotz, and W. Neighbour provided assistance in conducting the experiments. In addition, the authors would like to acknowledge the editorial assistance of M. C. Randall and the technical illustrations by D. Ullman. F. Jackson typed the manuscript. S. Viwanatepa deserves special thanks for his generous advice through all stages of the investigation.

TABLE OF CONTENTS

	<u>Page</u>
ABSTRACT	iii
ACKNOWLEDGEMENTS	iv
TABLE OF CONTENTS	v
LIST OF TABLES	vii
LIST OF FIGURES	viii
I. INTRODUCTION	1
1.1 General	1
1.2 Objectives and Scope	1
II. TEST SPECIMENS	3
2.1 Selection of Test Specimens	3
2.2 Description of Test Specimens	3
2.3 Material Properties	4
2.4 Fabrication of Test Specimens	5
III. EXPERIMENTAL TEST SET-UP AND INSTRUMENTATION	7
3.1 Testing Frame and Specimen Supports	7
3.2 Loading Apparatus	7
3.3 Instrumentation	7
3.3.1 Load And Reaction Measurements	8
3.3.2 Strain and Deformation Measurements	8
3.4 Recording Equipment	9
3.5 Test Procedures	10
IV. EXPERIMENTAL RESULTS AND DISCUSSION	13
4.1 Overall Response	13
4.1.1 Specimen BC7	14
4.1.2 Specimen BC8	15
4.1.3 Comparison of BC7 and BC8	17

	<u>Page</u>
4.2 Energy Dissipation	18
4.3 Visual Behavior	18
4.3.1 Specimen BC7	19
4.3.2 Specimen BC8	19
4.4 Slippage of Reinforcement and Fixed-End Rotation at Interior Joint	20
4.4.1 Specimen BC7	20
4.4.2 Specimen BC8	22
4.4.3 Comparison of Specimens BC7 and BC8	22
4.5 Strain of the Longitudinal Reinforcement	22
4.6 Effect of Shear	24
4.6.1 Specimen BC7	24
4.6.2 Specimen BC8	24
4.7 Sources of Deformation Contributing to the Total Horizontal Displacement	25
4.7.1 Specimen BC7	26
4.7.2 Specimen BC8	28
4.7.3 Comparison of Specimen BC7 with Specimen BC8	29
V. COMPARISON WITH NORMAL WEIGHT SPECIMENS	31
5.1 Specimens BC4 and BC7	31
5.2 Specimens BC3 and BC8	33
VI. BEHAVIOR OF SPECIMEN BC7 AS PREDICTED BY PRESENT R/C THEORY	35
VII. CONCLUSIONS AND RECOMMENDATIONS	
7.1 Conclusions	37
7.2 Recommendations	38
REFERENCES	41
TABLES	43
FIGURES	51
APPENDIX A	

LIST OF TABLES

<u>Table</u>		<u>Page</u>
2.1	Lightweight Concrete Mix	45
2.2	Concrete Mechanical Characteristics	45
3.1	Data Plotted by Recorders	46
4.1	Energy Dissipation Per Cycle	47
6.1	Measured and Caclulated Mechanical Characteristics of Members	48
6.2	Beam Deflections	49

LIST OF FIGURES

<u>Figure</u>		<u>Page</u>
2.1	Twenty-Story Building Prototype	53
2.2(a)	Gravity and Lateral Loads at Third Floor of Building . . .	53
2.2(b)	Moments Due to Gravity Loads (Above) and Moments Due to Lateral Loads (Below)	53
2.2(c)	Moments from Gravity and Lateral Load Effects	53
2.3	Definition of Forces and Displacements for a Subassemblage.	54
2.4	Test Specimen	54
2.5	Beam Section A-A	54
2.6	Column Section B-B	54
2.7	Concrete Stress-Strain Diagrams	55
2.8	Concrete Strength Gain Diagrams	55
2.9	Reinforcement Stress-Strain Diagram	
2.10	Cyclic Stress-Strain Diagram for Machined Specimen from #5 Bar	55
2.11	Reinforcement	56
2.12	Beam and Detail	56
2.13	Column and Detail	56
3.1	Beam-Column Test Set Up	57
3.2	Locations of Strain Gages	58
3.3(a)	Instrumentation on South Face of BC7	58
3.3(b)	Instrumentation on South Face of BC8	58
3.4	Supports for External Instrumentation	59
3.5(a)	Instrumentation on North Face of BC7	59
3.5(b)	Instrumentation on North Face of BC8	59
3.6	Load History of BC7	60

<u>Figure</u>	<u>Page</u>
3.7	Load History of BC8 60
4.1	Hysteretic Loops for BC7 - H vs. σ 61
4.2(a)	Hysteretic Cycles of BC7 at Service Load 61
4.2(b)	Hysteretic Loops for BC7 -- H_{RED} and H_{ER} vs. σ 61
4.3(a)	Pre-Yield Hysteretic Loops of BC8 -- H and H_{RED} vs. σ 61
4.3(b)	Post-Yield Hysteretic Loops of BC8 62
4.4(a)	Pre-Yield Hysteretic Loops of BC8 - H_{EQ} vs. σ 62
4.4(b)	Post-Yield Hysteretic Loops of BC8 - H_{EQ} vs. σ 62
4.4(c)	Comparison of Hysteretic Loops of BC7 and BC8 62
4.5	East Beam, BC7, at LP 23 63
4.6	North Face of BC7 at LP 49 63
4.7	Column Spall and Spall on Top of West Beam of BC7 63
4.8	West Beam of BC7 after Test 64
4.9	Spalling on West Column of BC8 Between LP 21 and LP 22 64
4.10	Spall on West Column of BC8 at LP 25 64
4.11	Spall on East Column of BC8 at LP 26, Exposing Reinforcement 65
4.12	Spalled Area Extending Along East Beam of BC8 by LP 28 65
4.14	Deep Spall on Top of East Beam, BC8 65
4.15(a)	Reinforcement Pullout from Column, BC7 West 66
4.15(b)	Reinforcement Pullout from Column, BC7 East 66
4.16(a)	Fixed-End Rotation of BC7 West at Column Face 66
4.16(b)	Fixed-End Rotation of BC7 East at Column Face 66
4.17(a)	Post-Yield Reinforcement Pullout from Column, BC8 West 67
4.17(b)	Post-Yield Reinforcement Pullout from Column, BC8 East 67
4.18(a)	Post-Yield Fixed-End Rotation of BC8 West at Column Face 67
4.18(b)	Post-Yield Fixed-End Rotation of BC8 East at Column Face 67

<u>Figure</u>	<u>Page</u>
4.19(a) Reinforcement Strain vs. Moment at Column Face, BC7 West	68
4.19(b) Reinforcement Strain vs. Moment at Column Face, BC7 East	68
4.20(a) Reinforcement Strain vs. Moment in Region 1 -- BC7 West .	68
4.20(b) Reinforcement Strain vs. Moment in Region 1 -- BC7 East .	68
4.21(a) Strain in Top Reinforcement at Column Face, BC8 West . .	69
4.21(b) Strain in Bottom Reinforcement at Column Face, BC8 West .	69
4.21(c) Strain in Top Reinforcement at Column Face, BC8 East . .	69
4.21(d) Strain in Bottom Reinforcement at Column Face, BC8 East .	69
4.22(a) Strain in Top Reinforcement in Region 1 -- BC8 West . . .	70
4.22(b) Strain in Bottom Reinforcement in Region 1 -- BC8 West .	70
4.22(c) Strain in Top Reinforcement in Region 1 -- BC8 East . . .	70
4.22(d) Strain in Bottom Reinforcement in Region 1 -- BC8 East .	70
4.23(a) Strain Variation in Shear Reinforcement, BC7 West	71
4.23(b) Strain in Variation in Shear Reinforcement, BC7 East . .	71
4.24(a) Shear Strain in Beam, Region 2 -- BC7 West	71
4.24(b) Shear Strain in Beam, Region 2 -- BC7 East	71
4.25(a) Strain Variation in Shear Reinforcement, BC8 West	72
4.25(b) Strain Variation in Shear Reinforcement, BC8 East	72
4.26(a) Shear Strain in Beam, Region 1 -- BC8 West	72
4.26(b) Shear Strain in Beam, Region 1 -- BC8 East	72
4.27(a) Shear Strain in Beam, Region 2 -- BC8 West	73
4.27(b) Shear Strain in Beam, Region 2 -- BC8 East	73
4.28(a) Moment vs. Beam Rotation in Region 1 -- BC7 West	73
4.28(b) Moment vs. Beam Rotation in Region 1 -- BC8 East	73
4.29(a) Moment vs. Beam Rotation in Region 1 -- BC8 West	74

<u>Figure</u>	<u>Page</u>
4.29 (b) Moment vs. Beam Rotation in Region 1 -- BC8 East	74
4.30 (a) Moment vs. Beam Rotation in Region 2 -- BC7 West	74
4.30 (b) Moment vs. Beam Rotation in Region 2 -- BC7 East	74
4.31 (a) Moment vs. Beam Rotation in Region 2 -- BC8 West	75
4.31 (b) Moment vs. Rotation in Region 2 -- BC8 East	75
4.32 (a) Components of Horizontal Displacement δ -- BC7 West	75
4.32 (b) Components of Horizontal Displacement δ -- BC7 West	75
4.32 (c) Components of Horizontal Displacement δ -- BC7 West	76
4.32 (d) Components of Horizontal Displacement δ -- BC7 West	76
4.32 (e) Components of Horizontal Displacement δ -- BC7 West	76
4.33 (a) Components of Horizontal Displacement δ -- BC7 West	76
4.33 (b) Components of Horizontal Displacement δ -- BC7 West	77
4.33 (c) Components of Horizontal Displacement δ -- BC7 West	77
4.33 (d) Components of Horizontal Displacement δ -- BC7 West	77
4.33 (e) Components of Horizontal Displacement δ -- BC7 West	77
4.34 (a) Components of Horizontal Displacement δ -- BC8 West -- First Cycle	78
4.34 (b) Components of Horizontal Displacement δ -- BC8 West -- Second Cycle	78
4.35 (a) Maximum Negative Horizontal Displacement δ -- BC8 West -- First Cycle	78
4.35 (b) Maximum Negative Horizontal Displacement δ -- BC8 West -- Second Cycle	78
4.36 (a) Maximum Positive Horizontal Displacement δ -- BC8 East -- First Cycle	79
4.36 (b) Components of Horizontal Displacement δ -- BC8 East -- Second Cycle	79
4.37 (a) Components of Horizontal Displacement δ -- BC8 East -- First Cycle	79

<u>Figure</u>	<u>Page</u>
4.37(b) Components of Horizontal Displacement δ -- BC8 East -- Second Cycle	79
5.1 Comparison of Hysteretic Loops of Specimens BC4 and BC7 .	80
5.2 Comparison of Hysteretic Loops of Specimens BC3 and BC8 .	80
6.1 Moment vs. Beam Rotation in Region 1 -- BC7 West	80
6.2 Moment vs. Beam Rotation in Region 1 -- BC7 East	80



1. INTRODUCTION

1.1 General

One of the guiding principles of earthquake-resistant design is to minimize the mass of the structure. For this reason the use of lightweight concrete in earthquake-resistant reinforced concrete (R/C) construction appears to have a good potential. Before this potential can be utilized, however, a better understanding of the behavior of lightweight concrete under simulated earthquake-like loading conditions is needed.

Recent studies have shown that one of the weakest links in R/C moment-resisting frames under seismic loadings is deterioration of bond (anchorage) of the main beam bars in the beam-column joints (1-4). Since the performance of bond in general in lightweight concrete is poorer than in normal weight concrete, as is recognized by standard building codes [5-6], the behavior of lightweight concrete structures under seismic loading becomes suspect. This combined with some poor performance of lightweight R/C structures during recent earthquakes, particularly during the 1971 San Fernando Earthquake [7], creates a need to better understand the seismic behavior of lightweight concrete and to compare this behavior with that of normal weight concrete.

1.2 Objectives and Scope

The behavior of the interior joint of a R/C ductile moment-resisting frame can only be properly assessed by studying the performance of the main structural elements, the beams, column and joint region as a single interconnected entity which forms a subassemblage of the frame. In this study the seismic behavior of lightweight R/C beam-column subassemblages is evaluated experimentally and compared with similar previously-tested normal weight R/C subassemblages. The first objective was to obtain experimental information regarding the strength, stiffness, deformation capacity (ductility) and energy absorption and energy dissipation capacities of lightweight R/C beam-column subassemblages under both monotonic and cyclic lateral loading. Thus

the behavior under cyclic loading, simulating seismic excitation, can be compared with that observed under monotonic loading, which is the basis of present design codes. The second objective was to conduct the experiments in a manner so the results could be compared with the previously-tested normal weight R/C subassemblages [1-4] .

To achieve these objectives, two lightweight R/C subassemblages, specimens BC7 and BC8, were constructed and tested. In the tests, a cyclically varying horizontal force was applied quasi-statically to the subassemblages, generating force-displacement hysteretic loops. In a pseudo-monotonic test on specimen BC7, a single large inelastic hysteretic loop was generated. The initial part of the loop provided information on the behavior of the subassemblage under monotonic loading. For the cyclic test, specimen BC8 was subjected to incrementally increasing cyclic loops until failure occurred. To aid the comparison of these specimens with the previously-tested normal weight subassemblages, specimens BC3 and BC4 [1-4] , the magnitude of the inelastic hysteretic loops at every stage in the tests was based on the ductility obtained at the similar stage in the previous tests. Ductility was used as a base of comparison rather than absolute displacement due to the lower stiffness (modulus of elasticity) of lightweight concrete.

This report contains the details of the experiments on BC7 and BC8, presentation and discussion of the experimental results, a comparison with the experimental results of BC3 and BC4, and finally a discussion of the results obtained regarding earthquake resistant design of lightweight R/C ductile moment resisting frames.

II. TEST SPECIMENS

2.1 Selection of Test Specimens

The test specimens in BC3 and BC4 were one-half scale models of an interior third floor beam-column connection in a 20 story normal weight R/C ductile moment resisting frame (refer to Fig. 2.1) designed to meet the requirements of the 1970 Uniform Building Code for buildings in seismic zone 3, which was at the time the zone of highest seismic activity. In designing specimens BC7 and BC8, the design for BC3 and BC4 was checked against the 1976 Uniform Building Code [6] for buildings constructed of lightweight concrete in seismic zone 4, the new code's zone of highest seismic activity. The only significant change was a slightly closer column tie spacing in the joint region. Note that the design used for BC7 and BC8 does not represent an interior third floor beam-column connection for the same 20-story frame made of lightweight concrete, since the design forces would be less, leading to smaller member sizes. Instead, the test specimens for BC7 and BC8 were just lightweight concrete versions of the test specimens used for BC3 and BC4, with the same member sizes and the same amount of main reinforcement.

Under severe earthquake excitation, the gravity load makes only a small modification to the moment diagram in a lower story frame since the lateral load predominates as is shown in Fig. 2.2. As a result, the points of inflection can be assumed to occur at midspan of the beams and midheight of the columns. This leads to the cruciform shaped subassemblages which are hinge supported at all four ends (refer to Figs. 2.3 and 2.4).

2.2 Description of Test Specimens

The subassemblages, which were half-scale models, consisted of 9 in. (229 mm) by 16 in. (406 mm) beams and a 17 in. (432 mm) square column as shown in Figs. 2.4 - 2.6. The overall length and height of the subassemblage was 12 ft. (3.66 m) and 6 ft., (1.83 m), respectively. All reinforcement was of Grade 60.

The main longitudinal reinforcement for the beams consisted of four #6 (19 mm diam.) reinforcing bars on the top and three #5 (16 mm diam.) bars along the bottom (Fig. 2.5). Thus, the bottom steel area was about one half of that of the top, the minimum amount required by the ACI Code, making the negative moment capacity about twice as large as the positive moment capacity. Shear reinforcement consisted of #2 (6 mm diam.) closed stirrups with a center-to-center spacing of 3.5 in. (89 mm). In addition, #2 hairpin-shaped stirrups were used with the same 3.5 in (89 mm) spacing to provide lateral support to the inside longitudinal reinforcement.

The longitudinal reinforcement for the columns consisted of twelve #6 bars (19 mm diam.) as shown in Fig. 2.16. Column ties were used to provide transverse shear reinforcement and confinement to the column core. The ties were made with #2 (6 mm diam.) underformed bars and spaced at 1.6 in. (41 mm) along both the column and joint regions. This spacing required nine ties in the joint region, whereas only seven ties were used in BC2 and BC4. This is the only major difference in the design of the subassemblages. One column tie consisted of 3 overlapping rectangular hoops. The two inner rectangular hoops acted as supplementary cross-ties.

2.3 Material Properties

The lightweight concrete mix used was designed to have a 4,500 psi (31 MPa) strength at 28 days in an attempt to duplicate the test strengths of BC3 and BC4. The mix design is listed in Table 2.1. The age and strength of each specimen at testing was 39 days and 4,615 psi (31.9 MPa) for BC7 and 28 days and 4,150 psi (28.6 MPa) for BC8. The concrete properties are summarized in Table 2.2. The stress-strain and strength-gain curves are shown in Figs. 2.7 and 2.8, respectively.

All reinforcement used was of Grade 60. The stress-strain curves for the #2 (6 mm diam.), #5 (16 mm diam.), and #6 (19 mm diam.) bars are shown in Fig. 2.9, while the results of a cyclic test performed on a machined #5 (16 mm diam.) bar are displayed in Fig. 2.10. The yield stress for the #5 (16 mm diam.) bar is considerably different in the two figures. This is probably due to the machining process, which

relieved much of the residual stresses in the cyclic test specimen, leading to a higher initial yield stress. The fact that the two tests were performed on different types of testing machines may have also had some influence on the results. In the strain hardening range, the envelope of the cyclic test agrees well with the monotonic tension test, indicating that very little degradation in material properties occurred under cyclic loading.

2.4 Fabrication of Test Specimens

The reinforcement cage (Fig. 2.11) was constructed to 1/8 in. (3 mm) tolerance and tied securely with 16-gage wire. Short steel pins were silver-soldered to the longitudinal reinforcement. The pins were later used to support clip gages to measure average strains in the reinforcement. Styrofoam and plastic tubing were placed around each pin to provide a gap between the pin and the concrete, enabling the pins to move independently of the concrete. Micro-dot strain gages were also welded to the longitudinal reinforcement of the beam to provide additional strain measuring devices.

Special end details for the beam and column were needed for mounting the beam shear transducers and column supports. These end details are shown in Figs. 2.12 and 2.13. The beam end detail consists of eight 5/8 in. (16 mm) diameter threaded rods butt and lap welded to the seven longitudinal reinforcing bars. To provide space for the welds, the shear reinforcement in the region of the end detail consisted of closed stirrups made with #3 (10 mm diam.) bars without any hairpin stirrups. To assist the shear key on the end plate in transferring the shear force from the support into the beam, four 1 in. (25 mm) diameter threaded rods extended 6 in. (150 mm) into the beam from each end plate. The column end detail consisted of eight 5/8 in. diameter threaded rods which were lap spliced with eight longitudinal reinforcing bars. Threaded rod was used in all of the end details so that it could easily be bolted to the end plates.

Once the reinforcement cage was completed, it was placed in an oiled wooden form. Plastic chairs were used to hold the cage in position. The form was levelled before casting. The concrete was cast in one day

using three lifts to prevent shrinkage cracks between the beams and column. A high-frequency vibrator was used to compact the concrete. After casting, wet burlap sacks and plastic covers were placed on the exposed concrete to aid curing. The forms were removed approximately one week before testing. Test cylinders were cured in closed metal cannisters.

III. EXPERIMENTAL TEST SET-UP AND INSTRUMENTATION

3.1. Testing Frame and Specimen Supports

The steel testing frame, available at the laboratory shown in Fig. 3.1, was used to support the subassemblages during the experiment. The subassemblage was supported by the frame at three points: both ends of the beams and at the top of the column. The beams were supported by rollers which allowed only rotation and horizontal translation. The top of the column was connected to the frame through a hinge which permitted rotation but no translational movement.

The main requirement which the testing frame had to fulfill was to remain nearly rigid throughout the testing. Theodolite measurements of the upper column hinge taken during the testing verified that this requirement had been met.

3.2. Loading Apparatus

A vertical force P and a horizontal force H were applied to the hinge support at the base of the column. The vertical force P simulates the column load at the third floor level of the 20 story prototype frame while the horizontal force H simulates the shear that would arise under seismic excitation.

The horizontal force H was applied through a double-acting hydraulic jack. Since the jack could apply a force in two directions, full load reversals could be simulated. A 600 kip (2670 kN) compression jack was used to apply the vertical force P . This jack was mounted on a movable cart so it could remain vertical while translating horizontally.

3.3. Instrumentation

Since the subassemblages were placed in an east-west direction when tested, compass directions (W, E, etc.) are used in the remainder of this report to describe and differentiate instrumentation, reactions, and deformations, for the two beams.

The instrumentation used can be subdivided into the following two categories: force and reaction measurements, and strain and deformation measurements. The instrumentation was denoted by the same names as in the previous tests for continuity.

3.3.1. Load and Reaction Measurements

Transducers were used to measure the applied vertical force P and the applied horizontal force H . Aluminum shear transducers of special design were used to measure the reactions, V_W and V_E , at the beam supports.

3.3.2. Strain and Deformation Measurements

Strain in the beam reinforcement was directly measured with eight weldable micro-dot strain gages. Four of the gages (RE1, RE11, RW1 and RW11) were placed on the hairpin stirrups. The location of the gages is shown in Fig. 3.2.

Rotations and average strains within regions along the beams and column near the interior joint were determined from measurements made with twenty clip gages. The location of these gages is shown in Fig. 3.3a for BC7 and Fig. 3.3b for BC8. Sixteen of the gages span four regions along the beams, and these gages are denoted by beginning with the letter "C" or "K". The letter "C" indicates the clip gage was mounted on the previously mentioned steel pins which were silver-soldered to the main longitudinal reinforcement (Fig. 3.4). The letter "K" indicates the clip gage was mounted on steel rods which were cast in the beam and span across its width. Thus the total rotations and average strains of the steel reinforcement can be compared with that of the concrete. By comparing Fig. 3.3a with Fig. 3.3b, it can be seen that the "K" clip gages on BC7 are offset horizontally from the "C" clip gages while both sets of clip gages are aligned on BC8. This change was made so interpretation of data would be facilitated. The four clip gages on the column are designated EU, EB, WU, and WB. They were mounted on steel pins silver-soldered to the main column reinforcement.

Shear deformations were measured with eight diagonal gages along two regions on each of the beams. These gages are shown in Fig. 3.3a for BC7 and Fig. 3.3b for BC8 and are denoted by having "S" for a first letter. On BC7 all eight gages were clip gages, while on BC8 the four gages nearest to the column were linear potentiometers. The gages near the column were connected to rods embedded in the column and in the beam. As a result, the shearing deformation across the interface cracks which developed between the beam and column could be measured. The gages further away from the column measured the shearing deformation in a region of high flexural-shear cracking.

Slippage of the rebars (pull-out) in the joint region was measured with the use of four linear variable differential transformers (LVDT's), designated PE1, PE11, PW1, and PW11 in Fig. 3.5a for BC7 and Fig. 3.5b for BC8. The LVDT's were attached to steel pins which were silver soldered to the main beam reinforcement at the intersection with the column faces. The LVDT's measured the relative displacement between the steel pins and the column face. With the information provided by the LVDT's, fixed-end rotations due to rebar slippage were also determined.

The interface cracks between the beams and column were measured with four additional LVDT's, designated as FE1, FE11, FW1 and FW11 in Fig. 3.5a for BC7 and Fig. 3.5b for BC8. These LVDT's were connected to steel rods embedded horizontally across the width of the beam. This set of LVDT's also provided an alternative route to calculate the fixed-end rotation.

The horizontal displacement of the lower column hinge, referred to as δ , was measured through the use of a 15 in. range linear potentiometer attached to the bottom hinge. Theodolite readings at certain stages during the testing were used to verify the accuracy of the linear potentiometer.

3.4. Recording Equipment

The data obtained by all the instrumentation was recorded on magnetic tape by a low-speed scanner data acquisition system. The

data from several gages and transducers were recorded continuously on XY and XYY' recorders. The data channels plotted on each recorder are listed in Table 3.1.

3.5. Test Procedures

After curing, each specimen was whitewashed. Grid lines were then drawn along each beam and the joint region to aid in detection and location of cracks during the testing. The specimen was then positioned in the testing frame and the external instrumentation and recording equipment were then connected and calibrated to complete the preparation before testing.

To begin the loading procedure, a 470 kip (2090 kN) vertical force was applied to the column. This value was maintained throughout the experiment. To simulate the negative moment at the interior joint due to gravity load, the beam supports were lowered by turning adjustment screws until a 3.5 kip (16 kN) downward reaction was measured at each support.

The horizontal load was now applied to the base of the column. The load histories for BC7 and BC8 are shown in Figs. 3.6 and 3.7, respectively. These load histories were similar to the ones used for the previously-tested subassemblages to aid in comparison. The BC7 load history, modelled after BC4, consisted of four small displacement cycles, simulating service load conditions, followed by one large displacement cycle. The small displacement cycles were controlled by the magnitude of the applied horizontal force. The range of the large loop was governed by displacement or, more accurately, the ductility which BC4 was subjected to. Ductility as used here refers to the ratio of a given horizontal displacement to the horizontal displacement at the first yield of the beam reinforcement and is denoted by the symbol μ . In the test on specimen BC4, a ductility of 5.7 was reached during the large displacement cycle. However, only a ductility of 5.4 was achieved during the test on BC7. This was due to a small initial offset in the displacement at the beginning of the working load cycles which was not noticed until data were reduced. This difference in ductility is so

small that it should not effect the validity of any comparisons made between the two subassemblages.

The BC8 load history consisted of incrementally increasing cycles patterned after BC3. In both of these experiments, each cycle was repeated once before moving to the next level. The cycles through LP 16 were controlled by the size of the applied horizontal force. The magnitude of the force was the same at each stage as in the previously-tested specimen, BC3. Beginning with LP 17, the size of the cycles was based on the ductility attained at the corresponding stage in the BC3 experiment. Ductility as used here is the ratio of a given horizontal displacement to the horizontal displacement when yielding of the specimen occurred as it was being loaded to LP 17 and is designated by the symbol μ_s . Yielding of the specimen occurs when the horizontal load capacity begins to level off as the yield moment is exceeded in both beams at the column face. Two different definitions or symbols for ductility are used to aid in the comparison later in this report of the lightweight R/C subassemblages with the previously-tested normal weight R/C subassemblages.



IV. EXPERIMENTAL RESULTS AND DISCUSSION

4.1. Overall Response

The main behavior of the subassemblage is represented by the horizontal force vs. horizontal displacement curve of the lower hinge. Figure 2.3 shows the main forces and displacements involved in this experiment. If the summation of moments are taken about the top hinge with the subassemblage in a displaced configuration, then:

$$(V_W - V_E)L = Hh + P\delta \quad (1)$$

Dividing the above equation by h and noting that $L = h$, the following equation results:

$$(V_W - V_E) = H_{EQ} = H + P\delta/h \quad (2)$$

The quantity $(V_W - V_E)$ represents the equivalent horizontal load capacity of the subassemblage, including the $P - \delta$ effect, and is denoted by H_{EQ} . Thus, by summing the absolute values of the beam reactions, the equivalent horizontal load capacity of the subassemblages, H_{EQ} , can be computed. H_{EQ} is directly proportional to the flexural capacity of the beams when the $P\delta$ effect is neglected.

The measured quantity H includes the frictional forces of the four hinges supporting the subassemblage. Thus the measured H is greater than the actual horizontal load being resisted by the subassemblage.

Solving equation (2) for H

$$H = (V_W - V_E) - P\delta/h \quad (3)$$

an equation results in which all the parameters on the right hand side are known at any given time during the experiment. Thus the actual horizontal load being resisted by the subassemblage can be reduced from the equilibrium of forces and is denoted by H_{RED} .

Theodolite readings taken after the experiment on BC7 indicated that the jack applying the column force P was not quite vertical, thereby

inducing a small horizontal load at the lower hinge which was constant throughout the experiment. Therefore for BC7 the following equation applies in the calculation of H_{RED} .

$$H_{RED} = (V_W - V_E) - P\delta/h + H_{COR} \quad (4)$$

In this equation H_{COR} is the constant horizontal load applied as a result of the column jack not being vertical.

The H , H_{RED} and H_{EQ} vs. δ graphs for BC7 and BC8 are shown in Figs. 4.1 - 4.4.

4.1.1 Specimen BC7

First yield of the beam reinforcement occurred at LP 23 at a displacement of 0.67 in. (17 mm). This corresponded to a ductility (μ) equal to one. The subassembly resisted a 37.3 kip (166 kN) load at first yield. As the displacement was increased further, the H and H_{RED} vs. δ curves in Fig. 4.1 give the impression that the capacity of the subassembly was diminishing. However, in Fig. 4.2b, the H_{EQ} vs. δ curve which includes the $P - \delta$ effect shows that the equivalent lateral load capacity increased by 27% to 47.4 kips (211 kN) from LP 23 to LP 32 where the maximum displacement of 3.70 in. (44 mm, $\mu = 5.4$) was reached. At this displacement, 50% of H_{EQ} was due to the $P - \delta$ effect. The load was then reversed until at LP 49 a load of 48.0 kips (214 kN) was being resisted. Again, the same observation as above can be noted between LP 43 and LP 49.

The area enclosed by the $H_{EQ} - \delta$ curve is a good indicator of the amount of energy dissipated by the subassembly. A comparison of Fig. 4.2a with Fig. 4.2b reveals that under the lateral service load cycles, the behavior of the subassembly is near-linear and does not dissipate much energy while under the large lateral displacement cycle, due to the inelastic deformation, the subassembly dissipated a great deal of energy.

The difference in the $H - \delta$ and $H_{RED} - \delta$ curves in Fig. 4.1 is due to the frictional forces in the four pin supports. The frictional forces have a maximum value of 7 kips (31 kN).

4.1.2. Specimen BC8

As mentioned previously, the loading history for BC8 (Fig. 3.7) was similar to the one used on the previously-tested specimen BC3. The early H - δ cycles (Fig. 4.3a) were not symmetrical; the negative displacements were larger than the positive displacements. Consequently, the bottom reinforcement on the east beam yielded first at LP 10 (Fig. 4.4a) at a displacement of -0.70 in. and a load of -35.5 kips (158 kN). At LP 13, at a displacement of 0.78 in. and a load of 34.5 kips (153 kN), the top reinforcement of the east beam yielded, and the bottom reinforcement on the west beam was on the verge of yielding. This explains the noticeable drop in stiffness from LP 11 to LP 13 in Fig. 4.3a and Fig. 4.4a. Until this point, almost no deterioration in stiffness was noted.

Shown in Fig. 4.3b and Fig. 4.4b are the cycles whose maximum displacements were based on the ductility obtained on the corresponding cycles on specimen BC3. Yielding of the specimen occurred at LP 17A at a load of 35.1 kips (156 kN) and a displacement of 0.86 in. (22 mm) corresponding to a ductility of one ($\mu_S = 1$). At LP 17 a displacement of 1.24 in. (31 mm, $\mu_S = 1.45$) was achieved while sustaining a load of 37.0 kips (165 kN). The peak resistance of -40.3 kips (-179 kN) was obtained at LP 18 ($\mu_S = 1.75$). A noticeable drop in stiffness occurred during the second cycle at this displacement as the slope of the curve leading to LP 19 decreased. Between LP 19 and LP 20 the hysteretic curve began to pinch, indicating diminishing energy dissipation. At LP 20, where a displacement of -1.51 in. (-38 mm, $\mu_S = 1.75$) was attained, the load was 5.2 kips (22 kN) or 13.1% less than at LP 18. This was the first significant drop in resistance from the first to second cycle at a given displacement. The capacity deteriorated even further as the subassembly was loaded to LP 21. At the same displacement as LP 19 on the curve leading to LP 21, the resistance at LP 21 was 8 kips (36 kN) or 23% less than at LP 19. At LP 21, with a displacement of 2.19 in. (56 mm, $\mu_S = 2.55$), the load on the specimen was 32.2 kips (143 kN), 14% less than at LP 17, indicating the resistance of the subassembly had already attained its peak value. A significant drop in resistance can also be noted by comparing the curve leading to LP 22 with LP 20.

At the same displacement as LP 20 on the previous cycle, the load at LP 22 was 9 kips (40 kN) or 26% less than that at LP 20. At LP 22 where the displacement was -2.35 in. (-60 mm, $\mu_S = 2.7$), the load was 29.2 kips (130 kN), 28% less than at LP 18. On the next cycle at these displacements, the stiffness degradation becomes even more pronounced. The load at LP 23 was 19.8 kips (88 kN), 38% less than at LP 21, while the load at LP 24 was 16.7 kips (74 kN), 43% less than at LP 22. At this point the hysteretic loops had become very narrow, and the sub-assembly was dissipating very little energy. The next two cycles were at a displacement of +3.43 in. (87 mm, $\mu_S = 4.0$) and -3.60 in. (91 mm, $\mu_S = 4.2$). By the end of the second cycle, the capacity of the subassembly was just a fraction of its peak values at LP 17 and LP 18. At LP 27 the load was 13.7 kips (61 kN), 37% of the value at LP 17, while at LP 28, the load was -19.4 kips (-86 kN), 48% of the value at LP 18. After LP 25, the H_{RED} curve started to have opposite sign of the H_{EQ} curve (Fig. 4.3b). This indicates that the capacity of the sub-assembly had diminished to the point where the horizontal load at the base of the column had to be applied in a direction to oppose the $P - \delta$ effect to maintain stability.

The remaining 1-1/2 cycles in the loading history (Fig. 3.8) are not shown in the graphs. Since the subassembly had already deteriorated very substantially, very little was to be learned from the remaining cycles. Although they were conducted, they are not shown since very few data records were taken.

By comparing the H and H_{RED} curves in Fig. 4.3b, the frictional forces in the pin supports can be determined. The maximum force due to friction is 7 kips, similar to BC7.

The following two general observations can be made concerning BC8 (Fig. 4.4b). First, the peak of H_{EQ} capacity of 40.3 kips (179 kN) occurred at LP 18 at a displacement of only -1.51 in. (-38 mm). Secondly, between LP 19 and LP 20, and then between LP 20 and LP 21, the hysteretic loop began to pinch, indicating that the bond in the joint had deteriorated, and the reinforcement was beginning to slip through the joint. This explains the decreasing capacity on the remaining cycles.

4.1.3 Comparison of BC7 and BC8

The first yield of the reinforcement in BC7 and BC8 occurred at virtually the same displacement, 0.67 in. (17 mm) vs. 0.70 in. (18 mm), and under similar loads, 37.3 kips (166 kN) vs. 35.5 kips (150 kN). The small difference in the loads was mainly due to the fact that the pre-yield cycles of BC8 (Fig. 4.4a) were larger than the working load cycles of BC7 (Fig. 4.2a), leading to some early degradation, and the concrete strength of BC7 was slightly greater than that of BC8, 4,615 psi (31.8 MPa) vs. 4,150 psi (28.6 MPa).

The behavior of BC7 and BC8 was drastically different in the inelastic range (refer to Fig. 4.4c). The lateral load resistance of BC7 reached maximum values at the two extreme displacements while the peak value for BC8 occurred at a displacement of only 1.50 in. (38 mm). This is an indication that repeated cycles of full reversal deformations led to early bond deterioration, and premature decrease in overall lateral resistance capacity. In a test such as BC7 where the specimen undergoes only one large inelastic cycle, anchorage of the reinforcement at a joint is not a problem since at any given point the tension reinforcement in each beam is anchored in the uncracked concrete (since it is under compression) in the adjoining beam. However, in a test such as the one performed on BC8 where the specimen is subjected to repeated inelastic cycles, interface cracks develop between each beam and the column as the reinforcement yields at the face of the column. As the reinforcement is being pulled from one side of the joint and pushed from the other, bond deterioration begins to occur and, after several cycles, eventually this deterioration extends throughout the width of the joint. This leads to complete slippage of the reinforcement, causing the resistance of the subassembly to decrease substantially. However, since the reinforcement is still anchored in the adjoining beam, the stiffness of the subassembly begins to increase at large displacements once the interface crack between the adjoining beam and the column closes. This behavior was exhibited by specimen BC8 beginning with LP 23.

The large difference in behavior by the two specimens shows that

the results from monotonic tests cannot be applied to predict the behavior under cyclic loading. The degradation of stiffness which occurs under cyclic loading demonstrates that the behavior of a subassemblage is dependent on its previous loading (or deformation) history.

4.2 Energy Dissipation

The ability to dissipate large amounts of energy is a very desirable characteristic in earthquake-resistant design. The area enclosed by the $H_{EQ} - \delta$ curves gives an indication of the amount of energy dissipated by each subassemblage. The areas of the large displacement cycle of BC7 and the post-yield cycles of BC8 are shown in Table 4.1.

The main observation that can be made is that in each cycle, specimen BC8 dissipated very little energy compared to specimen BC7. Premature slippage of the reinforcement in BC8 led to substantial pinching of the curves which diminished the energy dissipation capacity of the specimen. The largest amount of energy dissipated in one cycle by BC8 (which occurred at a low ductility on cycle 21-22) was only 26% of the value for BC7. From cycle 17-18 to cycle 19-20 which was between the same peak ductility values, the amount of energy dissipated decreased 28%, indicating severe deterioration had already occurred. At cycle 23-24 the amount of energy dissipated was 47% less than the quantity on the previous cycle, signifying more deterioration had taken place. The next cycle was at a comparable displacement to the large displacement cycle of BC7, yet the energy dissipated was only 22% of the amount for BC7. The total amount of energy dissipated by BC8 was 319.7 k-in. (36.10 kN-m). Coincidentally, this compared closely to the 300.6 k-in. (33.96 kN-m) of energy-dissipated by BC7. Yet the energy was dissipated over six inelastic cycles for BC8 compared to only one cycle for BC7: this emphasizes the substantial deterioration which occurred in specimen BC8 in the early inelastic cycles.

4.3 Visual Behavior

The visible damage experienced by each subassemblage was markedly different. Following is a brief description of the cracking and spalling which occurred in each specimen.

4.3.1 Specimen BC7

As the reinforcement yielded at LP 23, flexural-shear cracks up to 9 in. (229 mm) in length appeared along the bottom of the west beam and the top of the east beam (Fig. 4.5). The main cracking occurred over 20 in. (508 mm) regions near the column. More cracks developed as the maximum displacement was reached at LP 32. As the specimen was loaded in the opposite direction, flexural-shear cracking was observed along the top of the west beam and the bottom of the east beam. An interface crack between the beam and column developed, creating a very small (1/16 - 1/8 in.) (1.5 - 3 mm) gap, while small areas of the column cover toward the beams began to bulge. At LP 46, a few diagonal hairline cracks, 10 - 15 in. (254 - 381 mm) in length, appeared on the column in the joint region (Fig. 4.6). At LP 49, just as the maximum negative displacement was reached, the concrete spalled along the top of the west beam and the west face of the column immediately above the beam (Fig. 4.7). The cover of the beam spalled for a 6 in. (152 mm) length, exposing one reinforcing bar. The spall along the column was approximately 10 in. (254 mm) long and 6 in. (152 mm) wide. No reinforcement was exposed. As the cycle was completed, a 4 in. (102 mm) long spall along the bottom corner of the west beam occurred, exposing one reinforcing bar (Fig. 4.8).

4.3.2 Specimen BC8

The damage to specimen BC8 was distinguished by large, deep spalling along the beams and column and the development of wide interface cracks between each beam and the column. Between LP 21 and LP 22, the first spall occurred on the face of the column beneath the west beam (Fig. 4.9 and 4.10). The spall, which was 9 in. (229 mm) high and spanned the width of the column, exposed three column ties. By LP 22, interface cracks with a maximum width of 1/4 in. (6 mm) had developed between the beams and column. As the specimen reached the peak displacement at LP 26, spalling occurred along the lower column -- east beam junction (Fig. 4.11). The column cover spalled along a 10 in. (254 mm) high region across the width of the column, exposing three column ties. By LP 28, the spall extended along the bottom of the beam for about 4 in. (102 mm), uncovering all the main reinforcement (Fig. 4.12).

As the test continued, the interface cracks grew, and more spalling occurred. When the test was complete, the top and bottom reinforcement on both beams was exposed for a distance of 5 in. (127 mm) from the column (Fig. 4.13 and 4.14). Large spalls existed along the column above and below the west beam and below the east beam, each exposing column ties. The interface cracks enlarged until, near the end of the test, they reached a maximum width of approximately 1/2 in. (approx. 12.7 mm).

The flexural-shear cracking along the beams was not nearly as extensive as that of BC7. As the bond in the joint region deteriorated, the moments transmitted to the beams became small, minimizing cracking and flexural deflections along the beam. The large overall slippage of the reinforcement led to the extensive spalling along the beam-column junction and to the large interface cracks.

4.4 Slippage of Reinforcement and Fixed-End Rotation at Interior Joint

Overall slippage of a reinforcing bar through an interior joint is indicated by large pullout and push-in measurements on opposite sides of the joint. If the pullout measurement is large, while the push-in measurement remains small, then the strain of the reinforcement is in the strain hardening range and good bond still exists in the joint. When complete (total) slippage does occur, the stiffness of the sub-assembly decreases, and the fixed-end rotation of the beam relative to the column increases. Due to the instrumentation used, the fixed-end rotation can be based on the rotation whose measurement was based on the deformation of the reinforcement or of the concrete section as a whole.

4.4.1 Specimen BC7

The pullout and push-in of the reinforcement for BC7 is shown in Figs. 4.15a and b. Before yielding at LP 23, the pullout and push-in of the reinforcement was small. At the maximum displacement at LP 32, the pullout increased to 0.14 in. (3.6 mm) for the top reinforcement on the east beam and 0.13 in. (3.3 mm) for the bottom reinforcement on the west beam, while the push-in remained small. As the load was reversed, and the displacement returned to zero at LP 43, both beams had residual pullout for both the top and bottom reinforcement, indicating

the beam bars had elongated, and an interface crack had developed. The amount of elongation for the east beam was greater, due to the asymmetrical stiffness of the beams, i.e., more reinforcement on top than along the bottom. At this stage of the cycle, since interface cracks existed through the whole beam section at each column face, the moment at each of the column faces was resisted solely by the top and bottom reinforcement. Since the bottom reinforcement was smaller in area, it was being subjected to higher stresses.

As the specimen was loaded to LP 49, the top reinforcement on the east beam showed a positive pullout measurement, indicating that the interface crack did not close. At the same time, the bottom reinforcement was subjected to high stresses which were required to balance the large compressive forces being developed by the larger area of top reinforcement. The high stresses caused the bottom reinforcement to reach high strain levels leading to relatively large amounts of pullout at LP 49. Meanwhile, on the west beam a different phenomenon was occurring. Because of the larger area of the top reinforcement, acting in tension, the bottom reinforcement had to be stressed to higher compressive than tensile stresses, causing the interface crack to close quickly. Consequently at LP 49 the bottom reinforcement had a small push-in reading while the top reinforcement had a pullout reading which was substantially less than the bottom reinforcement on the east beam.

The maximum amount of pullout was 0.22 in. (5.6 mm) at LP 49 along the bottom reinforcement at the east side of the joint. The corresponding amount of push-in along the west side of the joint was less than 0.01 in. (0.25 mm). The small amount of push-in clearly indicates that overall slippage of the reinforcement had not occurred and that there was still good bond through the joint region.

The fixed-end rotation at the face of the column is depicted in Figs. 4.16a and b. The moment plotted along the vertical axis is simply the product of the reaction at the beam support and its lever arm of 63.5 in. (1.61 m) to the face of the column. In general the rotations based on the measured deformation of the concrete of the beam

were larger than the rotations based on the reinforcement deformation. This is due to some slippage of the concrete in the beam relative to the reinforcement. Comparing Fig. 4.16a with Fig. 4.16b, the two curves based on the concrete deformations agree very closely at all load points. The two curves based on the reinforcement deformations are not as similar due to the asymmetric stiffness of the beams. Bulging of the column cover between LP 43 and LP 49 disrupted the measurements on the east beam.

4.4.2. Specimen BC8

The pullout and push-in of the reinforcement for BC8 are shown in Figs. 4.17a and b. At LP 20, the bottom reinforcement had a pullout of 0.14 in. (3.6 mm) on the east side of the joint and a push-in of 0.07 in. (1.8 mm) on the west side which indicates that the bottom bars had begun to slip through the joint region. This explains the pinching of the $H_{EQ} - \delta$ hysteretic curve between LP 19 and LP 20. At LP 22 the top reinforcement had a pullout of 0.18 in. (4.6 mm) on the east side of the joint and a push-in of 0.12 in. (3.0 mm) on the west side, denoting large amounts of slippage of the reinforcement. Thus, slippage of both the top and bottom reinforcement had occurred at a horizontal displacement of only -2.35 in. (-60 mm, $\mu_s = 2.7$). It appears that the total slippage of the reinforcement through the joint was the main cause of the dramatic decrease in the lateral load capacity of the subassembly after LP 22.

4.4.3 Comparison of Specimens BC7 and BC8

The maximum amount of push-in of 0.03 in. (0.76 mm) for BC7 clearly indicates that total slippage of the reinforcement through the joint did not occur. For BC8 push-in greater than 0.25 in. (6.4 mm) and pullout in excess of 0.40 in. (10 mm) signifies that the bond deteriorated throughout the joint leading to total slippage of the reinforcement. The total slippage resulted in a peak fixed-end rotation (.054 rad) which was more than twice as large as the peak rotation (0.22 rad) for BC7.

4.5 Strain of the Longitudinal Reinforcement

The strain of the beam longitudinal reinforcement was determined

by two methods. In one method, the strain was directly measured by micro-dot strain gages welded to the reinforcement at the intersection with the column face. The second method involved clip gages which measured deformations in the reinforcement over a region adjacent to the column. The deformations were then divided by the 9 in. (229 mm) length of the region to determine the average strain. The second method provided an alternative way of determining an average strain after the strain gages broke.

The strains of the reinforcement for BC7 are shown in Figs. 4.19 and 4.20. As shown in the figures, the average strains were almost as large as the strains at the column face. This was probably due to the large amounts of diagonal tension cracking in the beams near the column. The bottom reinforcement maximum strain of 0.045 at LP 49 corresponds to a stress of about 90 ksi (620 MPa) (refer to Fig. 2.9) while the peak strain for the top reinforcement of 0.029 at LP 49 corresponds to a stress of about 83 ksi (572 MPa).

The strain of the reinforcement for BC8 is shown in Figs. 4.21 and 4.22. Two general observations can be made. The peak strains were much less than those of BC7 due to slippage of the reinforcement in the joint (≤ 0.018 which corresponds to a stress of about 75 ksi). Also slippage of the bottom reinforcement occurred first. At LP 20, which was the end of the second cycle at a peak displacement of -1.51 in. (38 mm), the strains of the bottom reinforcement failed to match those of LP 18, indicating the bars had pulled through. Total slippage of the top reinforcement occurred by LP 22 since the strain on the west side of the column failed to increase over that of LP 20, even though the peak displacements of the cycle had been increased.

As mentioned earlier, the bottom steel area was 50% of that at the top, the minimum amount required by the ACI Code, subjecting the bottom steel to higher amounts of stress for longer portions of each cycle when the moment at the face of the column was being resisted solely by the steel reinforcement. This led to the earlier total slippage of the bottom reinforcement in specimen BC8 and explains why the peak strains for the bottom reinforcement were larger than the top reinforcement for either specimen.

4.6 Effect of Shear

4.6.1 Specimen BC7

In specimen BC7 where the overall stiffness of the subassembly remained high, large shear forces on the order of $3.5 \sqrt{f'_c}$ psi ($.29 \sqrt{f'_c}$ MPa) led to extensive flexural-shear cracking causing the shear reinforcement to resist a substantial proportion of the load. The forces in the shear reinforcement became large enough to yield two of the four instrumented stirrups (Fig. 4.23). Since each beam had a higher stiffness in the negative moment direction, the largest shear forces in the west beam occurred at LP 49 and in the east beam at LP 32. From Fig. 4.23, it can be seen that these were also the points of peak strain in the shear reinforcement in each beam.

The shear strains in the two instrumented regions are shown in Fig. 4.24. The shear strains did not vary much between the first and second regions, substantiating that the interface crack remained small. Only at LP 49 where the interface crack attained its maximum width did the shear strain in the first region exceed that of the second region by a significant amount. The shear strain in the first region of the east beam at LP 49 was larger than in the west beam since the interface crack was wider due to the greater amount of pullout of the bottom reinforcement.

4.6.2. Specimen BC8

In specimen BC8 the shear behavior was dramatically different. The premature total slippage of the reinforcement in the joint region caused the peak shear forces to be about 15% lower than in BC7 and to occur at much lower displacements (LP 17 and LP 18), preventing the development of flexural-shear cracking over a very wide region of each beam and concentrating the shear deformation along the interface cracks. Consequently, the majority of the shear force along each beam was carried by the nearly-uncracked concrete section and the forces transmitted to the shear reinforcement were small, resulting in lower strains which were in the elastic range (Fig. 4.25). The peak strains occurred between LP 18 and LP 22, just before pull-through of the reinforcement was complete.

After slippage of the reinforcement occurred, the shear deformations across the interface crack (Fig. 4.26) became somewhat larger than in specimen BC7 since the width of the interface crack was much greater. As the interface crack developed, the shear force was resisted solely by the dowel action of the reinforcing bars. In Fig. 4.26, the shear strain was several times larger in the negative direction than in the positive due to the larger negative shear forces which led to a deterioration in shear resistance in the later cycles.

The shear deformations along the beam (Fig. 4.27) were much smaller than in specimen BC7. Since the flexural-shear cracking along the beam was not as pronounced or dispersed over as wide a region as in specimen BC7, much of the shear force was being resisted by the nearly uncracked concrete, minimizing shear deformations.

4.7 Sources of Deformation Contributing to the Total Horizontal Displacement

From the data obtained during the testing, the horizontal displacement at the bottom hinge of the column was decomposed into components due to flexure and shear in each beam, fixed-end rotations at the column faces, and the elastic deflection of the column. Following are definitions of each specific component:

Flexural Deformations in Beam

- δ_1 - component due to rotation within first region adjacent to column; based on information from Figs. 4.28 and 4.29.
- δ_2 - component due to rotation within second region from column; based on information from Figs. 4.30 and 4.31.
- δ_3 - component due to flexural deformation of remainder of beam; based on R/C beam theory.

Shear Deformations in Beam

- δ_{S1} - component due to shear strain within first region adjacent to column; based on information from Figs. 4.24 and 4.26.
- δ_{S2} - component due to shear strain within second region from column; based on information from Figs. 4.24 and 4.27.

Fixed-End Rotation of Beam

δ_{FE} - component due to fixed-end rotation at column face due to pull-out and push-in of reinforcement; based on information from Figs. 4.16 and 4.18.

Elastic Column Deflection

δ_{COL} - component due to elastic flexural deflection of column; based on elastic theory.

The shear deformations in the beam adjacent to the two instrumented regions were small and therefore neglected. The primary purpose of δ_{S1} was to measure the contribution due to shear across the interface crack. The letter E or W is placed after each component to distinguish between the two beams.

4.7.1 Specimen BC7

The components of the horizontal displacement for the west and east beams are shown in Figs. 4.32 and 4.33, respectively. The numbers along the diagonal dash lines designate the load points (LP's). Figs. 4.32a and 4.33a describe the behavior of the subassemblages until just after first yielding of the reinforcement. Each of the remaining four parts of each figure portray the behavior of the subassemblage for one-quarter of the cycle.

The column was nearly-rigid and always contributed less than 4% to the total deflection. At first yield of the reinforcement (LP 23), the fixed-end rotation contributed 11% on the west beam and 14% on the east beam. At LP 32 when the maximum displacement was reached, the contributions had grown to 18% on the west beam and 23% on the east beam. As cracking occurred at the higher displacements, the proportion due to both shear components increased from 1.4% on the west beam and 2.4% on the east beam at LP 23 to 4.3% on the west beam and 6.0% on the east beam at LP 32. δ_{S1} however remained very small, indicating that the interface crack had not become very large. The

shear deformation was greater in the east beam since it was bending about the stiffer direction and therefore resisting a greater shear force.

The behavior of the subassemblage as it was unloaded and returned to a nearly vertical position is shown in Figs. 4.32c and 4.33c. The applied horizontal force and beam reactions reverse sign between LP 37 and LP 38 causing δ_3 and δ_{COL} to make contributions to the displacement in the negative direction. (This is denoted on the graph as the lines cross-over between LP 37 and LP 38. Where criss-crossing of lines is confusing, slash marks are placed on one of the lines to indicate continuity.) The shear contribution reverses sign between LP 38 and LP 40. At LP 43 both beams were left with residual fixed-end rotations. However, the residual fixed-end rotation for the east beam was larger since the bottom reinforcement was now in tension working against the stiffer top reinforcement, while the reverse was occurring on the west beam. This also led to residual flexural rotations in both regions of the west beam compared to only the second region of the east beam.

By LP 44, shown in Figs. 4.32d and 4.33d, no residual rotations remained. From LP 45 to LP 49, the contribution due to fixed-end rotation increased from 16% to 19% in the west beam and 13% to 24% in the east beam, while the total shear contribution decreased from 13% to 8.5% in the west beam and 27% to 15% in the east beam. The contribution of the fixed-end rotation at LP 49 was larger in the east beam than in the west beam since its tension reinforcement, which was smaller in area, was strained to a higher degree.

Comparing the two extreme displacements, LP 32 with LP 49, the contribution due to fixed-end rotation remained virtually the same: a change from 18% to 19% in the west beam and from 23% to 24% in the east beam. The total shear contribution increased from 4.3% to 8.5% in the west beam and from 6.0% to 15% in the east beam. δ_{S1} increased as the interface crack developed and δ_{S2} increased as the cracking within the beams became more extensive.

The behavior during the last quarter cycle is depicted in Figs.

4.32e and 4.33e. At LP 55 the applied horizontal load and beam reactions reversed direction causing the contribution of δ_3 to switch sign. By LP 60, where the subassembly was returned to a near-vertical position, the fixed-end rotation in the west beam had reversed direction, leaving only the flexural components δ_{1W} and δ_{2W} with residual contributions in the negative displacement direction. However, at LP 60 the east beam had not only residual contributions from δ_{1E} and δ_{2E} but a residual fixed-end rotation due to the greater pull-out of its bottom reinforcement at LP 49.

4.7.2 Specimen BC8

The components of the horizontal displacement for the west and east beams are shown in Figs. 4.34 - 4.37. The load points correspond to the peak displacements on each cycle. The peak displacements in the positive direction are depicted in Fig. 4.34 for the west beam and Fig. 4.36 for the east beam. Similarly the peak displacements in the negative direction for the west and east beams are displayed in Figs. 4.35 and 4.37 respectively. Two cycles were performed at each displacement level. To present the information clearly, the components of the displacement for the second cycle are plotted separately from those on the first cycle. The changes in each component as the experiment progressed can best be understood by observing the load points in numerical order.

The most striking observation is the very large contribution of the fixed-end rotation early in the test. By LP 19 the contribution of the fixed-end rotation to the total displacement was 39% on the west beam and 29% on the east beam. At LP 20, the peak negative displacement on the same cycle, the contributions were 38% on the west beam and 48% on the east beam, indicating that total slippage of the reinforcement through the joint had begun to occur. The contribution of the fixed-end rotation continued to increase by substantial amounts through each of the remaining cycles.

4.7.3 Comparison of Specimen BC7 with Specimen BC8

The behavior of BC8 was strikingly different than that of BC7. Slippage of the reinforcement in the joint region in BC8 led to large fixed-end rotations. The total slippage began to occur at cyclic displacements of only 1.50 in. (38mm, $u_s = 1.8$). The behavior of BC7 indicated that although some local slippage had occurred, no total slippage of the reinforcement occurred as the contribution of the fixed-end rotation remained relatively small throughout the testing.

The behavior of both specimens indicates that analysis of R/C structures need to include the contribution of fixed-end rotations at the joint for both cyclic and monotonic loadings. Neglecting fixed-end rotations leads to underestimation of the actual inelastic displacement.

V. COMPARISON WITH NORMAL-WEIGHT SPECIMENS

The H_{EQ} curves for BC7 and BC4 are shown in Fig. 5.1, while the similar curves for BC8 and BC3 are depicted in Fig. 5.2. The horizontal axis in both graphs represent ductility. In Fig. 5.1, the ductility (μ) was based on the displacement at the first yield of the reinforcement while in Fig. 5.2 the ductility (μ_s) was based on the displacement when yielding of the specimen occurred as it was being loaded to LP 17.

The material strength properties of all four specimens were in relatively close agreement. The concrete strengths for BC4 and BC7 were 4570 psi (31.5 MPa) and 4615 psi (31.8 MPa), respectively and for BC3 and BC8, the concrete strengths were 4510 psi (31.1 MPa) and 4150 psi (28.6 MPa). The yield strength of the beam reinforcement was 71 ksi (489 MPa) for BC3 and BC4 while the yield strengths for the #5 and #6 bars were 67 ksi (462 MPa) and 65 ksi (448 MPa), respectively for BC7 and BC8. The minor variations in the material properties led to only small differences in the strength of each specimen, and, consequently the H_{EQ} curves can be compared directly.

5.1. Specimens BC4 and BC7

The strength of the two specimens was very similar. At first yielding of the reinforcement, LP 23, the load was 2 kips (9 kN) larger for BC4. At the peak displacement at LP 32, the capacity of BC4 was 49 kips, (218 kN), compared to 47 kips (209 kN) for BC7. The difference was partially due to the slightly smaller ductility which BC7 was subjected to. As the loading was reversed, the two curves crossed-over. As the maximum negative displacement was reached at LP 49; the capacity of BC7 exceeded that of BC4 by 2 kips (9 kN).

The magnitude of the fixed-end rotation indicates the amount of

bond degradation in the joint. At LP 32, the contribution of the fixed-end rotation to the total displacement was 18% in the west beam and 23% in the east beam of specimen BC 4, the same percentages as for specimen BC 7. At LP 49, the contributions for specimen BC4 were 18% in the west beam and 38% in the east beam. This compares with 19% in the west beam and 24% in the east beam of BC7. The greater contribution of the east beam of BC4 was due to the larger amount of pullout of the bottom reinforcement.

Since the modulus of elasticity of normal weight concrete is substantially higher than that of lightweight concrete, the initial stiffness of BC4 was greater than that of BC7. BC4 had an initial stiffness of 132 kip/in. (23.1 kN/mm) which was 52% greater than the initial stiffness of 87 kip/in. (15.2 kN/mm) for BC7. This was in close agreement with the relative moduli of elasticity of the two specimens; BC4 had a modulus of elasticity of 3.93×10^3 ksi (27.1×10^3 MPa) which was 46% greater than the modulus of 2.69×10^3 ksi (18.6×10^3 MPa) for BC7. As cracking of the concrete and yielding of the steel occurred at higher displacements, the stiffness of the specimens became more dependent on the steel reinforcement. This led to the similar stiffness of the two specimens for the remainder of the cycle, as is shown in Fig. 5.1.

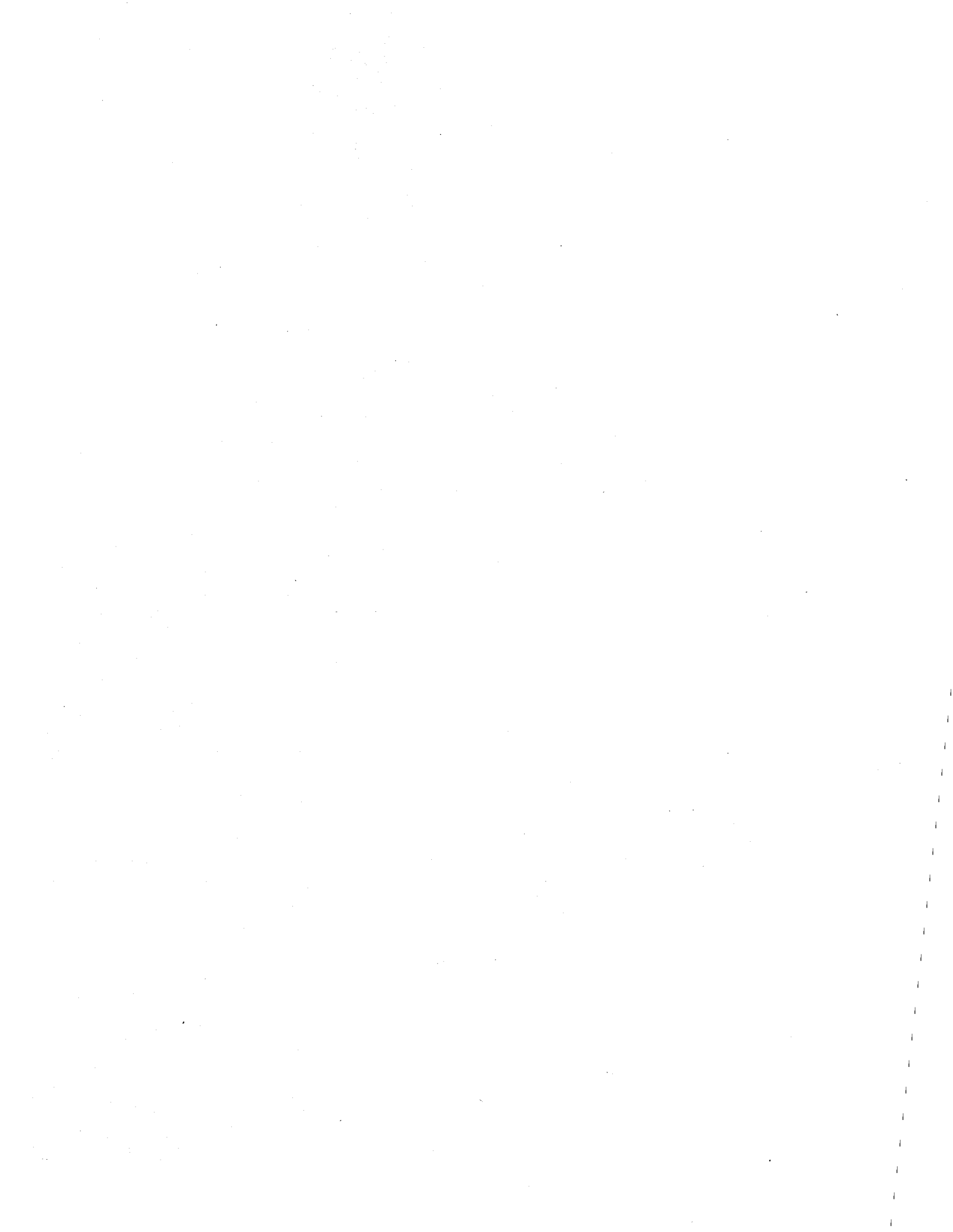
The greater flexibility of the lightweight concrete led to a displacement at first yield of 0.67 in. (17 mm) for BC7 which was 12% higher than the 0.60 in. (15 mm) displacement for BC4. This is important for designs in the inelastic range since for the same ductility lightweight concrete structures will have about 12% higher story drift, leading to more non-structural damage and higher $P - \delta$ forces.

Overall the behavior of the specimens were very similar. From the comparison, the main conclusion that can be drawn is that in a monotonic test, where degradation of the bond in the joint region does not occur, the performance of lightweight concrete is analogous to that of normal-weight concrete with regard to strength and fixed-end rotations.

5.2. Specimens BC3 and BC8

The performance of the two specimens as shown in Fig. 5.2 was dramatically different. Specimen BC3 reached a peak strength at LP 25 ($\mu_S = 3.9$) in the positive displacement direction and at LP 26 ($\mu_S = 4.2$) in the negative displacement direction. The strength of specimen BC8 peaked much sooner: at LP 17 ($\mu_S = 1.45$) and LP 18 ($\mu_S = 1.75$). At LP 22 ($\mu_S = 2.7$) the capacity of BC8 was already only 70% of that of BC3. This difference in behavior was due to the premature slippage of the reinforcement in specimen BC8.

The fixed-end rotation contributed less than 35% to the total deflection through LP 24 for BC3. By LP 24 ($\mu_S = 2.7$) on specimen BC8, over 75% of the total deflection was due to fixed-end rotation at the face of the column, indicating slippage of the reinforcement had occurred. Pull-through of the bars did not develop in BC3 until LP 29 ($\mu_S = 5.4$) when over 50% of the total deflection was due to fixed-end rotation. Clearly this strikingly different behavior under cyclic loading indicates that the bond of the reinforcement within the joint deteriorates earlier and at lower ductilities in lightweight concrete.



VI. BEHAVIOR OF SPECIMEN BC7 AS PREDICTED BY PRESENT R/C THEORY

Basic R/C beam theory was used to calculate several strength and stiffness properties of specimen BC7. The calculated properties were then compared with the measured ones to check the applicability of the theory for lightweight R/C structures.

The measured and calculated properties are shown in Tables 6.1 and 6.2. The necessary calculations are given in Appendix A. The measured flexural stiffnesses were obtained from Figs. 6.1 and 6.2. The calculated yield moments and loads were determined from simple R/C beam theory while the moments and loads at the maximum displacement, LP 32, were based on theory of confined concrete [9]. The measured tension steel strain at LP 32 was taken as known and the resulting moment and load to produce that strain were then determined. The curvatures at the face of the column were calculated from the strain distribution in the concrete section. The flexural stiffnesses were based on the cracked and uncracked transformed sections. The overall initial stiffness of the subassembly was determined by the flexural stiffnesses EI of each beam. In Table 6.2, the moment-area method was used to calculate the flexural deflections at yield while curvatures were used to determine the deflections in the inelastic range.

The results obtained, the conventional theory was found to be very good for determining moment capacities, and flexural stiffnesses of sections. While the calculated curvatures were rather close numerically to the measured curvatures, it must be remembered that the measured values are average curvatures over a 9 in. (229mm.) region. As a result, the calculated curvatures are to be expected to be higher than the measured curvatures. The reason that they were not is probably due to diagonal tension cracks which developed at yielding in the region of the beams near the column.

In Table 6.2 the calculated flexural components to the total

horizontal displacement were slightly less than the measured at first yield of the reinforcement. At the maximum deflection at LP 32, the flexural components were calculated two ways: first assuming a linear distribution of curvature over the length of the inelastic region and, second, assuming that the maximum calculated curvature at the face of the column was the average over the theoretical inelastic region (see Appendix A). The second method gave much better results, probably since it compensates for additional curvature due to diagonal tension cracks.

Overall the present R/C beam theory was very good for predicting strength and the cracked and uncracked flexural stiffnesses, and fair for predicting elastic and inelastic flexural deformations. Present theory however does not account for fixed-end rotations which reduce the overall stiffness of the subassemblage substantially in the inelastic range.

VIII. CONCLUSIONS AND RECOMMENDATIONS

7.1 Conclusions

As a result of this study, the following conclusions can be made regarding the behavior of reinforced lightweight concrete beam-column subassemblages. These conclusions are of a preliminary nature and are only valid for the two specimens tested.

1. Basic reinforced concrete theory can predict the strength and the cracked and uncracked flexural stiffness under monotonic loading with good accuracy. Even though flexural deformations are predicted with only fair accuracy, the basic theory does not include fixed-end rotations at the joint which make significant contributions to the total displacement even under monotonic loading.
2. Under monotonic loading, a ductility (μ) in excess of 5 can be achieved without observing total slippage of the reinforcement through the joint region and without a significant decrease in lateral resistance. The behavior of lightweight and normal weight specimens was very similar with regard to strength and fixed-end rotations up to a ductility of 5. However, for the same ductility, structures of lightweight concrete will have total displacements and story drifts which are about 12% greater than that of normal weight structures.
3. Under incrementally increasing cyclic loading, the behavior of the subassemblage was drastically different from that observed under monotonic loading. This was due to premature total slippage of the reinforcement through the joint region causing a substantial drop in stiffness and lateral resistance at a ductility (μ_S) as low as 2.5. As a result

the performance of lightweight concrete specimens is not as favorable as that of normal weight concrete since total slippage of the reinforcement did not occur until a ductility (μ_s) of 4.2 was exceeded in the normal weight concrete specimen.

4. If the beams do not have the same amount of reinforcement along the top and bottom, then the reinforcement which is smaller in area will be subjected to higher levels of strain leading to earlier bond deterioration.

7.2. Recommendations

From the conclusions, the following recommendations are made regarding earthquake resistant design of reinforced concrete ductile moment-resisting frames made with lightweight aggregate similar to that used in this investigation:

1. Designs using present code provisions should account for substantial decreases in stiffness and lateral load carrying capacity at lower ductilities than that of normal weight concrete structures.
2. Designs should account for lower initial stiffness, greater story drift, and consequently higher $P - \delta$ moments than that of normal weight concrete.

To handle the problem of bond deterioration in the joint, the following solutions and recommendations for future research are presented:

1. Studies are needed to determine the mechanism of bond deterioration in lightweight concrete.
2. The problem of bond deterioration can be minimized by preventing yielding of the reinforcement at the beam-column interface by moving the regions of inelastic action away from the joint. This can be done through the use of haunched beams or by bending and crossing the beam reinforcing bars a short distance from the joint. Some research has already been

conducted in the latter area (10).

3. Anchorage of the reinforcement can be improved by mechanical devices or better detailing practices.
4. Subassemblages with floor slabs need to be experimentally tested.
5. Analysis programs need to be developed, based on a stiffness degradation model, which include fixed-end rotations at the joint.

REFERENCES

1. Bertero, V. V., and Popov, E. P., "Seismic Behavior of Ductile Moment-Resisting Reinforced Concrete Frames," Reinforced Concrete Structures in Seismic Zones, Publication SP-53, American Concrete Institute, Detroit, 1977.
2. Popov, E. P., Bertero, V. V., Galunic, B., and Lantoff, G., "On Sismic Design of R/C Interior Joints of Frames," Proceedings of the Sixth World Conference on Earthquake Engineering, New Delhi, India, January, 1977, pp. 5.191-5.196.
3. Viwathanatepa, S., "Hysteretic Behavior of Reinforced Concrete Beam-Column Subassemblages," Ph.D. Thesis, Department of Civil Engineering, University of California, Berkeley, Dec. 1978.
4. Soleimani, D., "Reinforced Concrete Ductile Frames under Earthquake Loadings with Stiffness Degradation," Ph.D. Thesis, Department of Civil Engineering, University of California, Berkeley, Dec. 1978.
5. ACI Standard Building Code Requirements for Reinforced Concrete (ACI 318-71), American Concrete Institute, Detroit, Michigan, 1971.
6. International Conference of Building Officials, "Uniform Building Code," 1976 Edition, Vol. I, Washington, D. C., 1973.
7. U. S. Department of Commerce, National Oceanic and Atmospheric Administration, "San Fernando, California, Earthquake of February 9, 1971," Vol. I, Washington, D. C., 1973.
8. Bertero, V. V., and Popov, E. P., "Hysteretic Behavior of Ductile Moment-Resisting Reinforced Concrete Frame Components," Report No. EERC 75-16, University of California, Berkeley, April, 1975.
9. Park, R. , and Paulay, T., Reinforced Concrete Structures, John Wiley & Sons, Inc., 1975.
10. Galunic, B., Bertero, V. V., and Popov, E. P., "An Approach for Improving Seismic-Resistant Behavior of Reinforced Concrete Interior Joints," Report No. UCB/EERC-77/30, Earthquake Engineering Research Center, University of California, Berkeley, 1977.
11. Bertero, V. V., Bresler, B., Selna, L. G., Chopra, A. K., and Koretsky, A. V., "Design Implications of Damage Observed in the Olive View Medical Center Buildings," Proceedings of the Fifth World Conference on Earthquake Engineering, Rome, 1973.
12. Brelser, B., Bertero, V. V., "Olive View Medical Center Materials Study--Phase 1," Report No. EERC 73-19, Earthquake Engineering Research Center, University of California, Berkeley, December, 1973.

T A B L E S

TABLE 2.1

LIGHTWEIGHT CONCRETE MIX
(FOR 1 CU. YD. OF CONCRETE)

MATERIAL	BRAND	WEIGHT OR VOLUME
CEMENT	1 & 2	528.3 lb
SAND	OLYMPIA 1.5	1473.1 lb
AGGREGATE	PORT COSTA 5/8" EXP. SHALE FORMULA 43 V-7	806.3 lb
WATER	-	295.7 lb
TOTAL		3103.4 lb
WATER REDUCING AGENT	POZZOLITH 300N	434.8 ml
AIR ENTRAINING AGENT	MBAE - 10	32.6 ml

WATER/CEMENT = 0.56 (BY WEIGHT)

TABLE 2.2

CONCRETE MECHANICAL CHARACTERISTICS

SPECIMEN	AGE (DAYS)	COMPRESSIVE STRENGTH F'_c (psi)	MODULUS OF ELASTICITY E_c (psi)	MODULUS OF RUPTURE f_t (psi)	DRY UNIT WEIGHT (pcf)	AIR (%)
BC7	39	f615	2.69×10^6	248	117	4.5-5.0
BC8	28	4150	2.44×10^6	286	117	4.5-6.0

TABLE 3.1 DATA PLOTTED BY RECORDERS

RECORDER NO.	TYPE	X-AXIS	Y-AXIS	Y^1 -AXIS
1	$XY Y^1$	δ	H	$H_{EQ} (=V_W - V_E)$
2	$XY Y^1$	H	V_W	V_E
3	XY	RW11	V_W	-
4	XY	RE11	V_E	-
5	$XY Y^1$	V_W	(FW11-FW1)	(PW11-PW1)
6	$XY Y^1$	V_E	(FE11-FE1)	(PE11-PE1)

TABLE 4.1 ENERGY DISSIPATION PER CYCLE

SPECIMEN	CYCLE	TOP BOTTOM μ_S / μ_S	TOP BOTTOM H_{EO} / H_{EO} kips/kips (kN/kN)	TOP AREA kip-In (kN-m)	BOTTOM AREA kip-In (kN-m)	TOTAL AREA kip-In (kN-m)
BC7	32-49	4.3 [*] / 4.1 [*]	47.3/48.0 (210/214)	121.7 (13.75)	178.9 (20.21)	300.6 (33.96)
BC8	17-18	1.45/1.75	37.0/40.3 (165/179)	18.1 (2.05)	34.9 (3.94)	53.0 (5.99)
	19-20	1.45/1.75	35.0/35.1 (156/156)	20.1 (2.27)	18.2 (2.06)	38.3 (4.33)
	21-22	2.55/2.7	32.2/29.5 (143/131)	40.0 (4.52)	39.4 (4.45)	79.4 (8.97)
	23-24	2.55/2.7	19.8/19.8 (88/88)	19.1 (2.16)	15.0 (1.69)	34.1 (3.85)
	25-26	4.0/4.2	23.4/24.3 (104/108)	30.7 (3.47)	34.6 (3.91)	65.3 (7.38)
	27-28	4.0/4.2	17.3/19.4 (77/86)	24.6 (2.78)	25.0 (2.82)	49.6 (5.60)

* DETERMINED BY CONVERSION ($\mu_S = 0.78\mu$)

TABLE 6.1 MEASURED AND CALCULATED MECHANICAL CHARACTERISTICS OF MEMBERS

PROPERTY	MEASURED	CALCULATED
M_Y^+ kip-in (kN-m)	928 (104.8)	821 (92.6)
M_Y^- kip-in (kN-m)	1552 (175.3)	1439 (162.5)
H_{EQY} kips (kN)	39.0 (173)	35.6 (158)
M_{32}^+ kip-in (kN-m)	1131 (127.8)	1063 (120.1)
M_{32}^- kip-in (kN-m)	1877 (212.1)	1791 (202.3)
$H_{EQ 32}$ kips (kN)	47.3 (210)	44.9 (200)
ϕ_Y^+ Radians	$2.18 \times 10^{-4} *$	2.09×10^{-4}
ϕ_Y^- Radians	$2.17 \times 10^{-4} *$	2.43×10^{-4}
ϕ_{32}^+ Radians	$3.08 \times 10^{-3} *$	2.95×10^{-3}
ϕ_{32}^- Radians	2.54×10^{-3}	2.47×10^{-3}
E_c ksi (MPa)	2.69×10^3 (18.6×10^3)	2.84×10^3 19.6×10^3
E_c^{I+} kip-in ² (kN-m ²) uncr	9.63×10^6 (27.6×10^3)	1.09×10^7 (31.4×10^3)
E_c^{I-} kip-in ² (kN-m ²) uncr	1.08×10^7 (31.0×10^3)	1.09×10^7 (31.4×10^3)
E_c^{I+} kip-in ² (kN-m ²) cr	3.36×10^6 (9.64×10^3)	3.73×10^6 (10.7×10^3)
E_c^{I-} kip-in ² (kN-m ²) cr	4.85×10^6 (13.9×10^3)	5.51×10^6 (15.8×10^3)
$K_{initial} (= \frac{H_{EQ}}{S})$ kip/in (kN/mm)	87 (15.2)	95 (16.6)

* AVERAGE CURVATURE IN 9 in. (229 mm) REGION
ADJACENT TO COLUMN

NOTE: (+) - POSITIVE MOMENT DIRECTION
(-) - NEGATIVE MOMENT DIRECTION
ALL MOMENTS ARE AT FACE OF COLUMN

TABLE 6.2 BEAM DEFLECTIONS

	COMPONENT DUE TO FLEXURE		TOTAL DEFLECTION IN (mm)
	MEASURED IN (mm)	CALCULATED IN (mm)	
S_{Y}^{+}	0.41 (10.4)	0.38 (9.7)	0.67 (17.0)
S_{Y}^{-}	0.48 (12.2)	0.33 (8.4)	0.86 (21.9)
S_{32}^{+}	2.55 (64.8)	1.42 (36.1) 2.28 (57.9) *	3.70 (94.0)
S_{32}^{-}	2.26 (57.4)	1.19 (30.3) 2.06 (52.3)	3.70 (94.0)

* ASSUMING ϕ AT COLUMN FACE IS AVERAGE OVER THEORETICAL LENGTH OF INELASTIC REGION

NOTE: (+) - POSITIVE MOMENT DIRECTION

(-) - NEGATIVE MOMENT DIRECTION

F I G U R E S

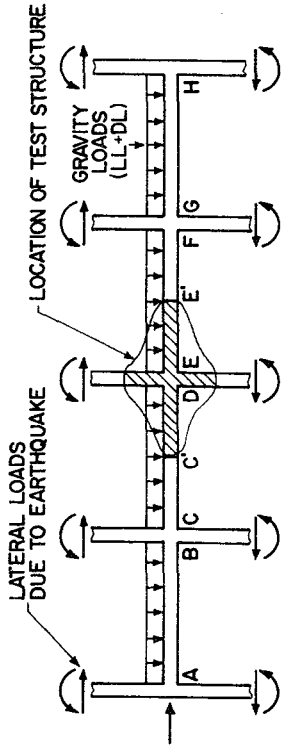


FIG. 2.2 (a) GRAVITY AND LATERAL LOADS AT THIRD FLOOR OF BUILDING

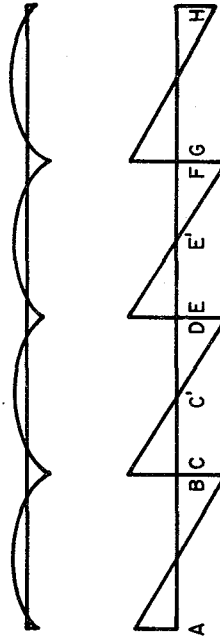


FIG. 2.2 (b) MOMENTS DUE TO GRAVITY LOADS (ABOVE) AND MOMENTS DUE TO LATERAL LOADS (BELOW)

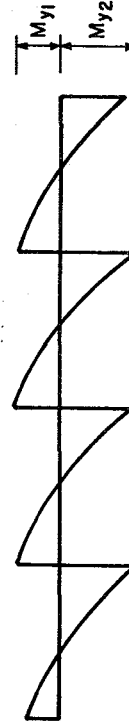


FIG. 2.2 (c) MOMENTS FROM GRAVITY AND LATERAL LOAD EFFECTS

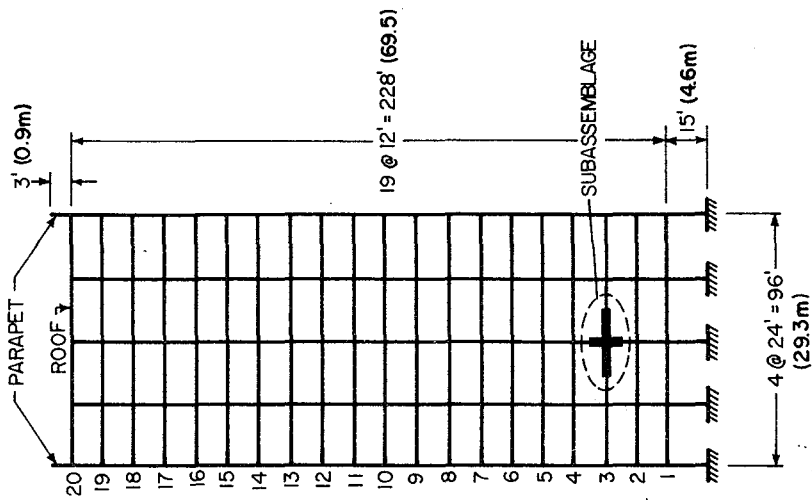


FIG. 2.1 TWENTY-STORY BUILDING PROTOTYPE

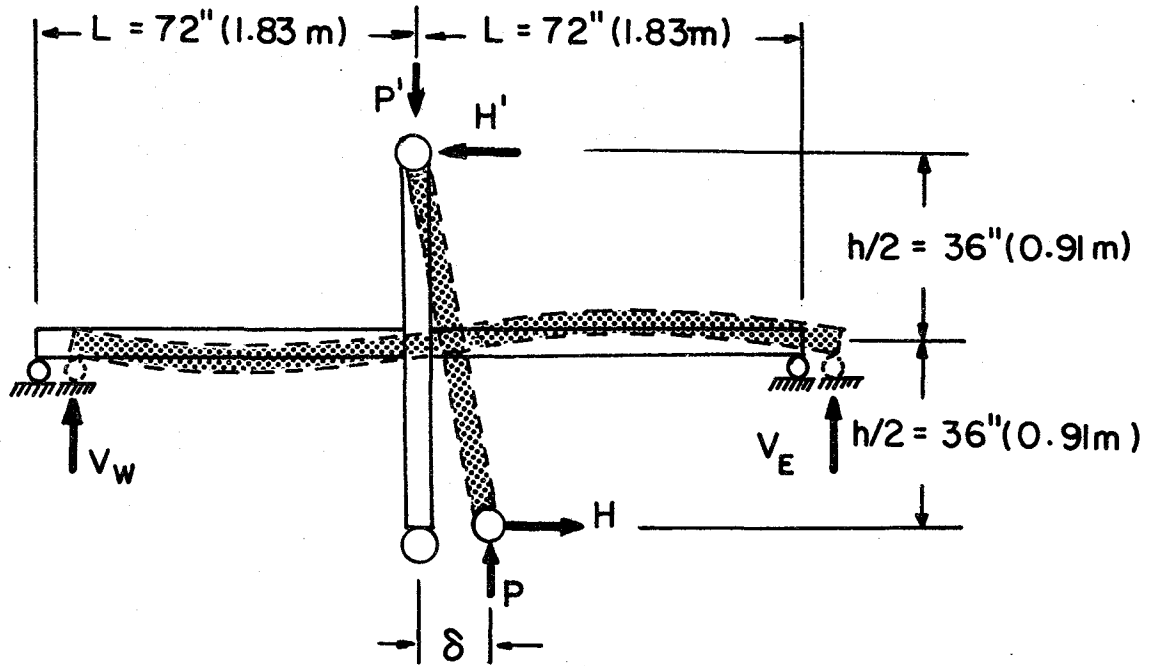


FIG. 2.3 DEFINITION OF FORCES AND DISPLACEMENTS FOR A SUBASSEMBLAGE

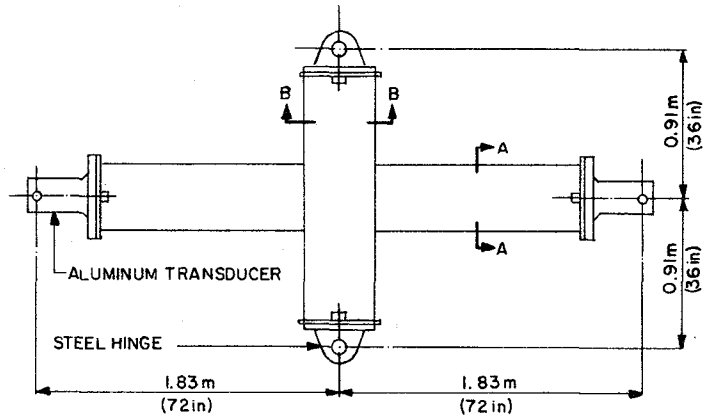


FIG. 2.4 TEST SPECIMEN

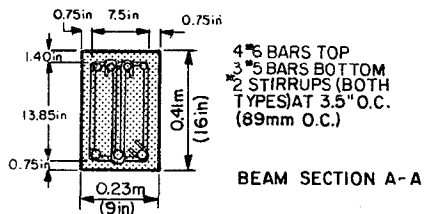


FIG. 2.5 BEAM SECTION A-A

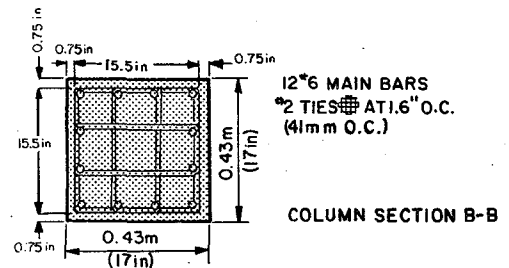


FIG. 2.6 COLUMN SECTION B-B

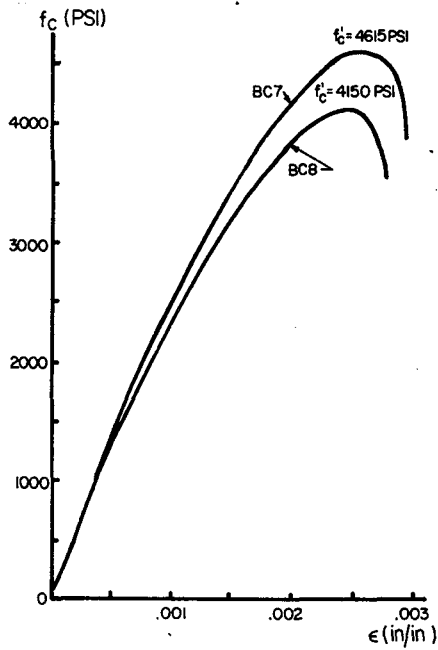


FIG. 2.7 CONCRETE STRESS - STRAIN DIAGRAMS

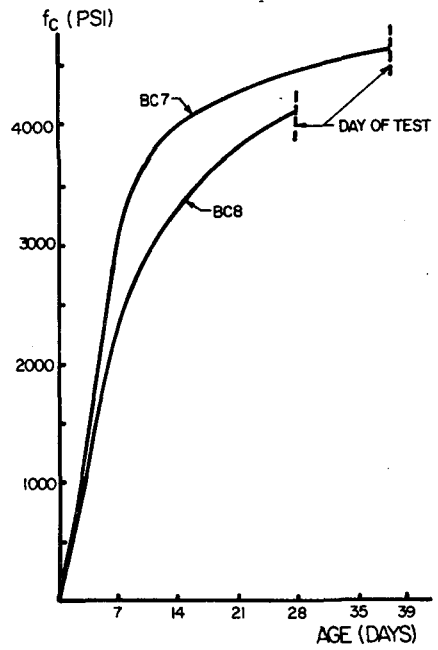


FIG. 2.8 CONCRETE STRENGTH GAIN DIAGRAMS

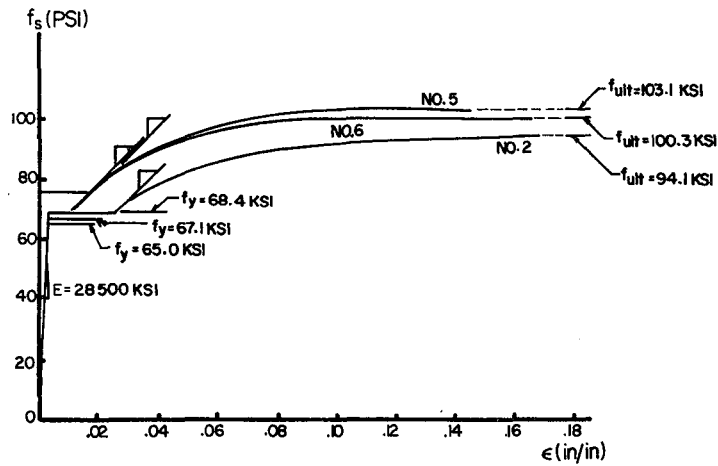


FIG. 2.9 REINFORCEMENT STRESS-STRAIN DIAGRAM

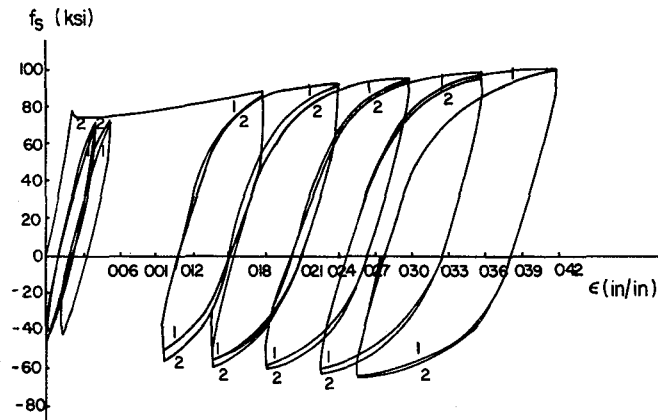


FIG. 2.10 CYCLIC STRESS-STRAIN DIAGRAM FOR MACHINED SPECIMEN FROM #5 BAR

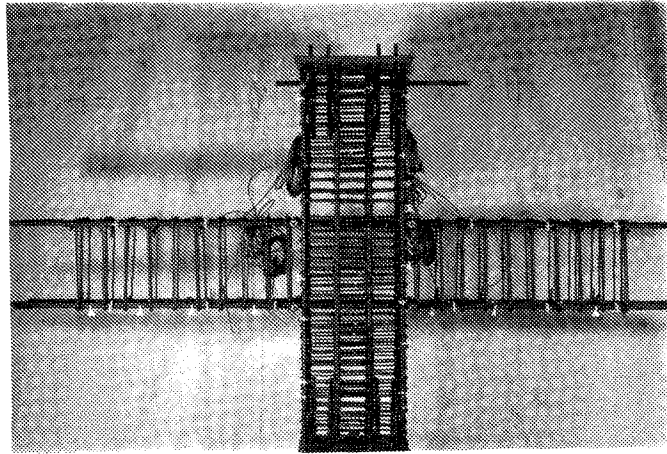


FIG. 2.11 REINFORCEMENT

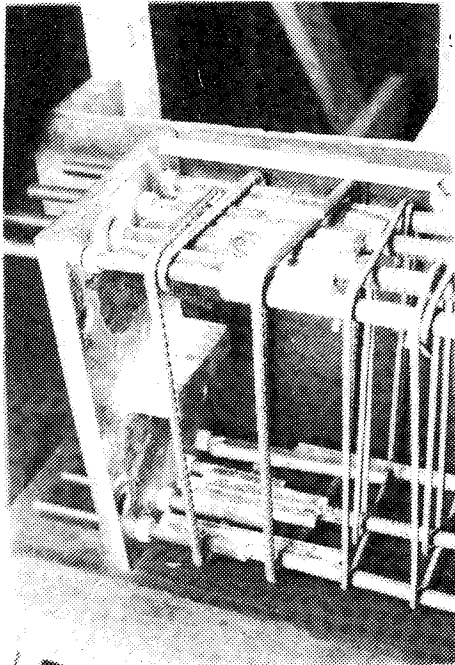


FIG. 2.12 BEAM AND DETAIL

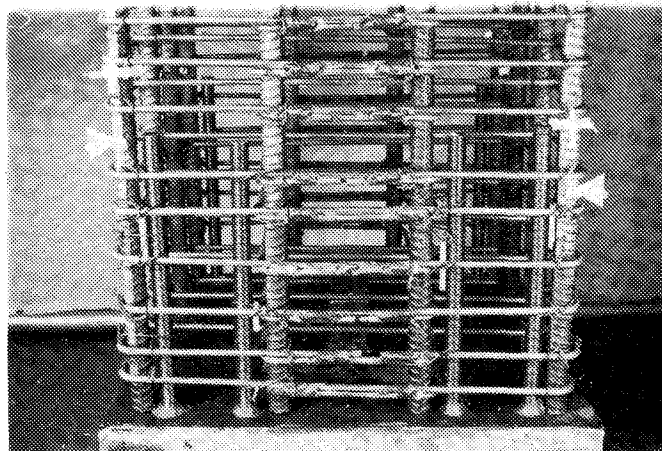


FIG. 2.13 COLUMN AND DETAIL

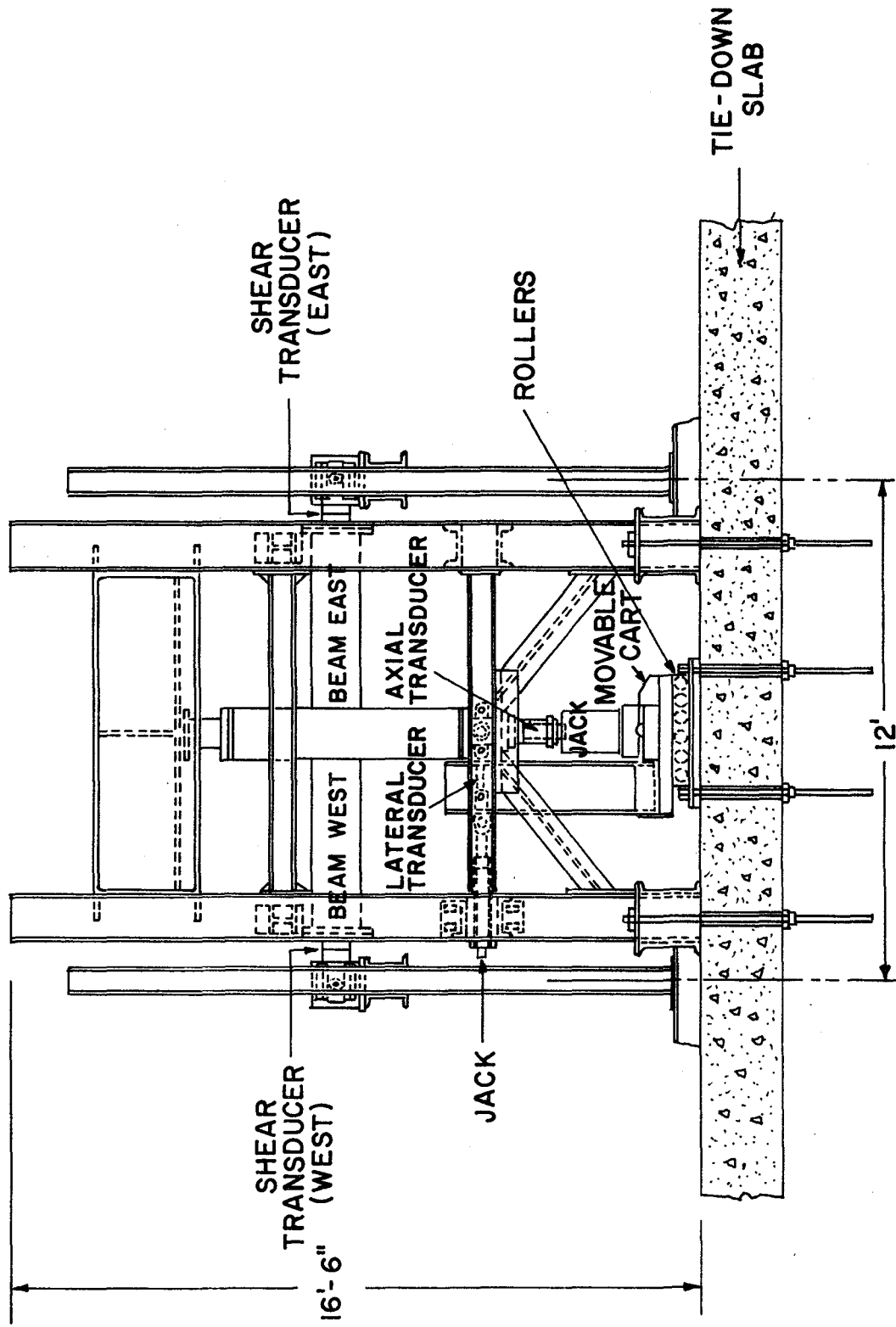


FIG. 3.1 BEAM-COLUMN TEST SET UP

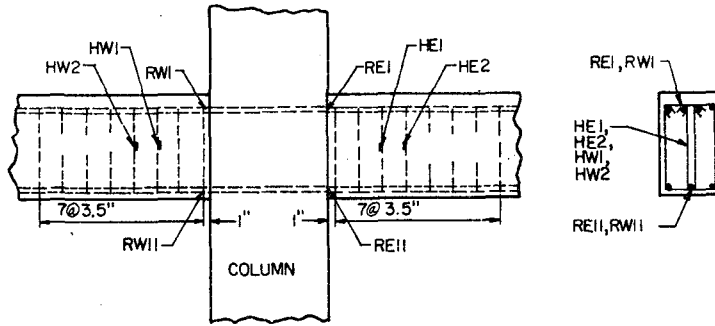


FIG. 3.2 LOCATIONS OF STRAIN GAGES

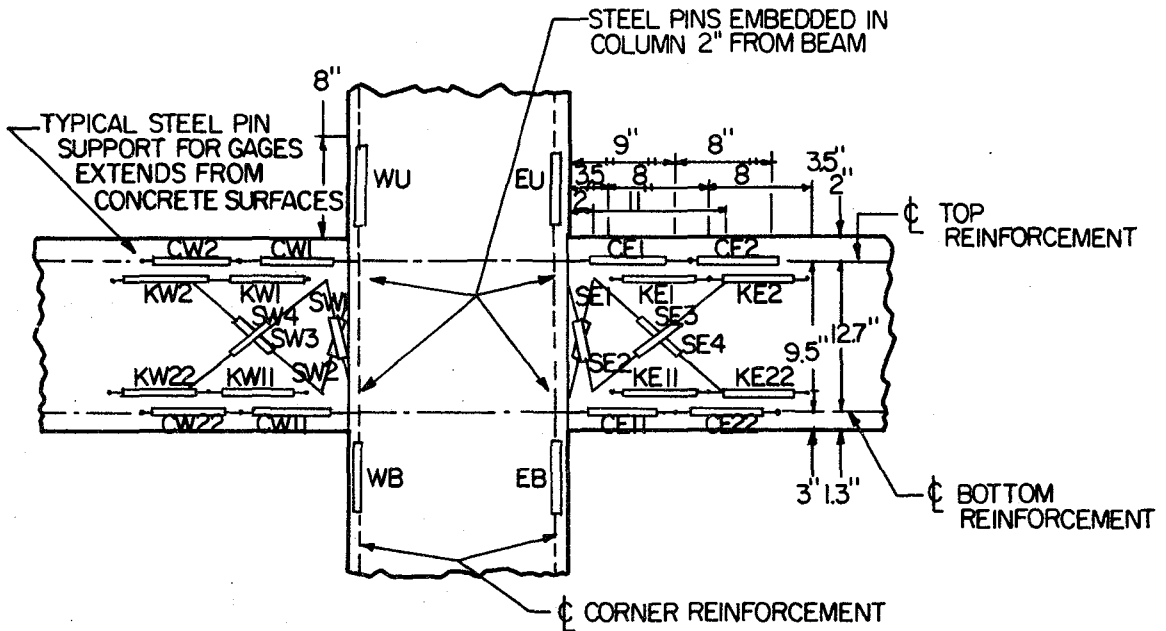


FIG. 3.3(a) INSTRUMENTATION ON SOUTH FACE OF BC7

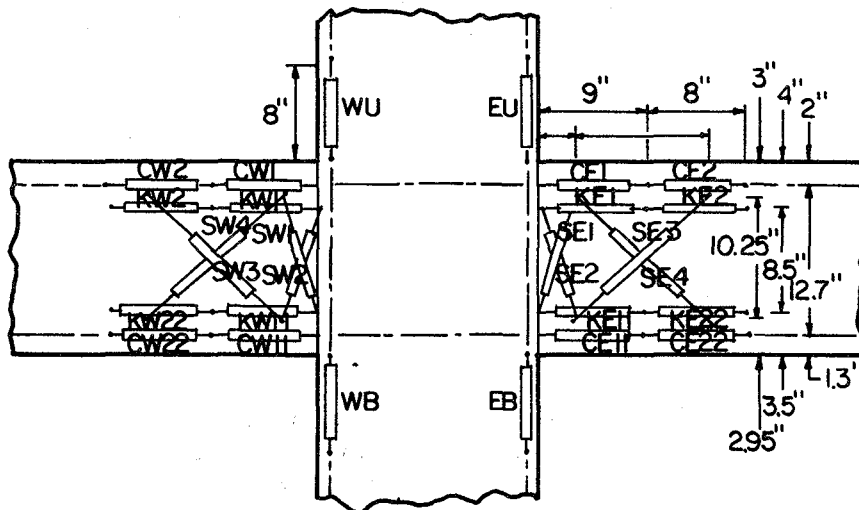


FIG. 3.3(b) INSTRUMENTATION ON SOUTH FACE OF BC8

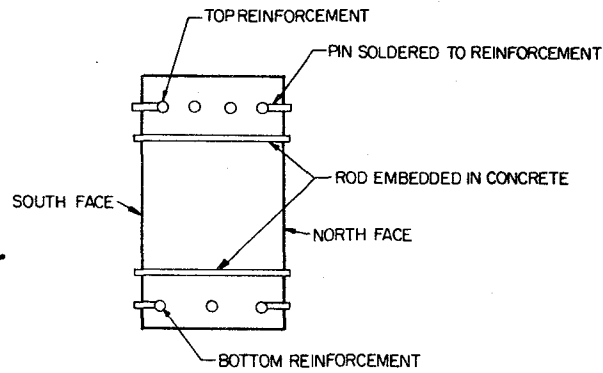
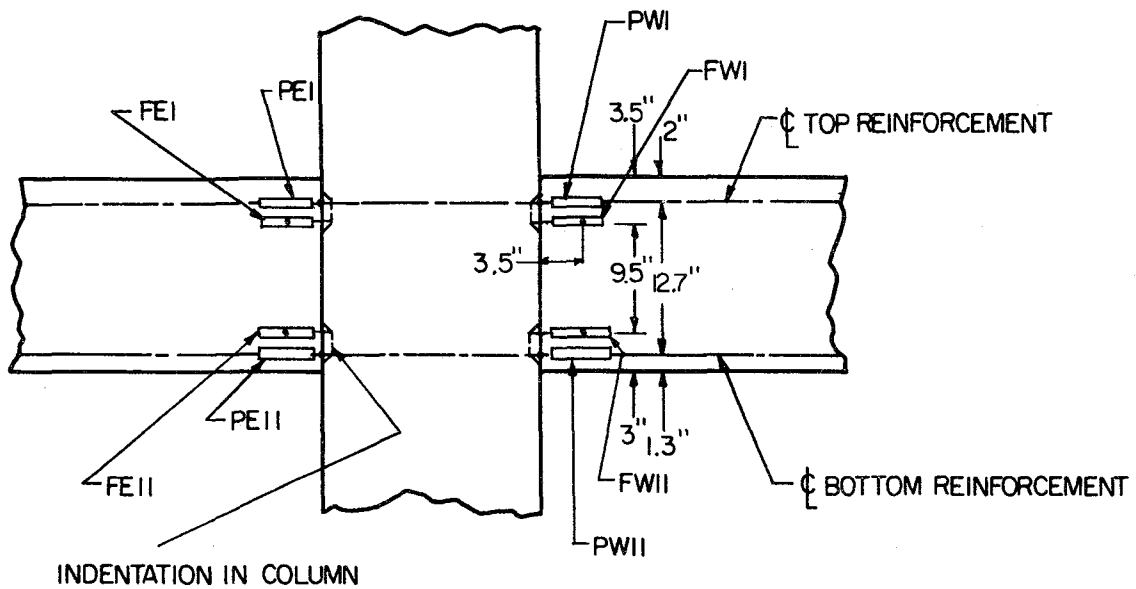


FIG. 3.4 SUPPORTS FOR EXTERNAL INSTRUMENTATION



INDENTATION IN COLUMN

FIG. 3.5 (a) INSTRUMENTATION ON NORTH FACE OF BC7

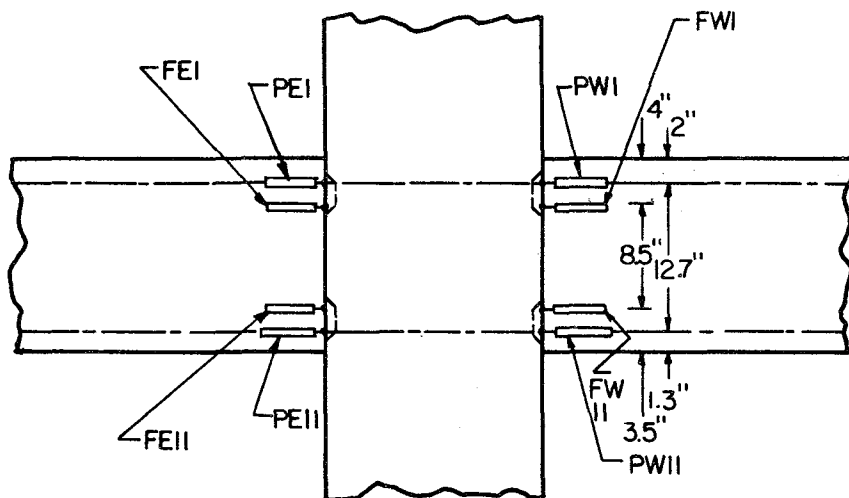


FIG. 3.5 (b) INSTRUMENTATION ON NORTH FACE OF BC8

HORIZONTAL DISPLACEMENT δ (IN)

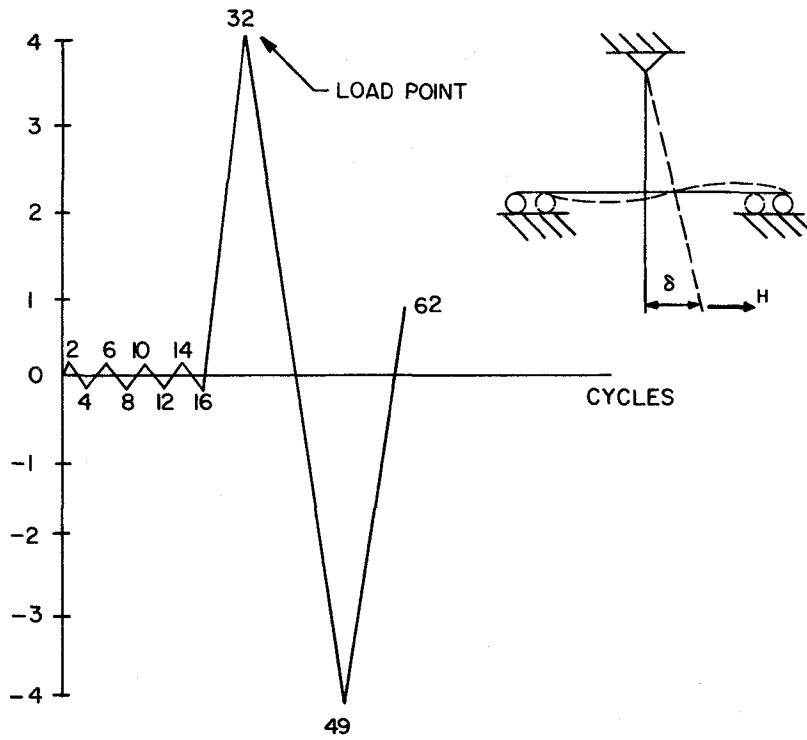


FIG. 3.6 LOAD HISTORY OF BC7

HORIZONTAL DISPLACEMENT δ (IN)

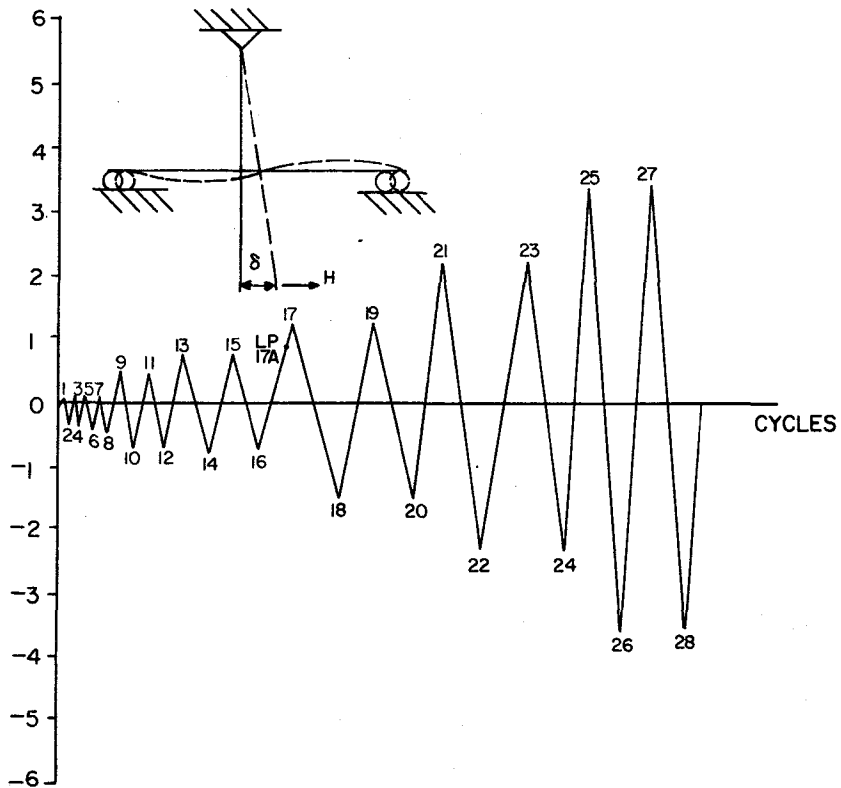


FIG. 3.7 LOAD HISTORY OF BC8

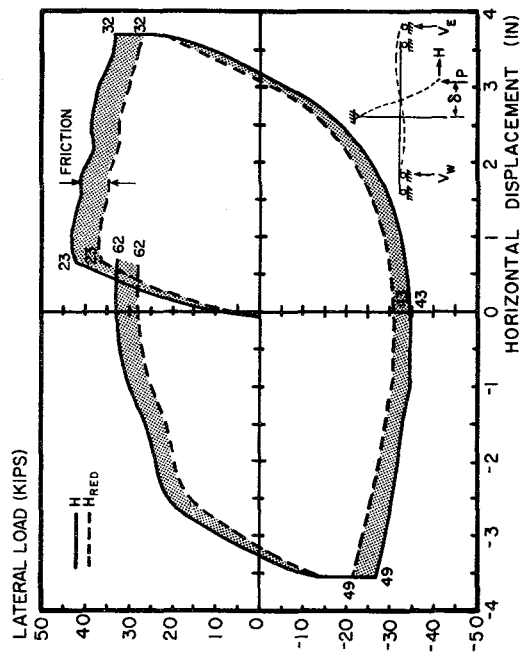


FIG. 4.1 HYSTERETIC LOOPS FOR BC7 -- H VS. σ

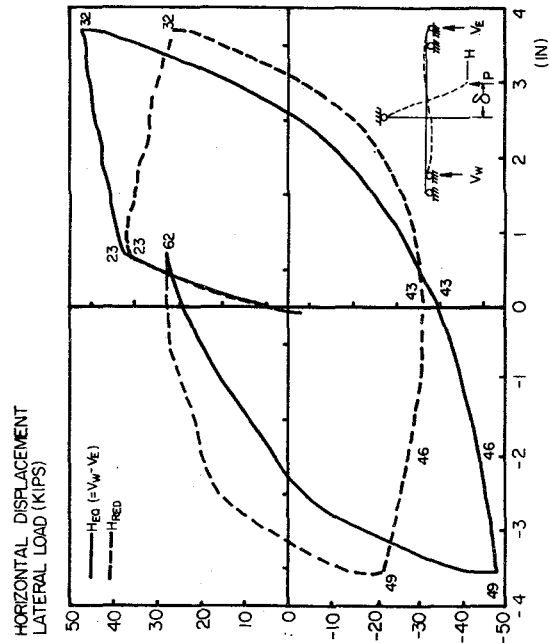


FIG. 4.2 (b) HYSTERETIC LOOPS FOR BC7 -- H_{RED} AND H_{ER} vs. σ

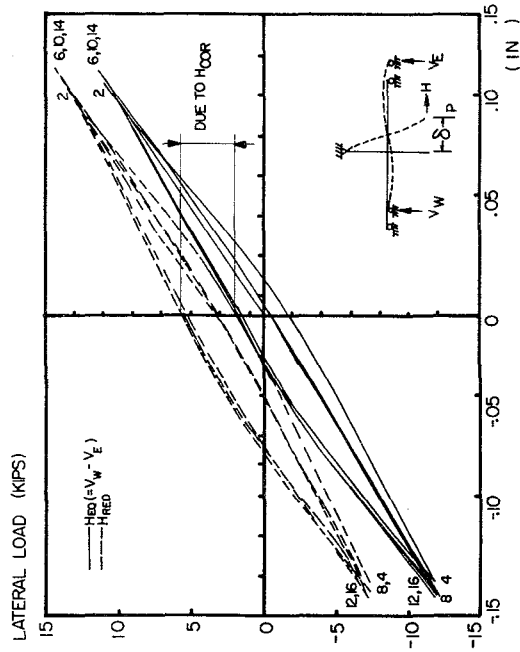


FIG. 4.2 (a) HYSTERETIC CYCLES OF BC7 AT SERVICE LOAD

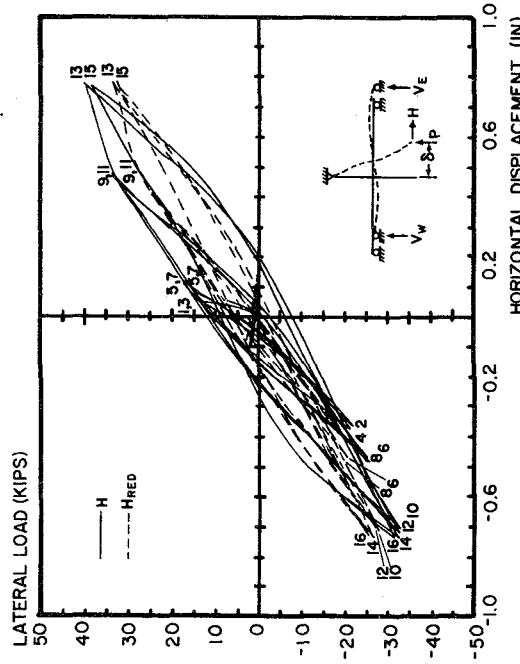


FIG. 4.3 (a) PRE-YIELD HYSTERETIC LOOPS OF BC8 -- H AND H_{RED} vs. σ

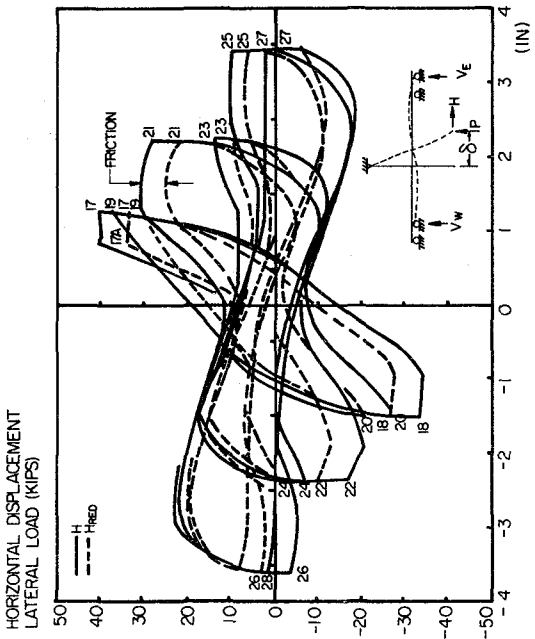


FIG. 4.3 (b) POST-YIELD HYSTERETIC LOOPS OF BC8

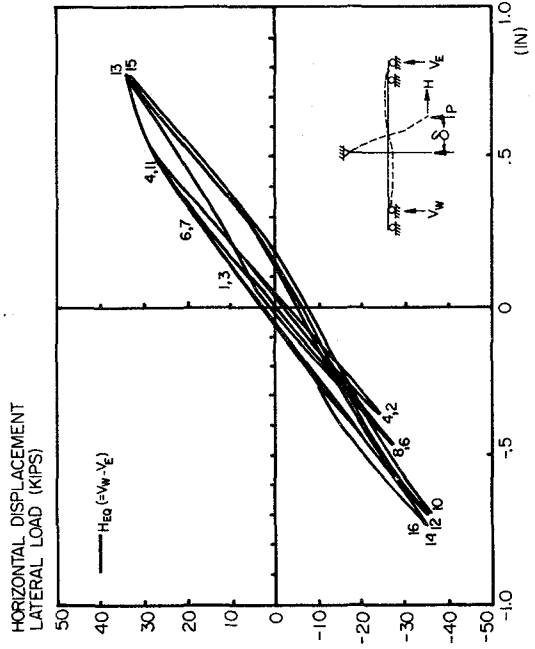


FIG. 4.4 (a) PRE-YIELD HYSTERETIC LOOPS OF BC8 -- H_{EQ} vs. σ

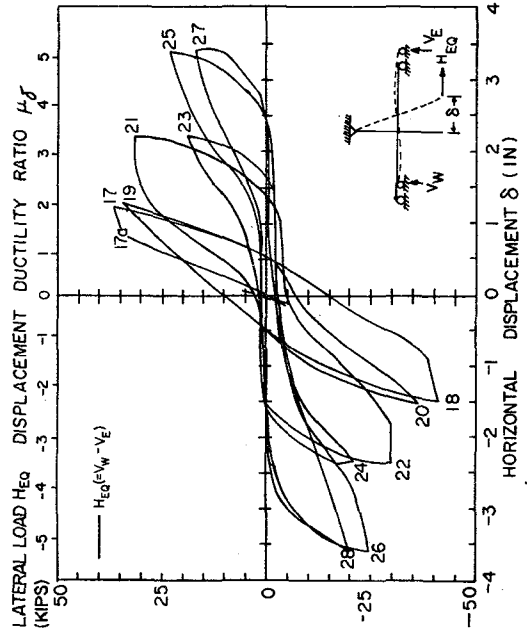


FIG 4.4 (b) POST-YIELD HYSTERETIC LOOPS OF BC8-- H_{EQ} vs. σ

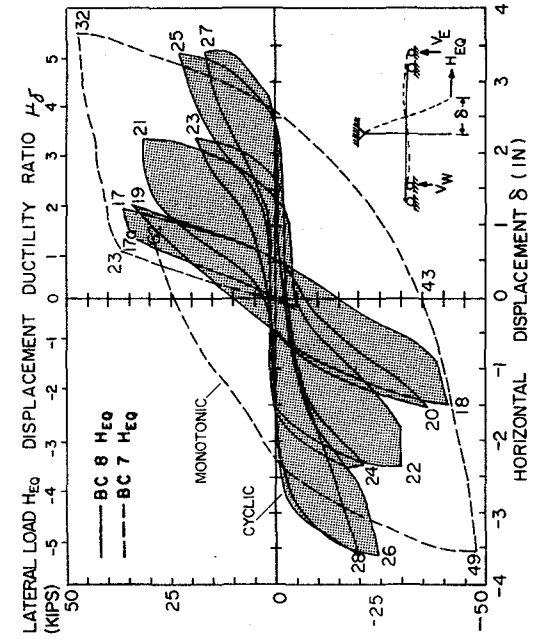


FIG. 4.4 (c) COMPARISON OF HYSTERETIC LOOPS OF BC7 AND BC8

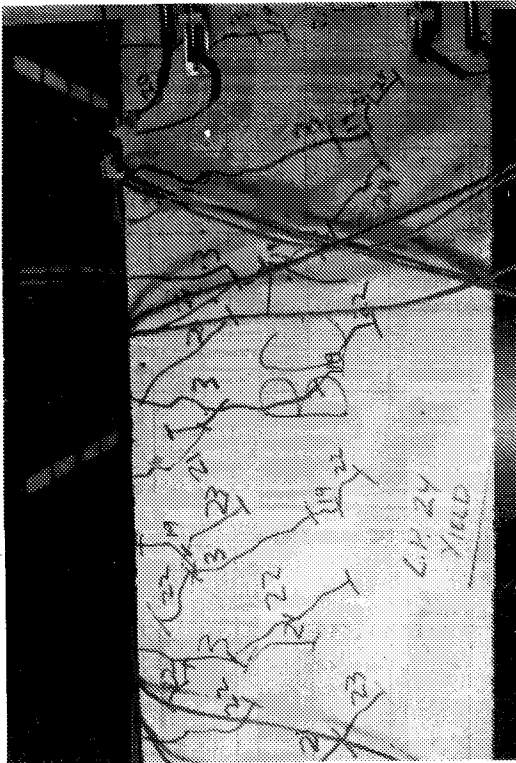


FIG. 4.5 EAST BEAM, BC7, AT LP23

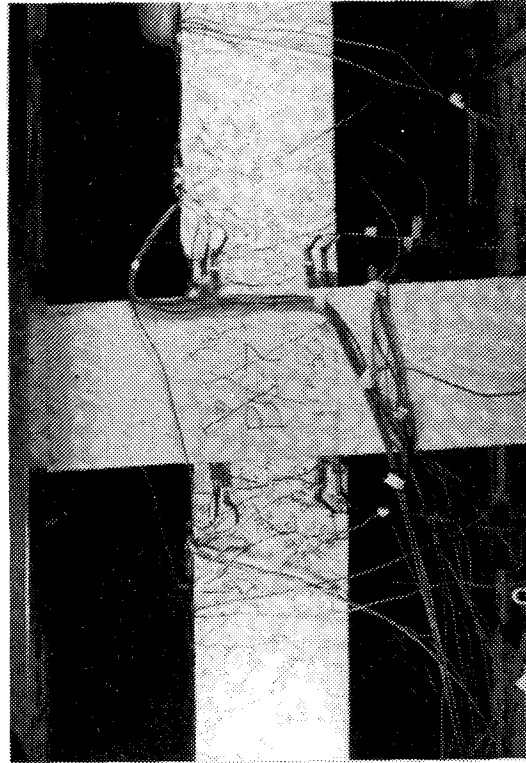


FIG. 4.6 NORTH FACE OF BC7 AT LP 49. (NOTE DIAGONAL CRACKS ON COLUMN)

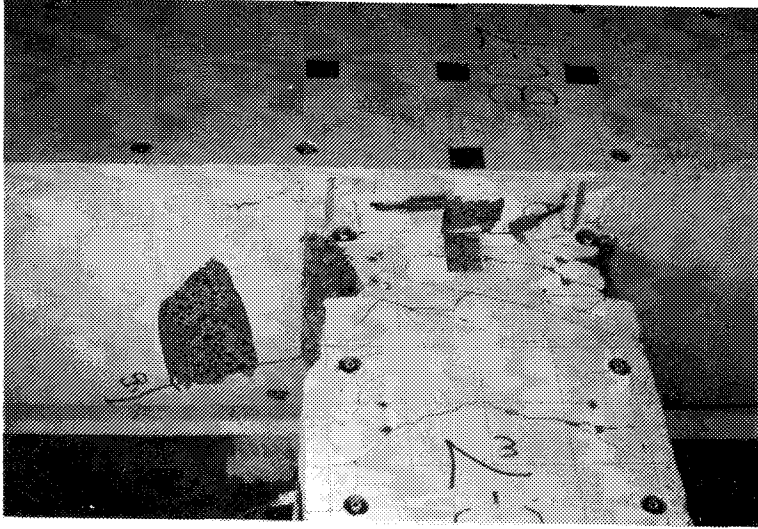


FIG. 4.7 COLUMN SPALL AND SPALL ON TOP OF WEST BEAM OF BC7

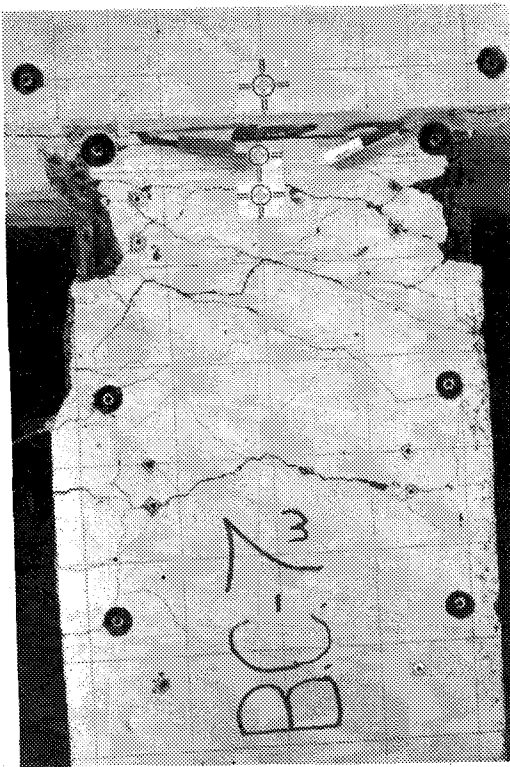


FIG. 4.8 WEST BEAM OF BC7 AFTER TEST. (NOTE SPALLS ON BOTH THE TOP AND BOTTOM OF BEAM AT COLUMN AND REGION OF EXTENSIVE FLEXURAL-SHEAR CRACKING.)

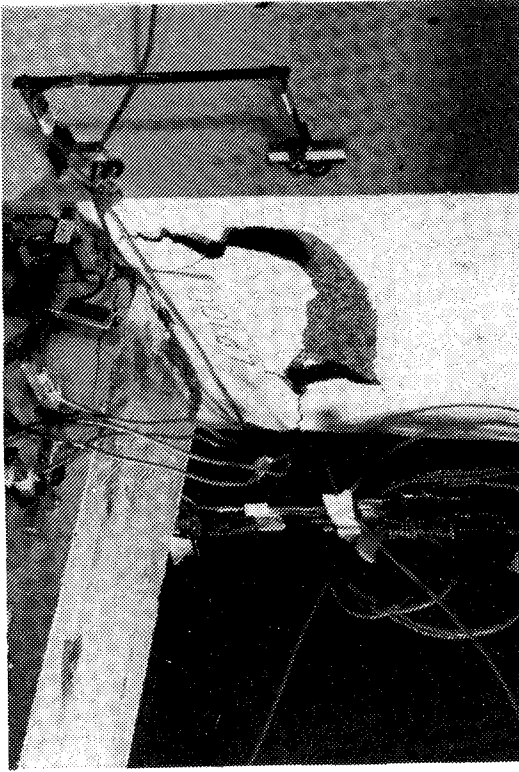


FIG. 4.9 SPALLING ON WEST COLUMN OF BC8 BETWEEN LP 21 AND LP 22

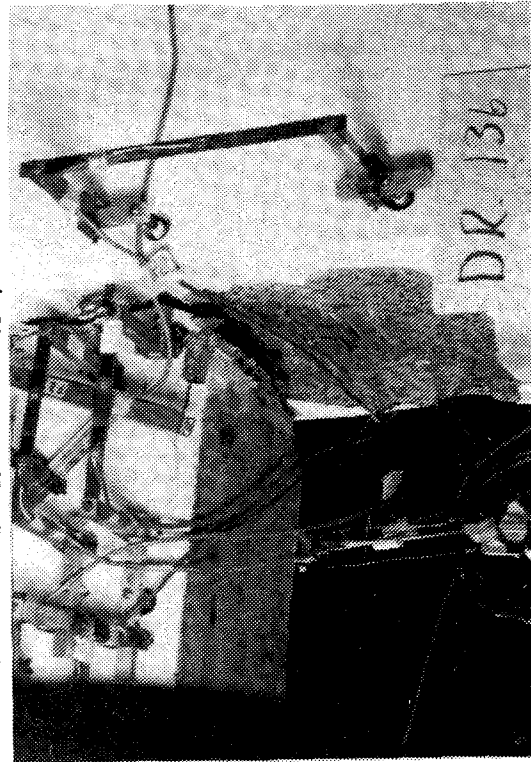


FIG. 4.10 SPALL ON WEST COLUMN OF BC8 AT LP25. (NOTE EXPOSED REINFORCEMENT ON COLUMN AND WIDE INTERFACE CRACK BETWEEN BEAM AND COLUMN.)

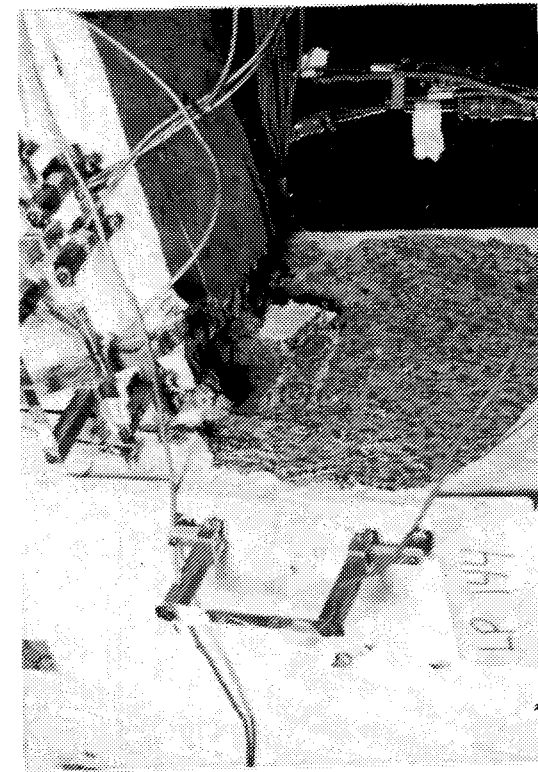


FIG. 4.11 SPALL ON EAST COLUMN OF BC8 AT LP 26, EXPOSING REINFORCEMENT

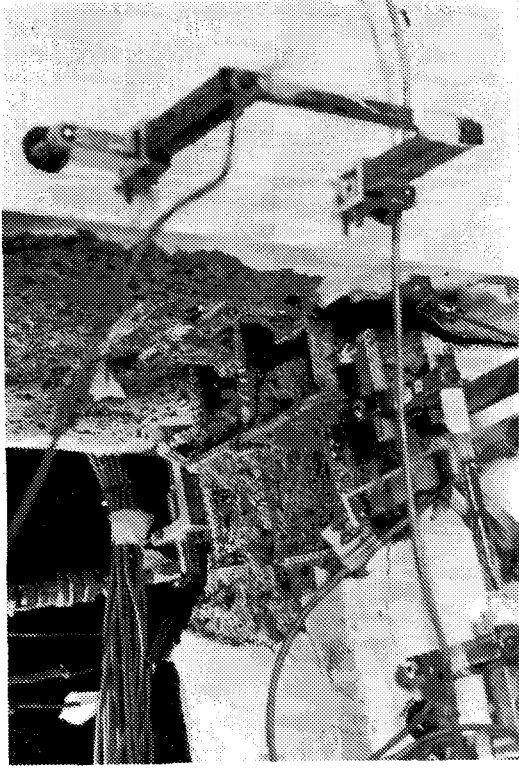


FIG. 4.12 SPALLED AREA EXTENDING ALONG EAST BEAM OF BC8 BY LP 28. (NOTE LARGE INTERFACE CRACK.)

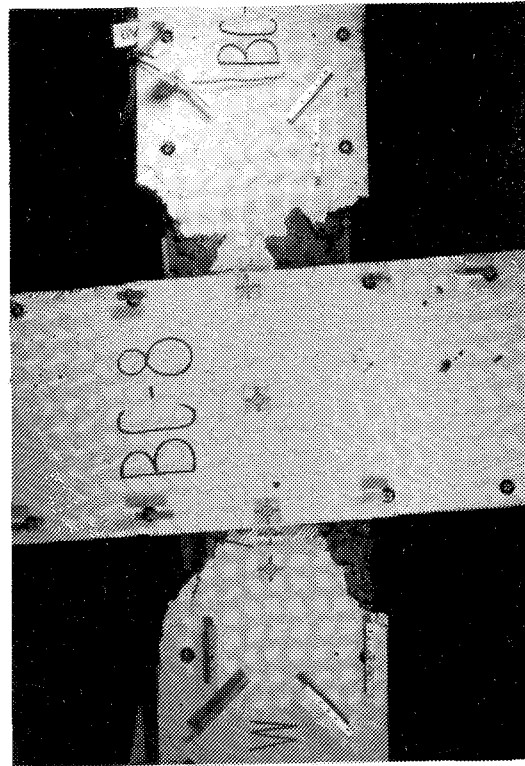


FIG. 4.13 BC8 AT END OF RST



FIG. 4.14 DEEP SPALL ON TOP OF EAST BEAM, BC8

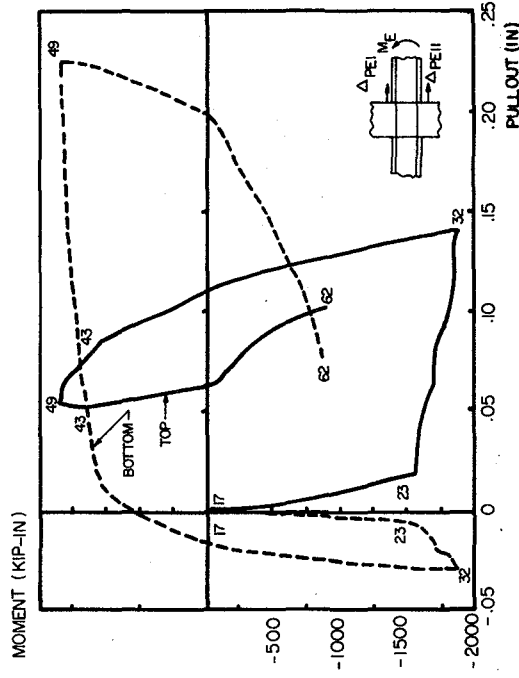


FIG. 4.15 (b) REINFORCEMENT PULLOUT FROM COLUMN, BC7 EAST

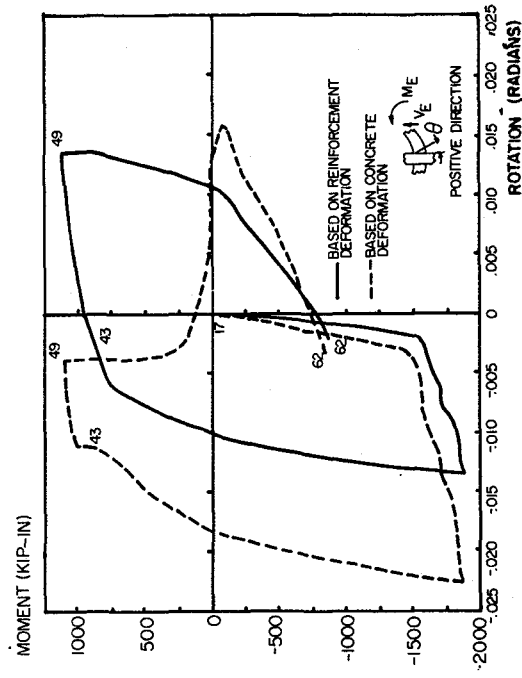


FIG. 4.16 (b) FIXED-END ROTATION OF BC7 EAST AT COLUMN FACE

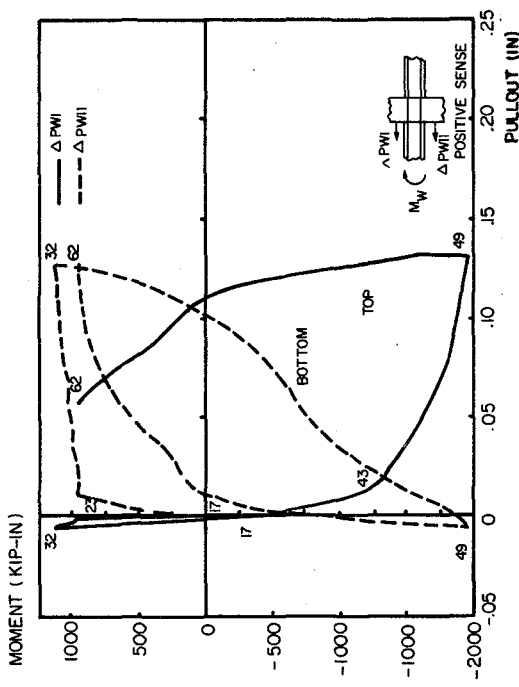


FIG. 4.15 (a) REINFORCEMENT PULLOUT FROM COLUMN, BC7 WEST

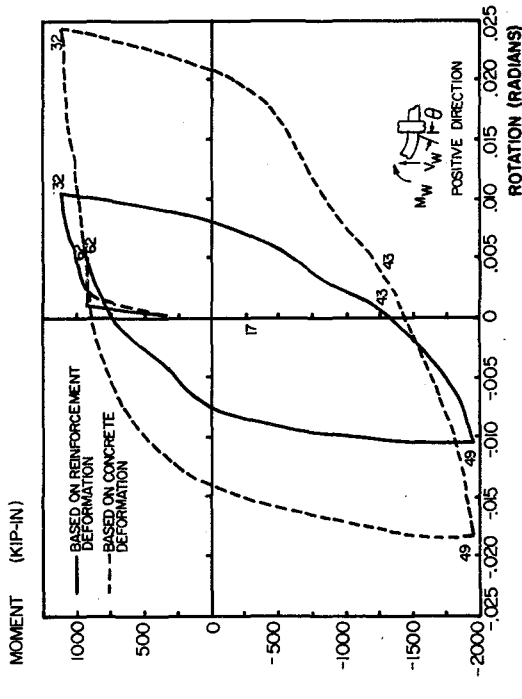


FIG. 4.16 (a) FIXED-END ROTATION OF BC7 WEST AT COLUMN FACE

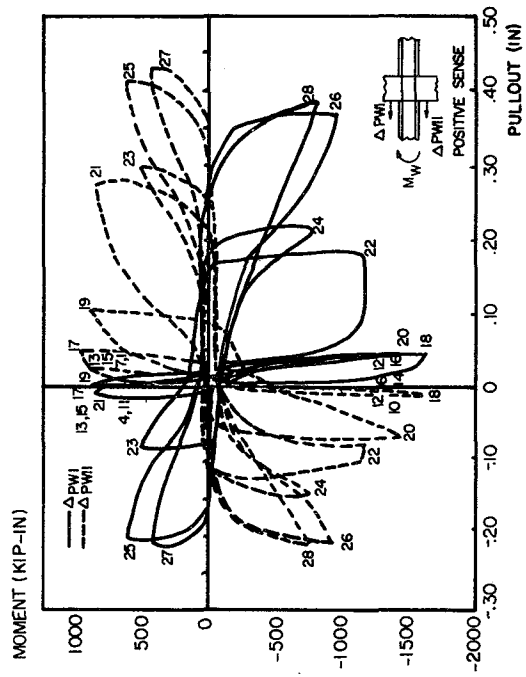


FIG. 4.17(a) POST-YIELD REINFORCEMENT PULLOUT FROM COLUMN, BC8 WEST

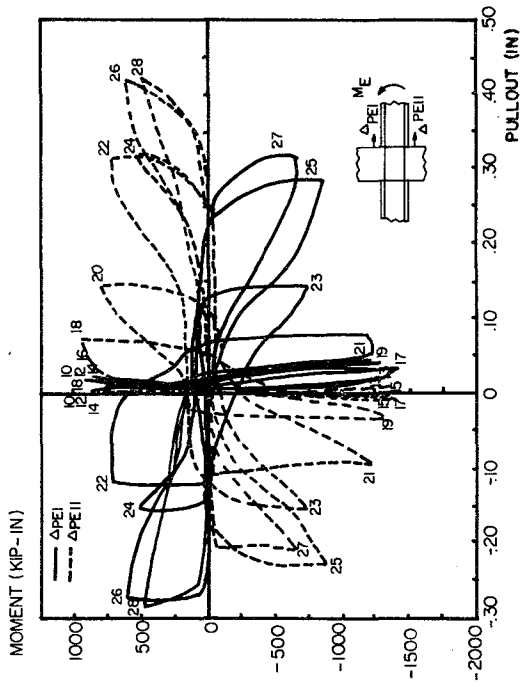


FIG. 4.17(b) POST-YIELD REINFORCEMENT PULLOUT FROM COLUMN, BC8 EAST

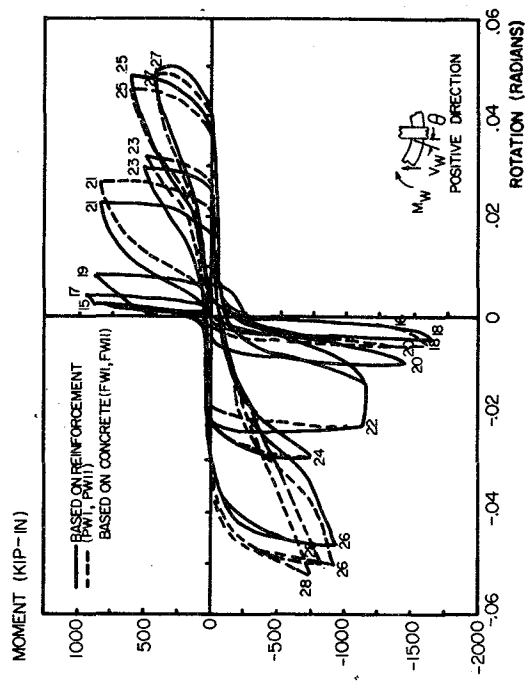


FIG. 4.18(a) POST-YIELD FIXED-END ROTATION OF BC8 WEST AT COLUMN FACE

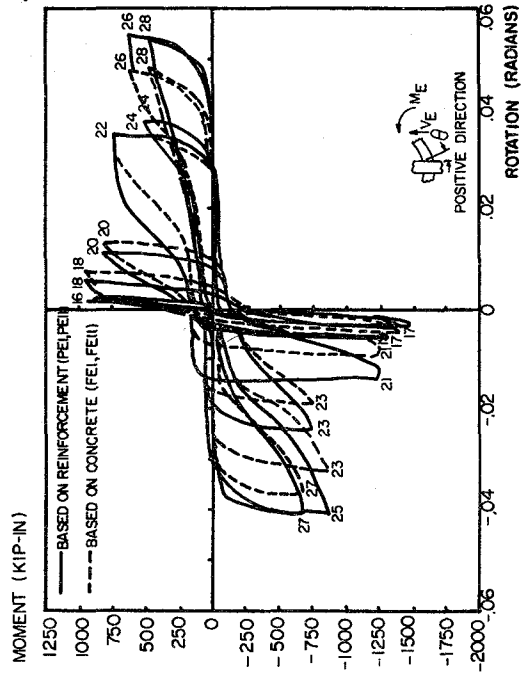


FIG. 4.18(b) POST-YIELD FIXED-END ROTATION OF BC8 EAST AT COLUMN FACE

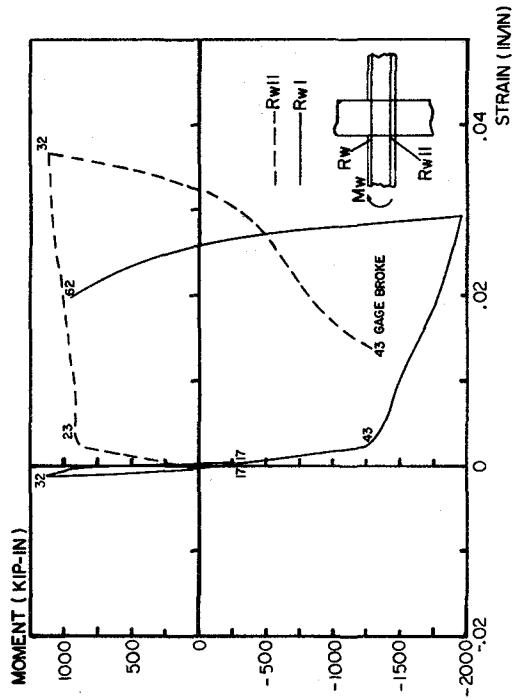


FIG. 4.19 (a) REINFORCEMENT STRAIN VS. MOMENT AT COLUMN FACE, BC7 WEST

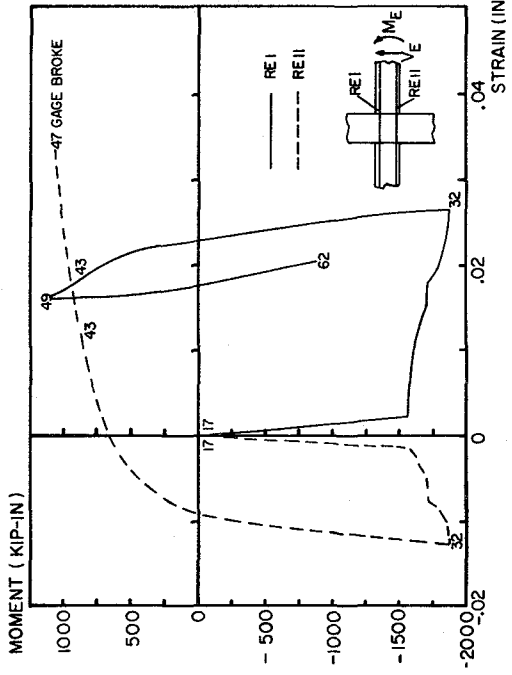


FIG. 4.19 (b) REINFORCEMENT STRAIN VS. MOMENT AT COLUMN FACE, BC7 EAST

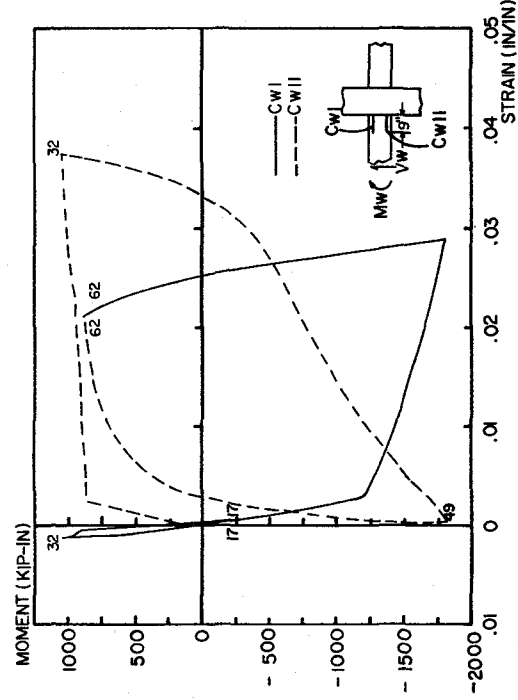


FIG. 4.20 (a) REINFORCEMENT STRAIN VS. MOMENT IN REGION I -- BC7 WEST

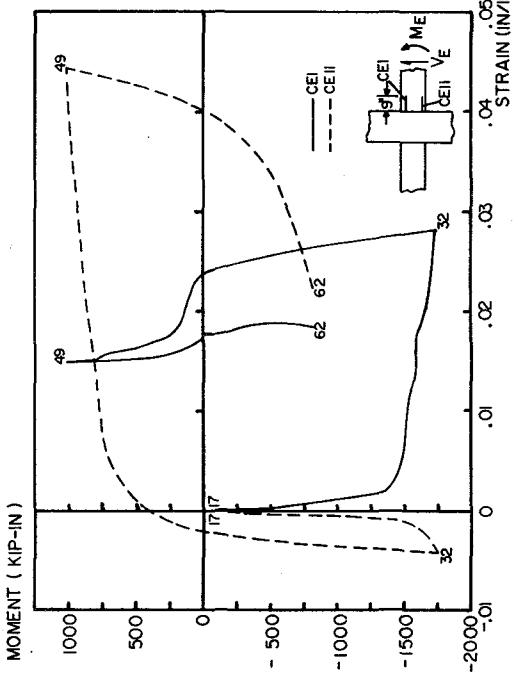


FIG. 4.20 (b) REINFORCEMENT STRAIN VS. MOMENT IN REGION I -- BC7 EAST

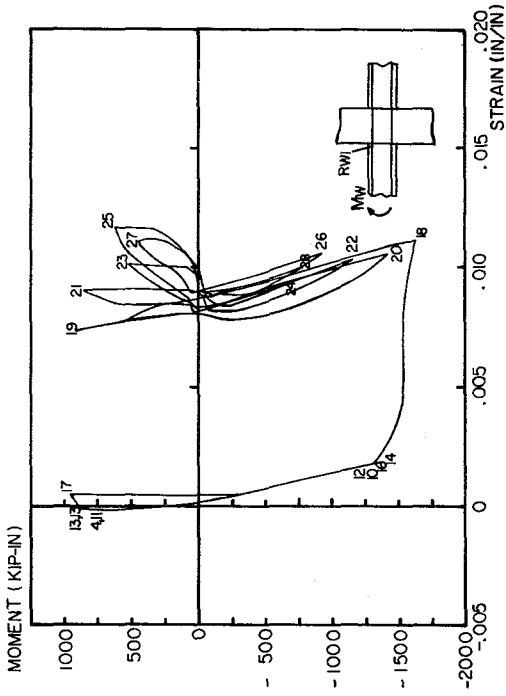


FIG. 4.21 (a) STRAIN IN TOP REINFORCEMENT AT COLUMN FACE, BC8 WEST

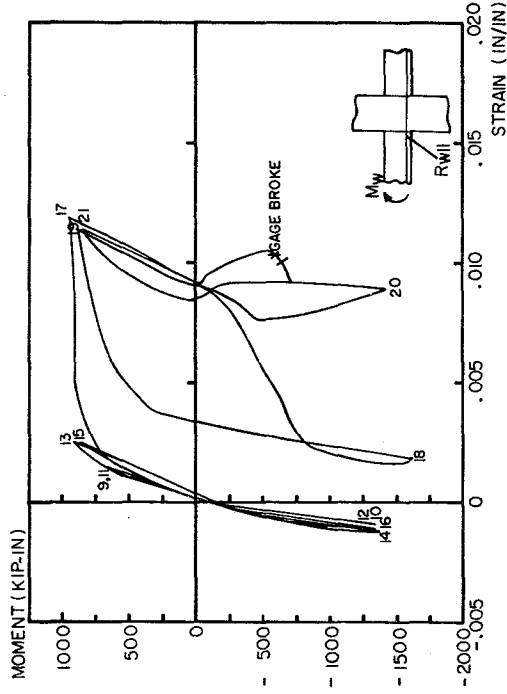


FIG. 4.21 (b) STRAIN IN BOTTOM REINFORCEMENT AT COLUMN FACE, BC8 WEST

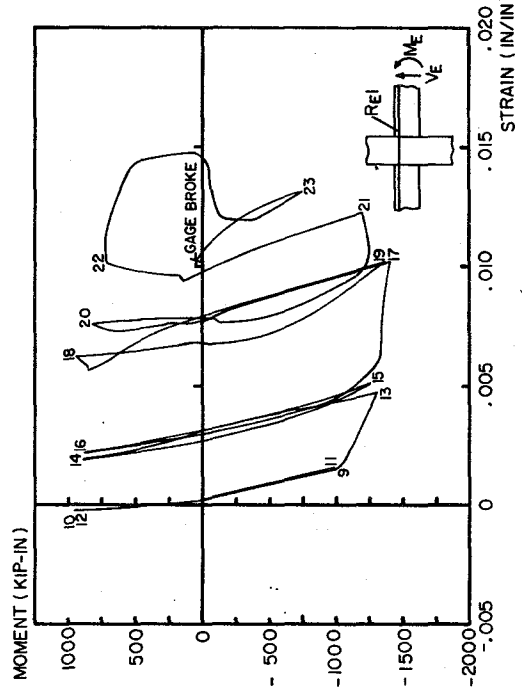


FIG. 4.21 (c) STRAIN IN TOP REINFORCEMENT AT COLUMN FACE, BC8 EAST

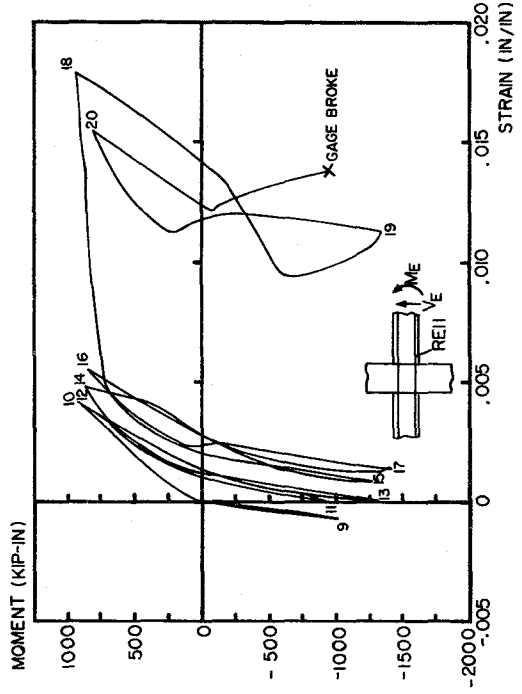


FIG. 4.21 (d) STRAIN IN BOTTOM REINFORCEMENT AT COLUMN FACE, BC8 EAST

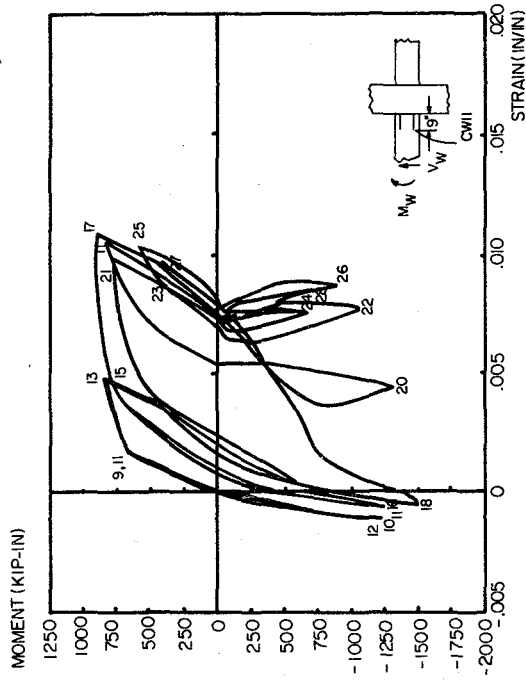


FIG. 4.22 (b) STRAIN IN BOTTOM REINFORCEMENT IN REGION 1 -- BC8 WEST

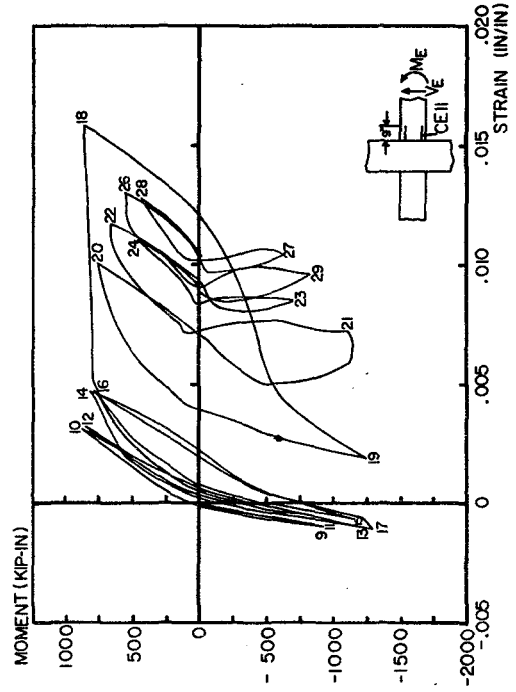


FIG. 4.22 (d) STRAIN IN BOTTOM REINFORCEMENT IN REGION 1 -- BC8 EAST

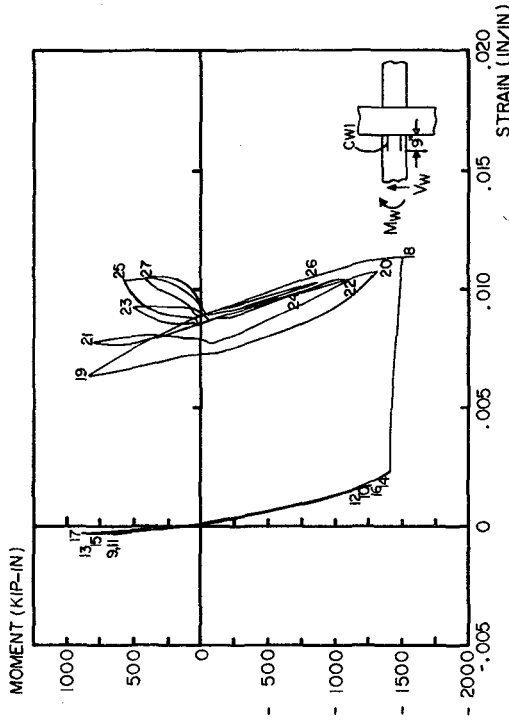


FIG. 4.22 (a) STRAIN IN TOP REINFORCEMENT IN REGION 1 -- BC8 WEST

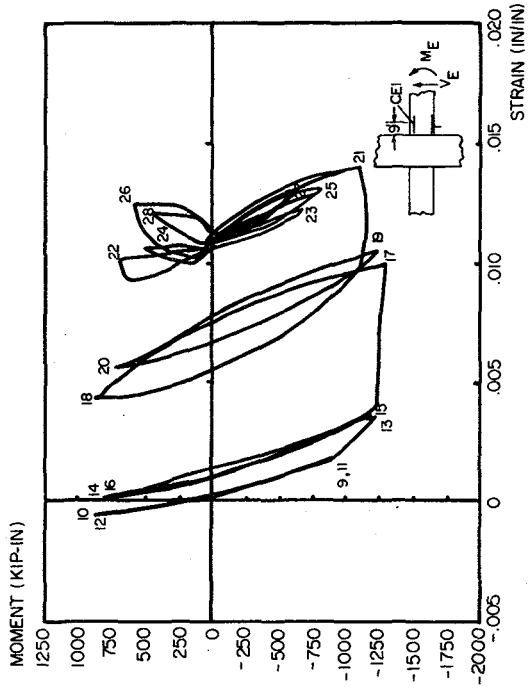


FIG. 4.22 (c) STRAIN IN TOP REINFORCEMENT IN REGION 1 -- BC8 EAST

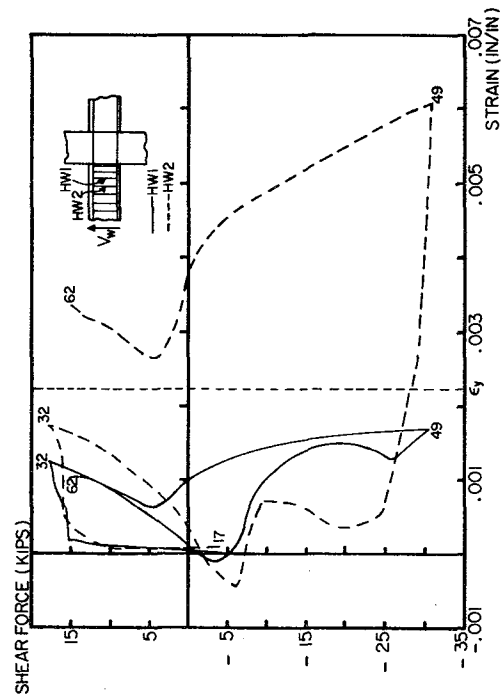


FIG. 4.23 (a) STRAIN VARIATION IN SHEAR REINFORCEMENT, BC7 WEST

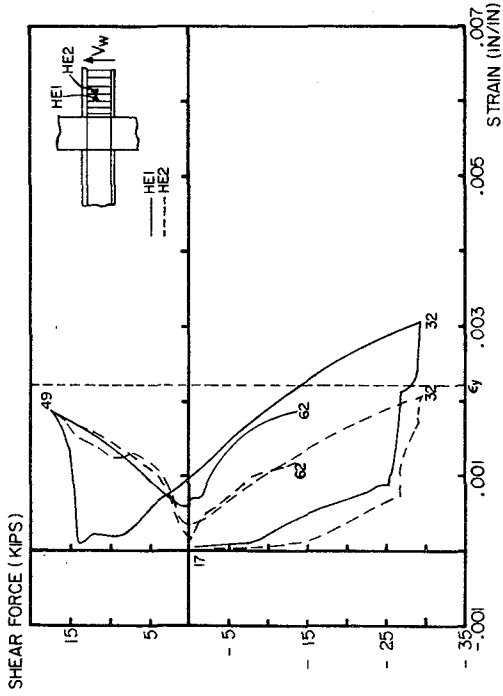


FIG. 4.23 (b) STRAIN IN VARIATION IN SHEAR REINFORCEMENT, BC7 EAST

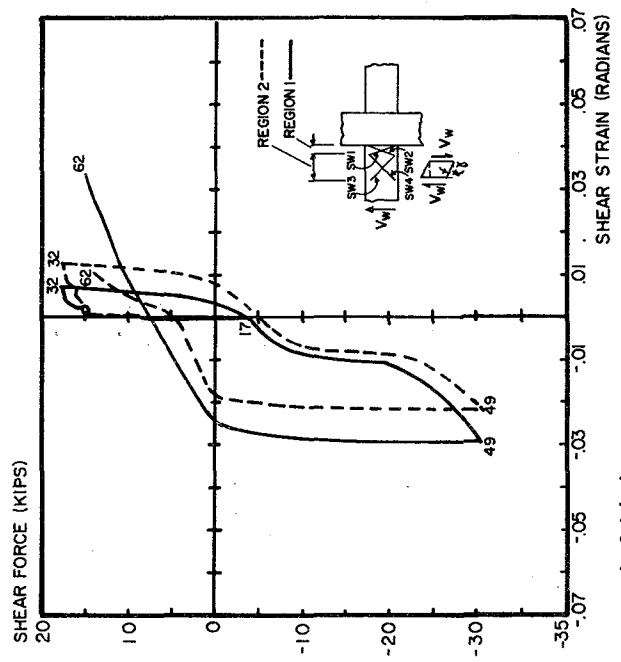


FIG. 4.24 (a) SHEAR STRAIN IN BEAM, REGION 2 -- BC7 WEST

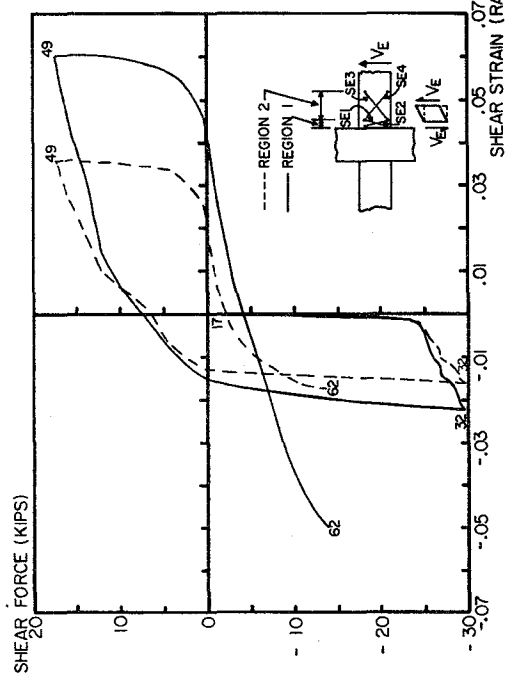


FIG. 4.24 (b) SHEAR STRAIN IN BEAM, REGION 2 -- BC7 EAST

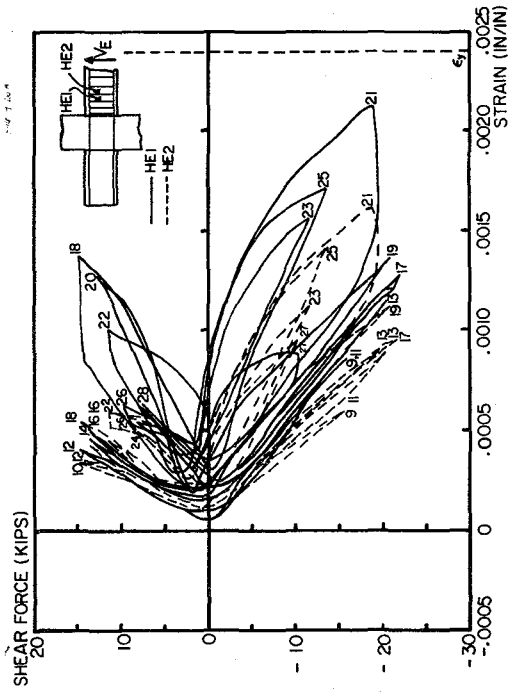


FIG. 4.25 (b) STRAIN VARIATION IN SHEAR REINFORCEMENT, BC8 EAST

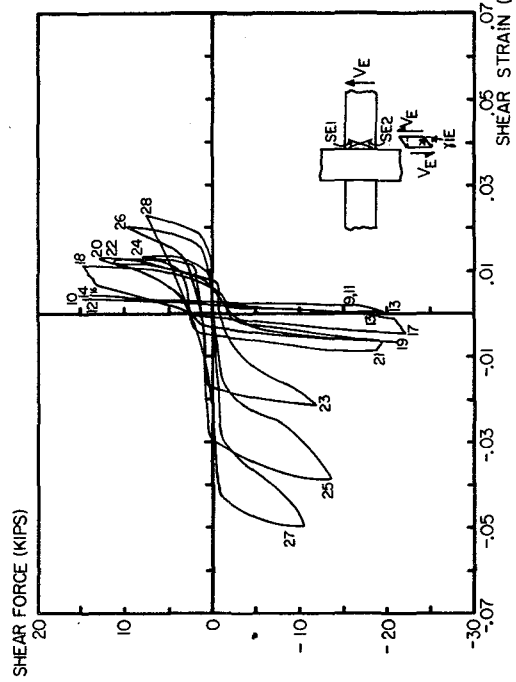


FIG. 4.126 (b) SHEAR STRAIN IN BEAM, REGION 1 --- BC8 EAST

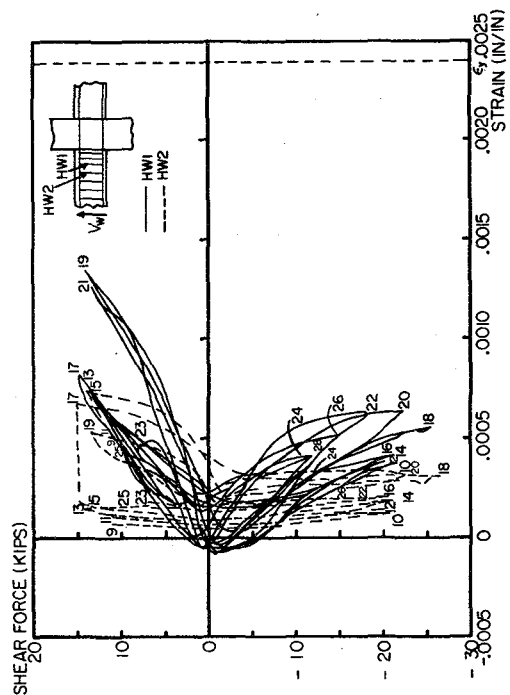


FIG. 4.25 (a) STRAIN VARIATION IN SHEAR REINFORCEMENT, BC8 WEST

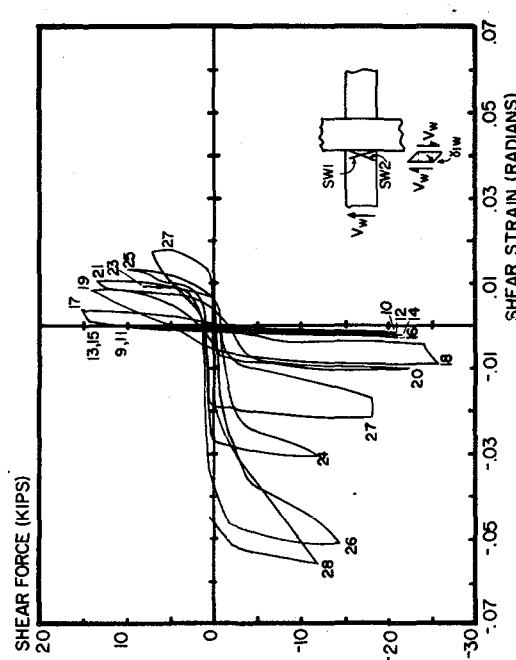


FIG. 4.26 (a) SHEAR STRAIN IN BEAM REGION 1 --- BC8 WEST

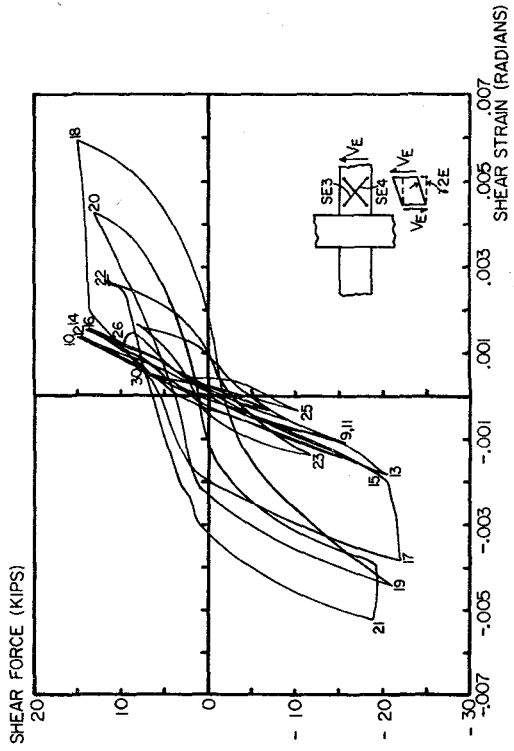


FIG. 4.27(a) SHEAR STRAIN IN BEAM, REGION 2 -- BC8 WEST

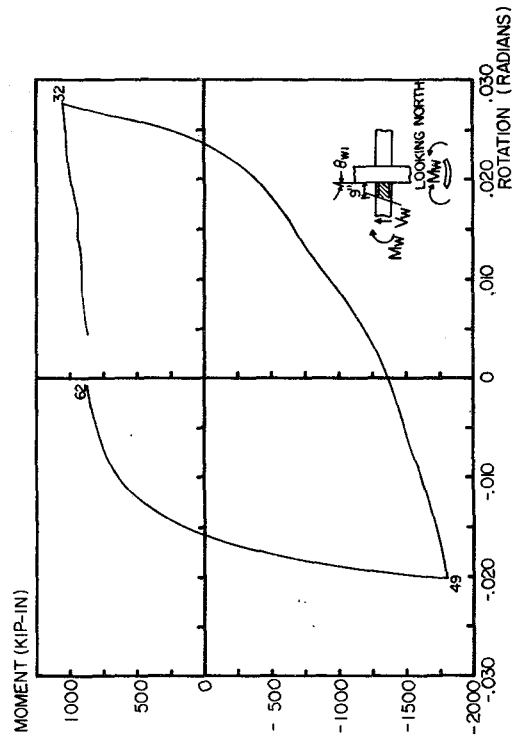


FIG. 4.28(a) MOMENT vs. BEAM ROTATION IN REGION 1 -- BC7 WEST

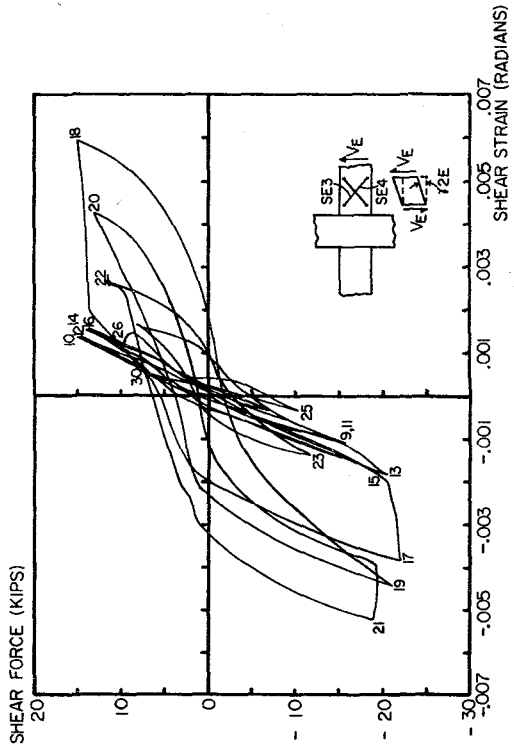


FIG. 4.27(b) SHEAR STRAIN IN BEAM, REGION 2 -- BC8 EAST

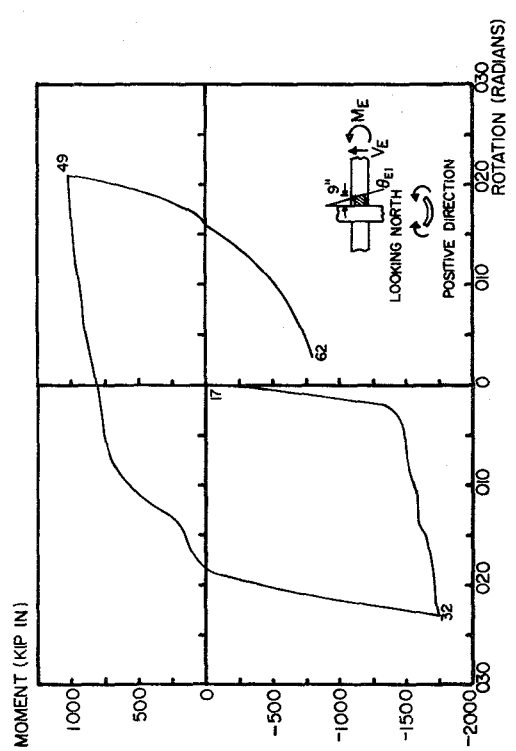


FIG. 4.28(b) MOMENT vs. BEAM ROTATION IN REGION 1 -- BC8 EAST

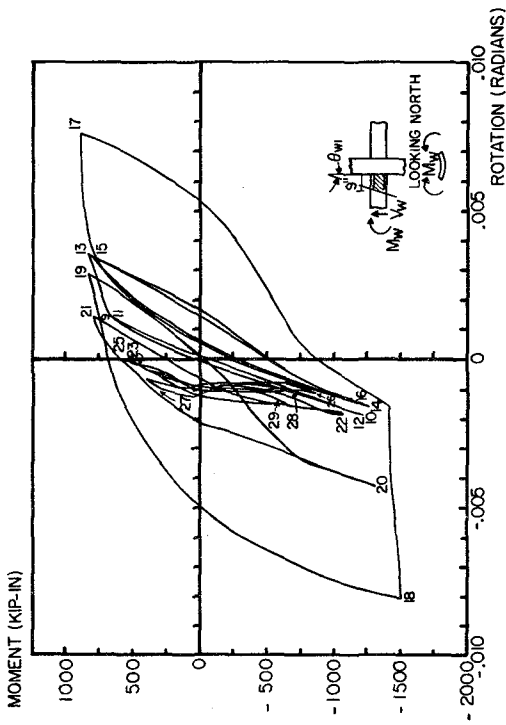


FIG. 4.29 (a) MOMENT vs. BEAM ROTATION IN REGION 1 -- BC8 WEST

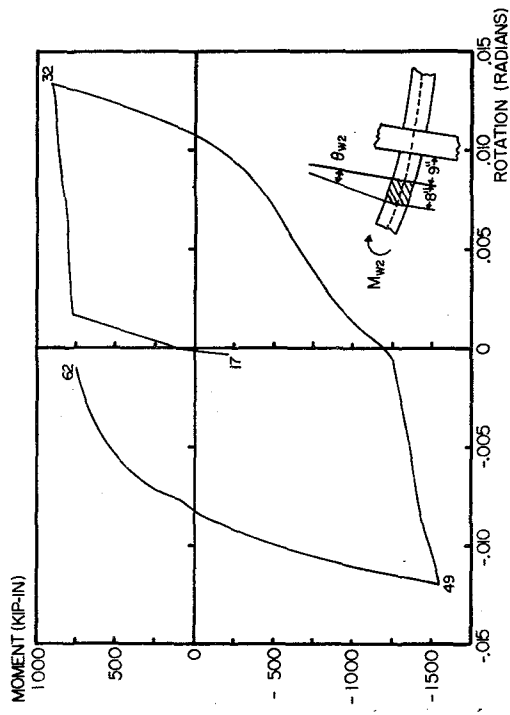


FIG. 4.30 (a) MOMENT vs. BEAM ROTATION IN REGION 2 -- BC7 WEST

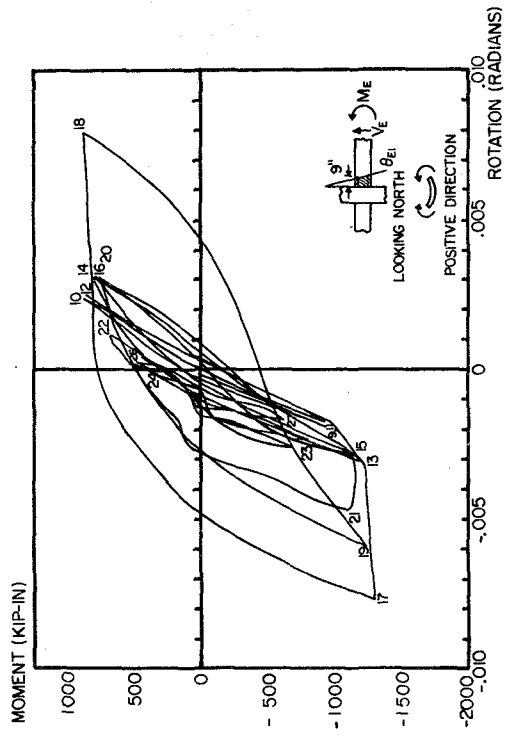


FIG. 4.29 (b) MOMENT vs. BEAM ROTATION IN REGION 1 - BC8 EAST

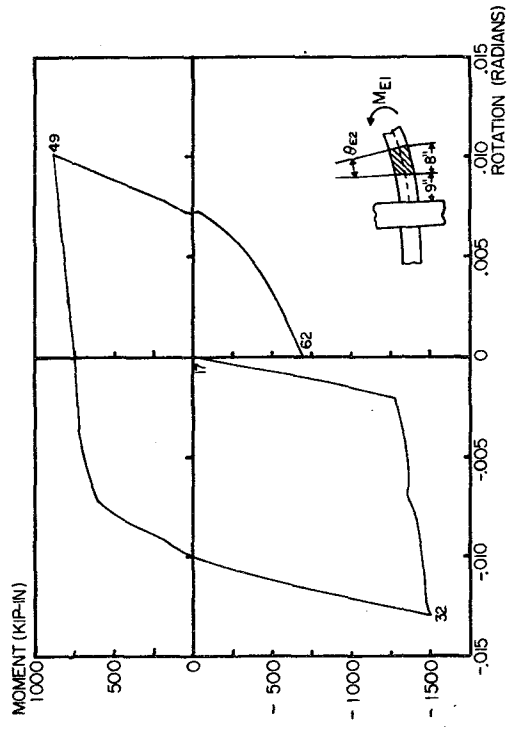


FIG. 4.30 (b) MOMENT vs. BEAM ROTATION IN REGION 2 -- BC7 EAST

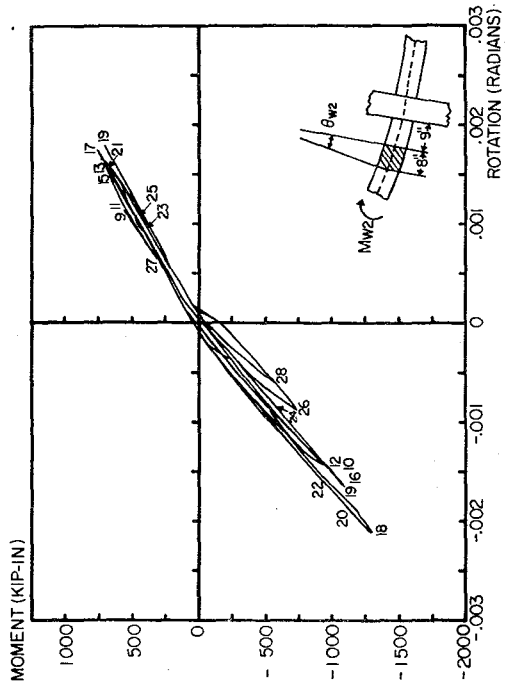


FIG. 4.31(a) MOMENT VS. BEAM ROTATION IN REGION 2 -- BC8 WEST

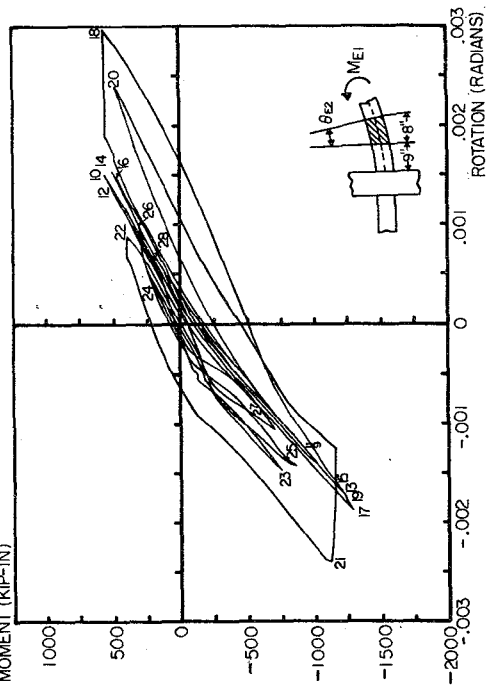


FIG. 4.31(b) MOMENT VS. BEAM ROTATION IN REGION 2 -- BC8 EAST

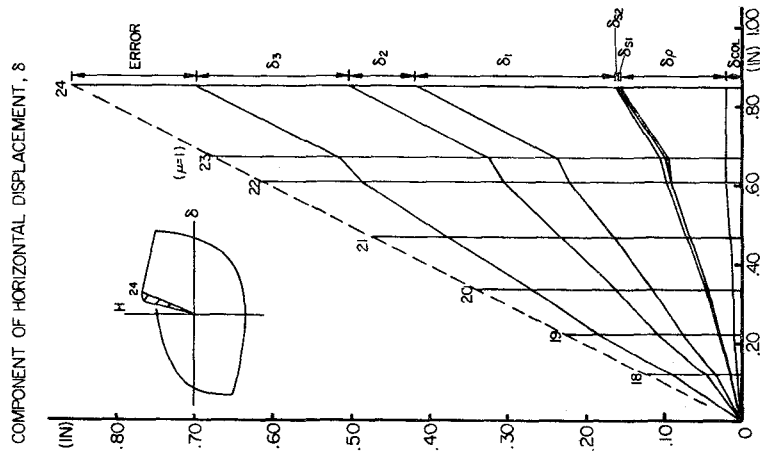


FIG. 4.32 (a) COMPONENTS OF HORIZONTAL DISPLACEMENT δ -- BC7 WEST

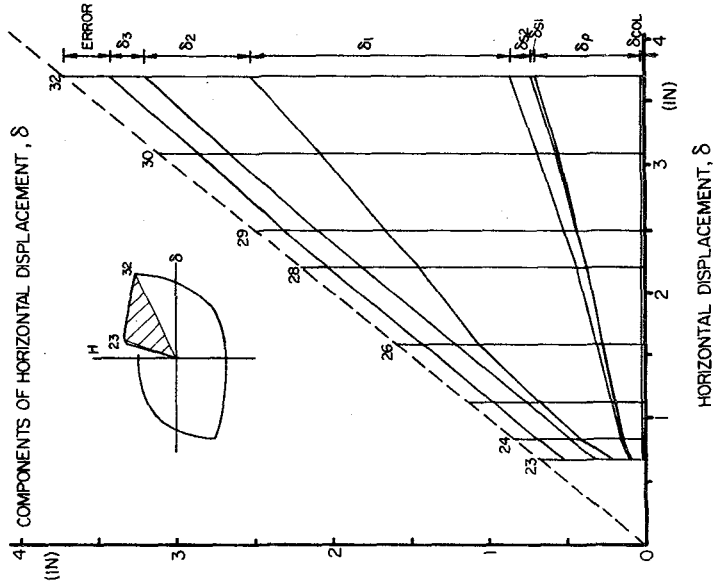


FIG. 4.32 (b) COMPONENTS OF HORIZONTAL DISPLACEMENT δ -- BC7 WEST

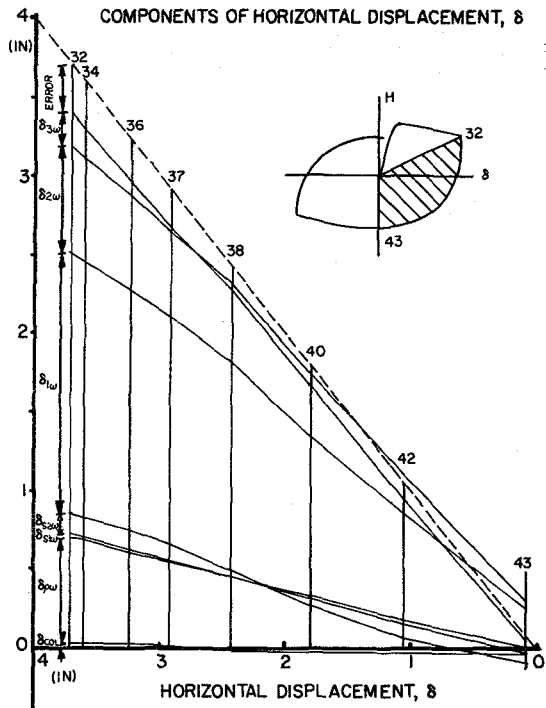


FIG. 4.32(c) COMPONENTS OF HORIZONTAL DISPLACEMENT δ -- BC7 WEST

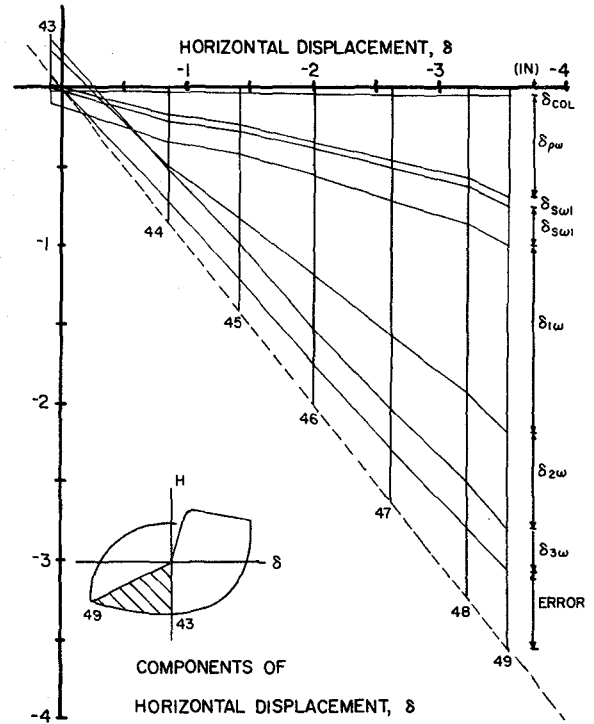


FIG. 4.23(d) COMPONENTS OF HORIZONTAL DISPLACEMENT δ - BC7 WEST

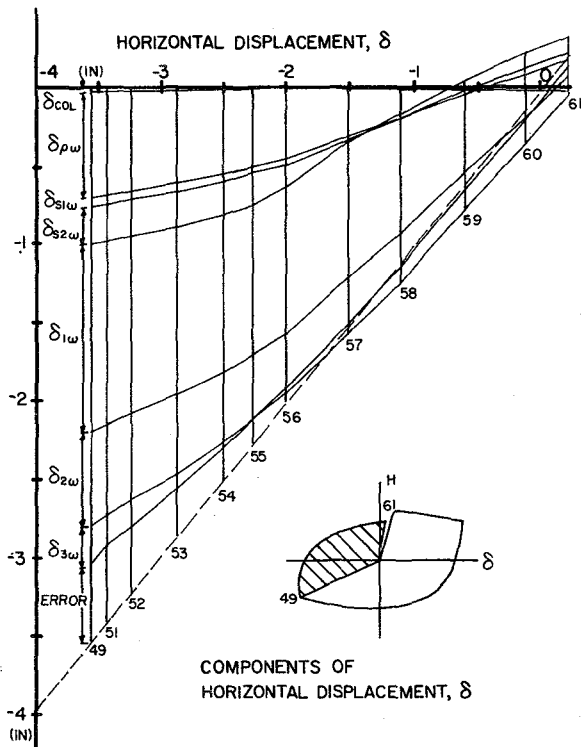


FIG. 4.32(e) COMPONENTS OF HORIZONTAL DISPLACEMENT δ - BC7 WEST

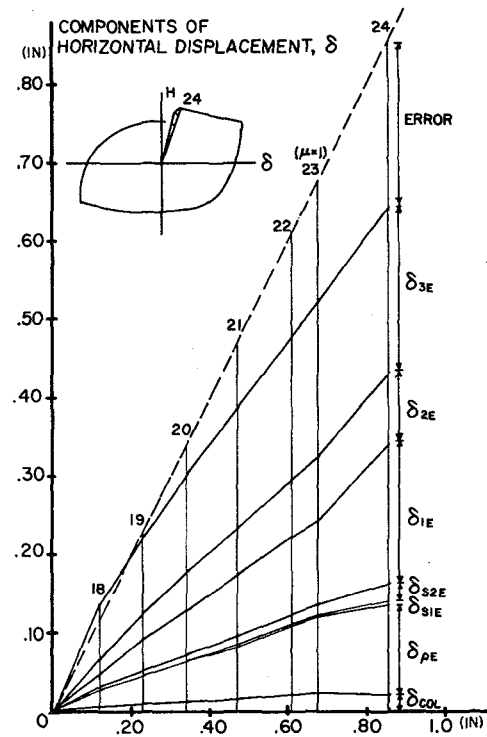


FIG. 4.33(a) COMPONENTS OF HORIZONTAL DISPLACEMENT δ - BC7 WEST

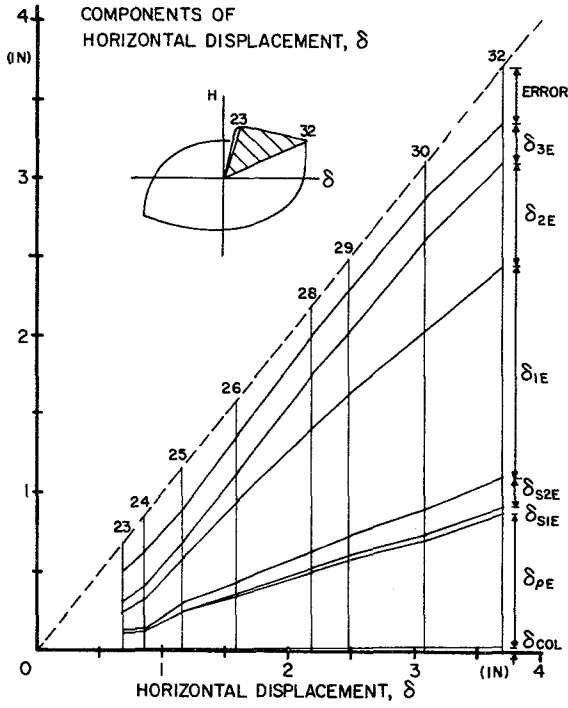


FIG. 4.33(b) COMPONENTS OF HORIZONTAL DISPLACEMENT δ -- BC7 WEST

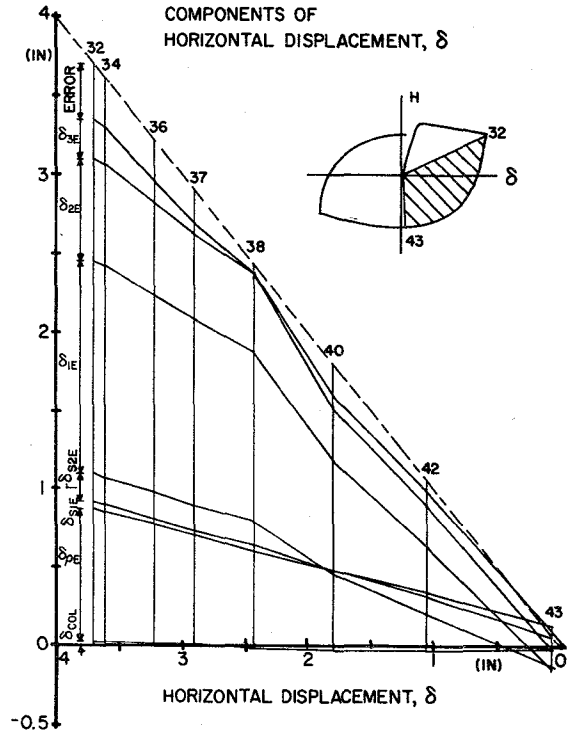


FIG. 4.33(c) COMPONENTS OF HORIZONTAL DISPLACEMENT δ -- BC7 WEST

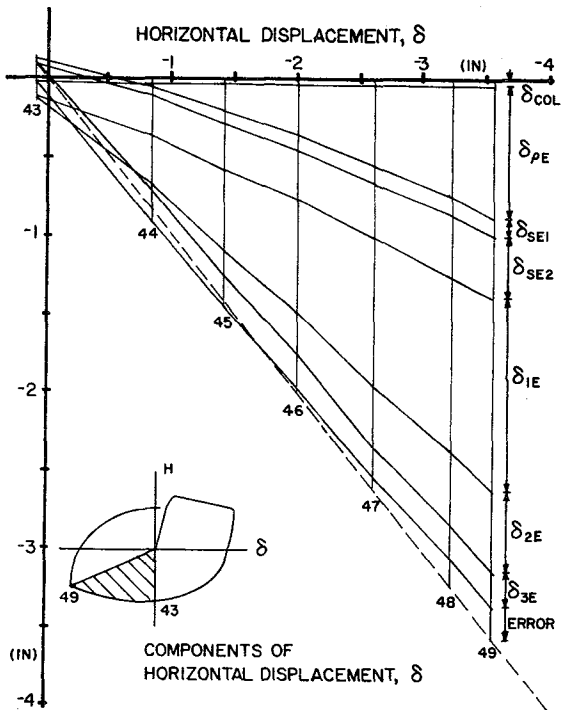


FIG. 4.33(d) COMPONENTS OF HORIZONTAL DISPLACEMENT δ -- BC7 WEST

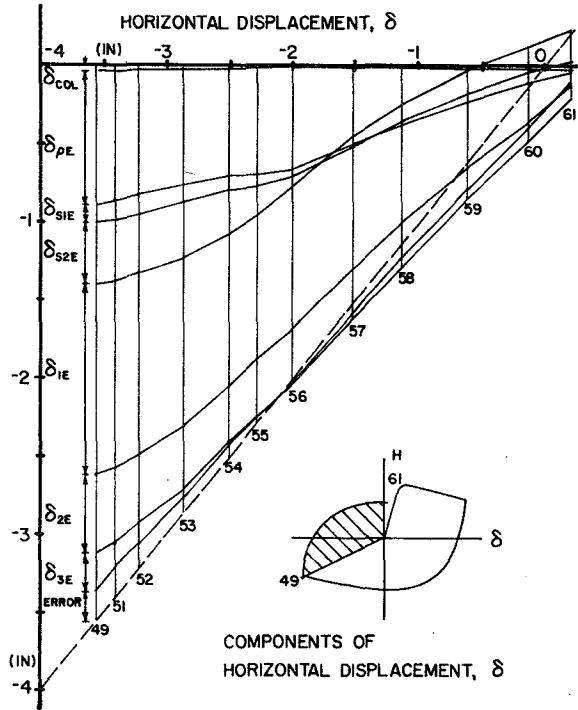
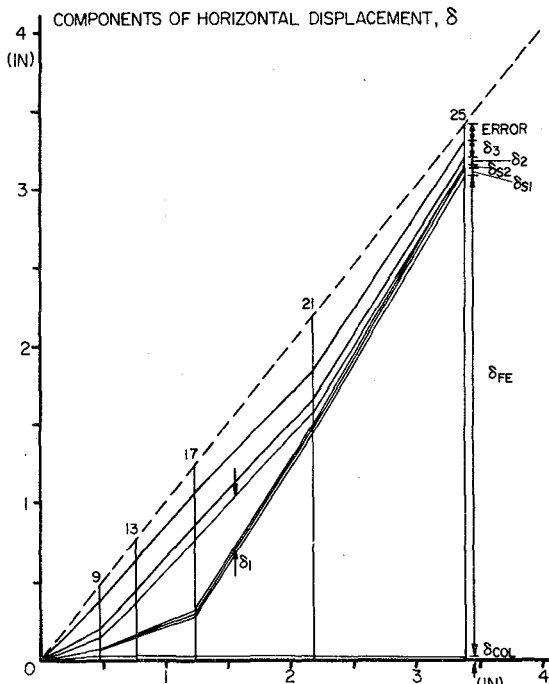
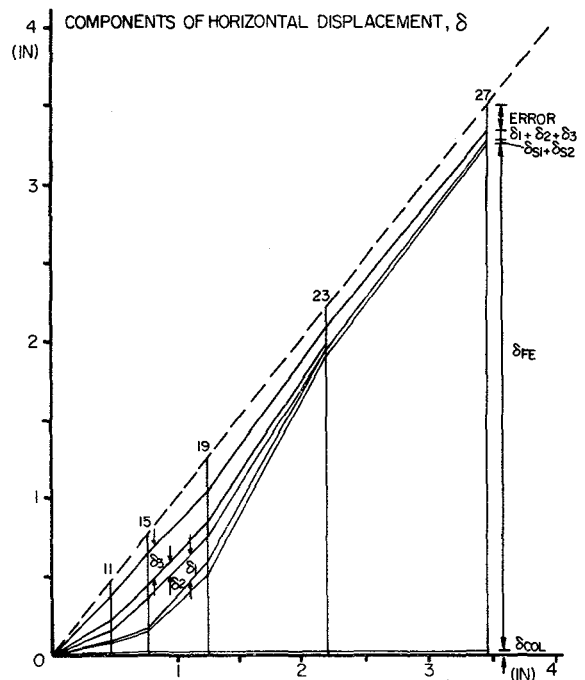


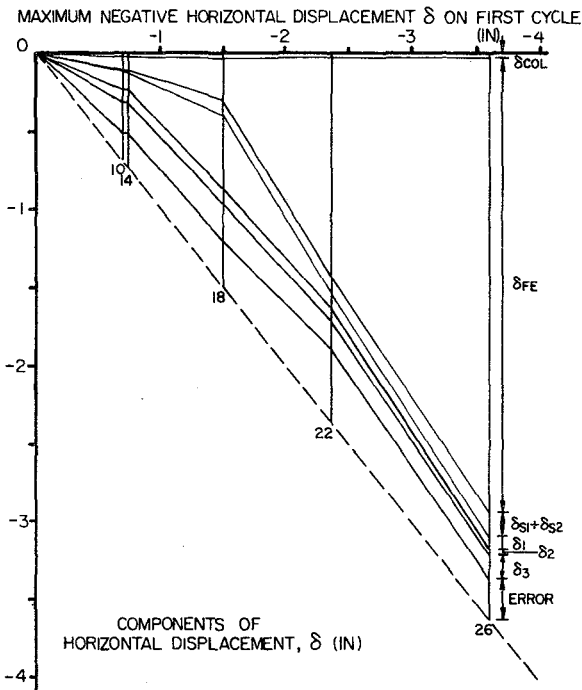
FIG. 4.33(e) COMPONENTS OF HORIZONTAL DISPLACEMENT δ -- BC7 WEST



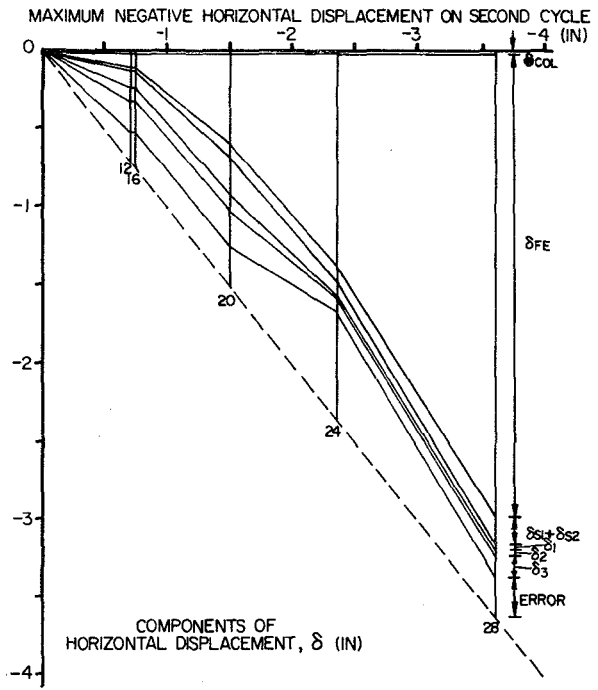
MAXIMUM POSITIVE HORIZONTAL DISPLACEMENT δ ON FIRST CYCLE
 FIG. 4.34(a) COMPONENTS OF HORIZONTAL DISPLACEMENT δ -- BC8 WEST -- FIRST CYCLE



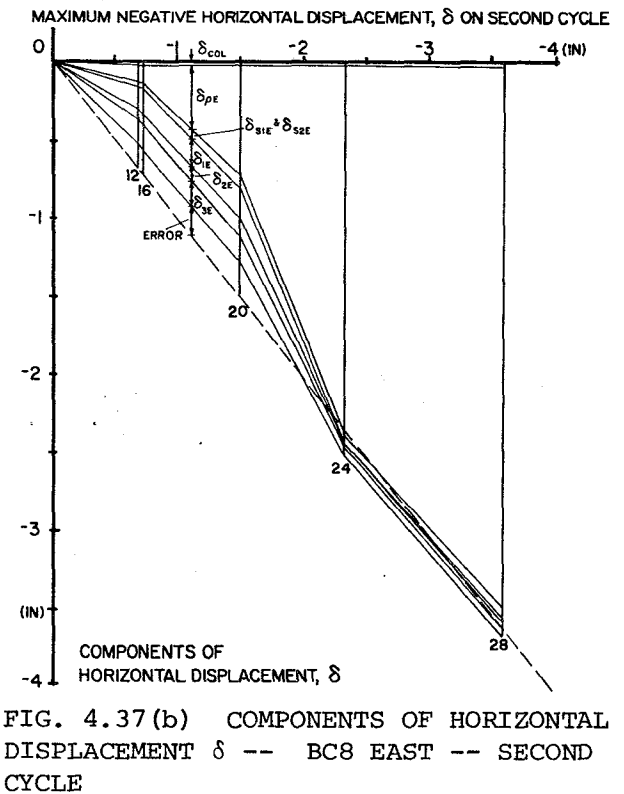
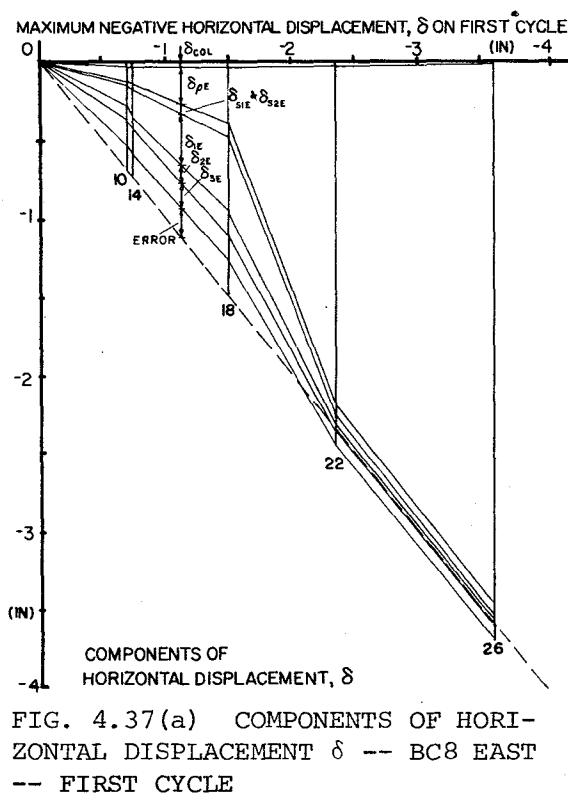
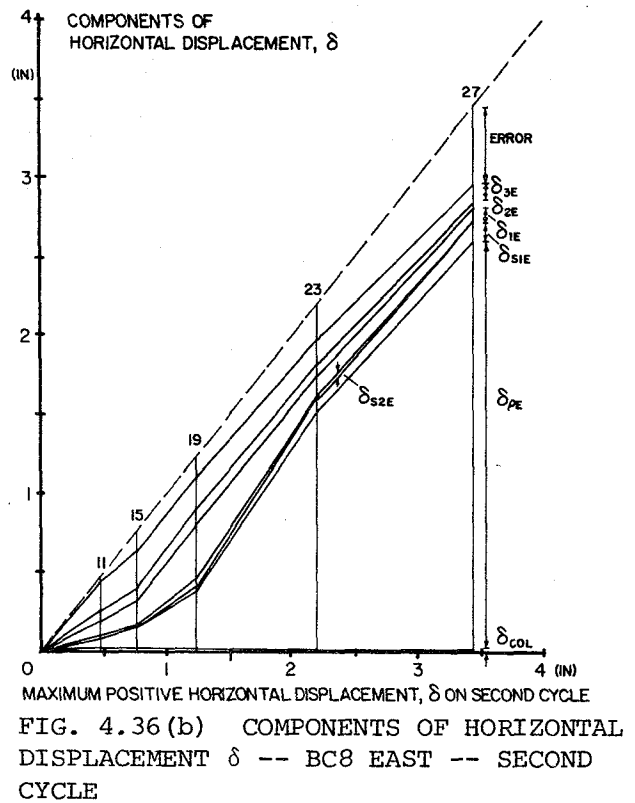
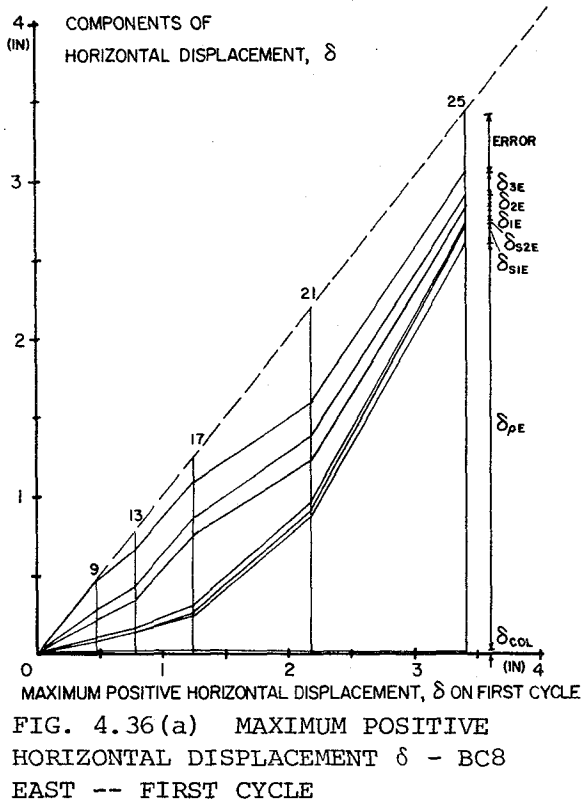
MAXIMUM POSITIVE HORIZONTAL DISPLACEMENT δ ON SECOND CYCLE
 FIG. 4.34(b) COMPONENTS OF HORIZONTAL DISPLACEMENT δ -- BC8 WEST -- SECOND CYCLE



MAXIMUM NEGATIVE HORIZONTAL DISPLACEMENT δ ON FIRST CYCLE
 FIG. 4.35(a) MAXIMUM NEGATIVE HORIZONTAL DISPLACEMENT δ -- BC8 WEST -- FIRST CYCLE



MAXIMUM NEGATIVE HORIZONTAL DISPLACEMENT ON SECOND CYCLE
 FIG. 4.35(b) MAXIMUM NEGATIVE HORIZONTAL DISPLACEMENT δ -- BC8 WEST -- SECOND CYCLE



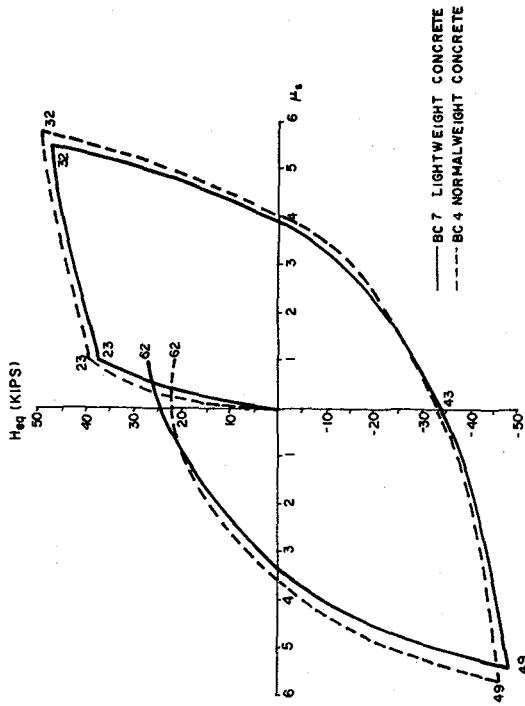


FIG. 5.1 COMPARISON OF HYSTERETIC LOOPS OF SPECIMENS BC4 and BC7

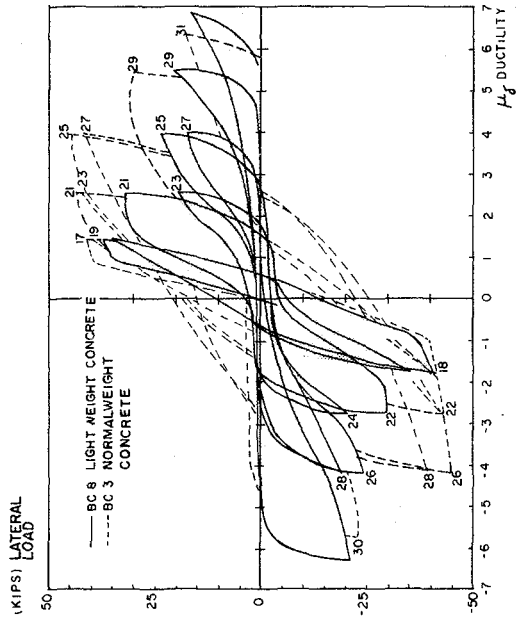


FIG. 5.2 COMPARISON OF HYSTERETIC LOOPS OF SPECIMENS BC3 AND BC8

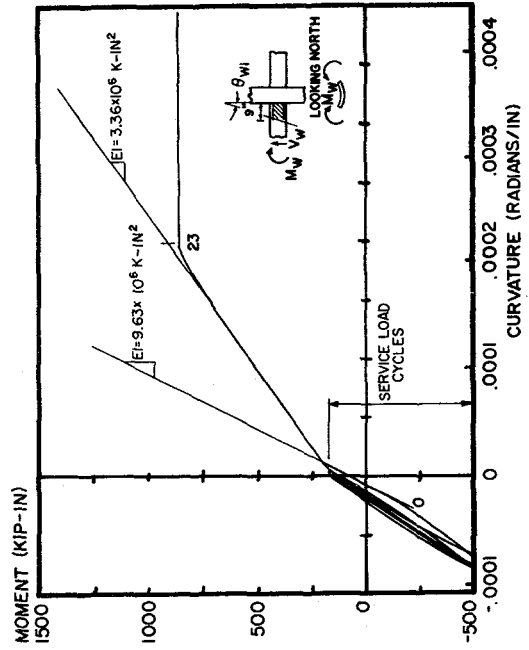


FIG. 6.1 MOMENT VS. BEAM ROTATION IN REGION 1 -- BC7 WEST

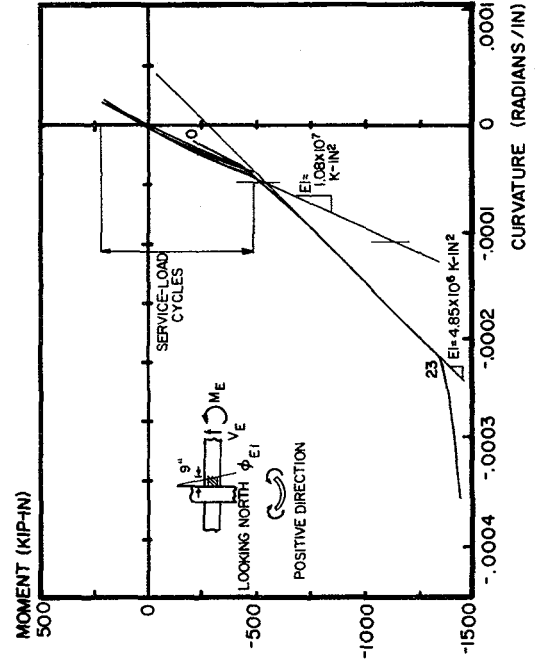


FIG. 6.2 MOMENT VS. BEAM ROTATION IN REGION 1 -- BC7 EAST

APPENDIX A

CALCULATED PROPERTIES FOR SPECIMEN BC7

From experimental data

$$f_y = 65 \text{ ksi} \quad \text{FOR \#6}$$

$$f_y = 67 \text{ ksi} \quad \text{FOR \#5}$$

$$E_s = 2.85 \times 10^4 \text{ ksi}$$

$$E_c = 2.69 \times 10^3 \text{ ksi}$$

$$f'_c = 4.615 \text{ ksi}$$

Refer to Fig. 2.5 for dimensions of beam section

YIELD MOMENTS

Assume concrete stress to be linear

$$M_y = f_y A_s j d + f'_s \left(\frac{kd}{3} - d' \right) A'_s$$

$$K = [m^2 (p' + p)^2 + 2m(p + p' \frac{d'}{d})]^{1/2} - m(p + p')$$

POSITIVE MOMENT DIRECTION

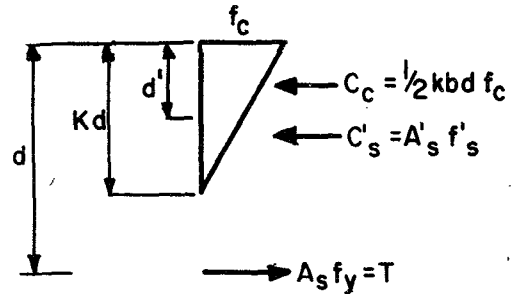
$$p = \frac{A_s}{bd} = \frac{0.92}{9(14.69)} = 0.00696$$

$$p' = \frac{A'_s}{bd} = \frac{1.77}{9(14.69)} = 0.0134$$

$$m = \frac{E_s}{E_c} \quad \text{For strength calculations, use } E_c \text{ for normal weight concrete}$$

$$E_c = 33w^{1.5} \sqrt{f'_c} = 33(150)^{1.5} \sqrt{4615} = 4.12 \times 10^3 \text{ ksi}$$

$$m = \frac{2.85 \times 10^4}{4.12 \times 10^3} = 6.9 \sim 7.0$$



$$d' = 2 \text{ in. } d = 14.7 \text{ in.}$$

$$\text{Substituting } k = 0.236$$

$$y = 1 - \frac{k}{3} = 0.921$$

$$M_y^+ = 67 (0.92) (0.921) (14.7) + 8.8 \left[\frac{0.236(14.7)}{3} - 2 \right] 1.77$$

$$= 821 \text{ k-in. } (92.6 \text{ kN-m})$$

$$\phi_y^+ = \frac{\epsilon_y}{d(1-k)} = \frac{67/28500}{147(1-0.236)} = 2.09 \times 10^{-4} \text{ radians}$$

$$f_c = E_c \epsilon_c = E_c \epsilon_y \frac{k}{(1-k)} = 2.69 \times 10^3 \left(\frac{67}{28500} \right) \frac{0.236}{(1-0.236)}$$

$$= 1.95 \text{ ksi} = 0.42 f_c' < 0.7 f_c'$$

∴ Linear stress distribution is adequate

NEGATIVE MOMENT DIRECTION

$$p = \frac{1.77}{9(14)} = .0140$$

$$p' = \frac{0.92}{9(14)} = .0073$$

$$d' = 1.31 \text{ in. } d = 14 \text{ in.}$$

$$\text{Substituting } k = 0.329$$

$$\alpha = 0.890$$

$$f_s' = \frac{0.329(14) - 1.31}{14(1-0.329)} 65 = 22.8 \text{ ksi}$$

Substituting

$$M_y^- = 1439 \text{ k-in. } (162.6 \text{ kN-m})$$

$$\phi_y^- = \frac{65/28500}{14(1-0.329)} = 2.43 \times 10^{-4} \text{ radians}$$

$$f_c = E_c \epsilon_c = E_c \epsilon - l \frac{k}{(1-k)} = 2.69 \times 10^3 \left(\frac{65}{28500} \right) \frac{0.329}{(1-0.329)}$$

$$= 3.01 \text{ ksi} = 0.65 f'_c < 0.7 f'_c$$

∴ Linear stress distribution is adequate

LOAD AT YIELD

Since both beams yield almost simultaneously:

$$H_{EQ} = \frac{M_Y^- + M_Y^+}{l} \quad l - \text{distance from beam reaction to column face}$$

$$= 63.5 \text{ in.}$$

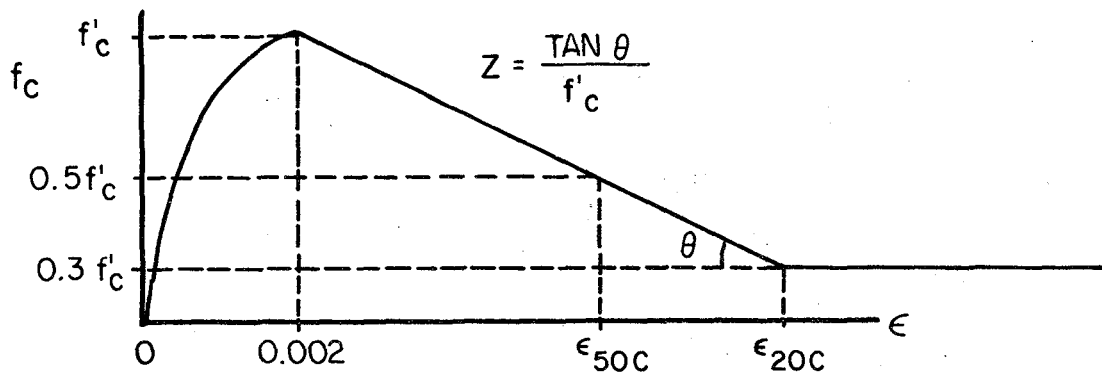
$$H_{EQ} = \frac{1439 + 821}{63.5} = 35.6 \text{ kips (158 kN)}$$

APPLIED MOMENT AT LP32

From test: East beam $\epsilon_s = 0.0266$ $f_s = 82.5 \text{ ksi}$ (negative moment direction)

West beam $\epsilon_s = 0.0367$ $f_s = 89 \text{ ksi}$ (positive moment direction)

To balance high stresses in steel, the concrete confined by closed stirrups must reach high strain levels.



STRESS-STRAIN CURVE ASSUMED FOR CONFINED CONCRETE [REF. 9, CH. 2, 6]

For $0.002 \leq \epsilon_c \leq \epsilon_{20c}$

$$f_c = f'_c [1 - z(\epsilon_c - 0.002)]$$

$$\text{where } z = \frac{0.5}{\epsilon_{50u} + \epsilon_{50h} - 0.002}$$

$$\epsilon_{50u} = \frac{3 + 0.002 f'_c}{f'_c - 1000}$$

$$\epsilon_{50h} = \frac{3}{4} P_s \sqrt{\frac{b''}{S_h}}$$

$$\epsilon_{50c} = \epsilon_{50u} + \epsilon_{50h}$$

where f'_c is in psi

P_s = Ratio of volume of transverse reinforcement to volume of concrete core measured to outside of hoops

b'' = width of confined core measured to outside hoops

S_h = spacing of hoops

$$P_s = \frac{A_b \ell_s}{b'' d''}$$

A_b = area of reinforcing bar

ℓ_s = length of stirrup

d'' = height of confined core

$$P_s = \frac{(0.049)(43.25)}{(7.5)(14.625)} = 0.019$$

$b'' = 7.5$ in.

$S_h = 3.5$ in.

$$E_{soh} = \frac{3}{4} (0.019) \sqrt{\frac{7.5}{3.5}} = 0.021$$

$$E_{sou} = \frac{3 + 0.0002(4615)}{4615 - 1000} = 0.0034$$

$$Z = \frac{0.5}{0.003 + 0.021 - 0.002} = 22.1$$

NEGATIVE MOMENT DIRECTION

$$T = F_s A_s = 82.5(1.77) = 146 \text{ kips}$$

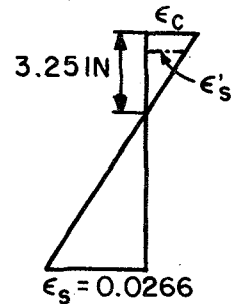
Assume $c = 3.25$ in.

$$E_c = E_s \frac{c}{d-e} = 0.0266 \frac{3.25}{14-3.25} = 0.0080$$

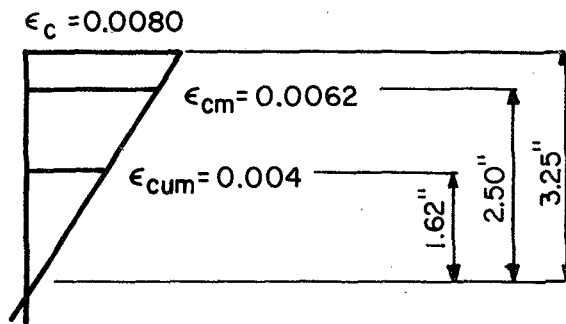
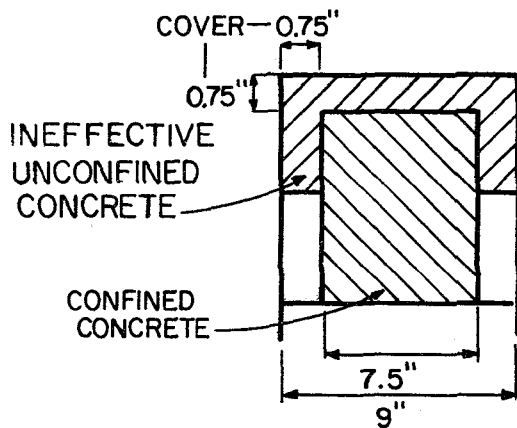
$$E_s' = E_c \frac{c-d}{c} = 0.0080 \frac{3.25-1.3}{3.25} = 0.0048$$

$$E_y < E_s' < E_{sh} \quad F_s' = F_y = 67 \text{ ksi}$$

$$C_s' = F_s' A_s' = 67(0.92) = 61.6 \text{ kips}$$



Assume Unconfined Concrete $w/E_c > 0.004$ Ineffective



Confined Concrete:

From Table 6.2 Ref. 9 $w/Z = 22.1$

$$E_{cm} = 0.0062$$

$$\gamma = 0.860$$

$$\gamma = 0.456$$

Where $C_c = \gamma F_c 'c' b$ acting $\gamma c'$ from extreme compression fiber

C' - Distance from neutral axis to extreme compression fiber in question

$$C_c = 0.860(4.615) (7.5) (2.50) = 74.4 \text{ kips}$$

$$C_c \text{ ACTS } 14 - 0.75 - 0.456(2.5) = 12.11 \text{ in. from tension of steel}$$

Unconfined Concrete

$$E_{cum} = 0.004$$

$$Z = 22.1$$

From Table 6.2

$$\gamma = 0.822$$

$$\gamma = 0.429$$

$$C_{cu} = 0.822(4.615) (1.5) (1.62) = 9.2 \text{ kips}$$

$$C_{cu} \text{ ACTS } 14 - 3.25 + 1.62 - 0.429(1.62) = 11.68 \text{ in. from tension of steel}$$

$$C = C_c + C_{cu} + C_s' = 74.4 + 9.2 + 61.6 = 145.s \text{ kips} \approx T = 146 \text{ kips}$$

$$c = 3.25 \text{ is correct}$$

Summing Moments About Tension Steel

$$M_{32} = 74.4(12.11) + 9.2(11.68) + 61.6(12.7) = 1791 \text{ kip-in} \\ = (202.3\text{kN-m})$$

$$\phi_{32} = \frac{E_c + E_s}{h} = \frac{0.008 + 0.0266}{h} = 2.47 \times 10^{-3} \text{ radians}$$

POSITIVE MOMENT DIRECTION

$$T = F_s A_s = 89(0.92) = 82 \text{ kips}$$

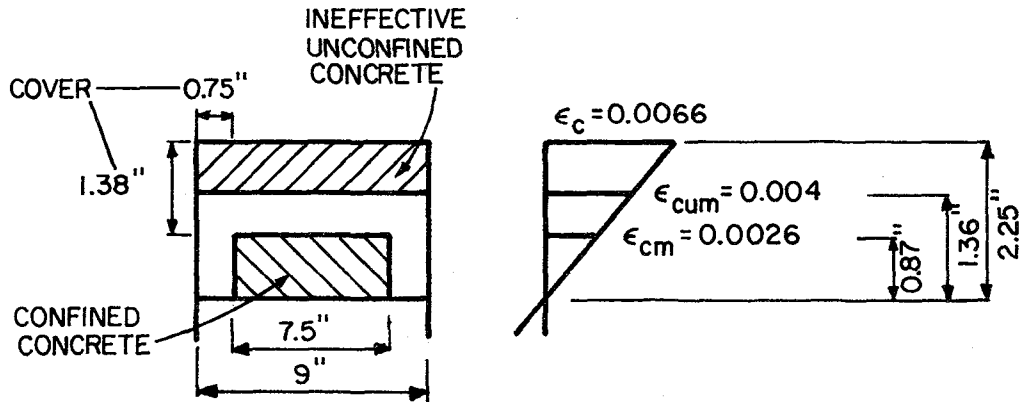
Assume $C = 2.25 \text{ in.}$

$$E_c = E_s \frac{c-d}{c} = 0.0367 \frac{2.25}{14.7 - 2.25} = 0.0066$$

$$E_s' = E_c \frac{c-d}{c} = 0.0066 \frac{(2.25-2)}{2.25} = 0.0007 < E_y$$

$$F_s' = E_s E_s' = 28500(0.0007) = 20.0 \text{ ksi}$$

$$C_s' = F_s' A_s' = 20.0(1.77) = 35.4 \text{ kips}$$



Since unconfined concrete is more effective than confined concrete there is no need to differentiate between the two in the analysis

From Table 6.2 $W/E_{cum} = 0.004$

$$Z = 22.1$$

$$\gamma = 0.822$$

$$\gamma = 0.429$$

$$C_c = 0.822(4.615)(9)(1.36) = 46.4 \text{ kips}$$

C_c acts $14.7 - 2.25 + 1.36 - 0.429(1.36) = 13.23$ in. from tension steel

$$C_1 = C'_s + C_{1c} = 35.4 + 45.4 = 81.8 \approx T = 82 \text{ kips}$$

$\therefore C = 2.25$ in. is correct

Summing moments about tension steel

$$M_{32}^+ = 46.4(13.23) + 35.4(12.7) = 1063 \text{ kip/in. (120.1 kN-m)}$$

$$\phi_{32}^+ = \frac{E_c + E_s}{d} = \frac{0.0066 + 0.0367}{14.7} = 2.95 \times 10^{-3} \text{ radians}$$

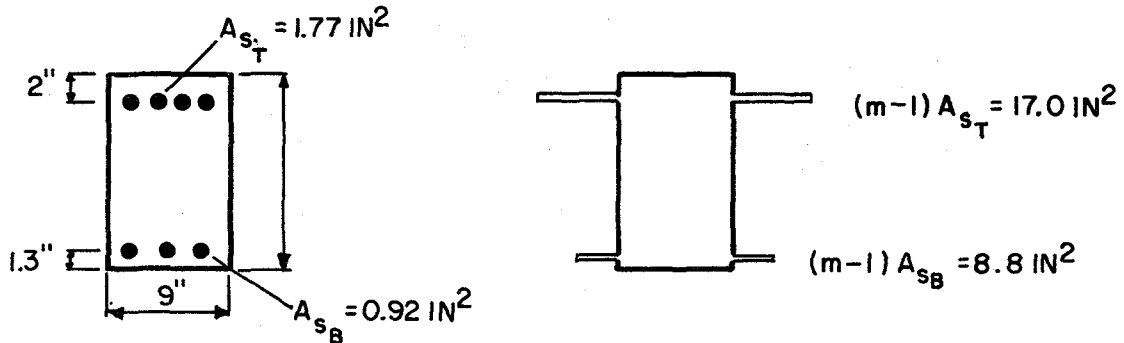
LOAD AT LP32

$$H_{EQ32} = \frac{M_{32}^- + M_{32}^+}{l} = \frac{1791 + 1063}{63.5} = 44.9 \text{ kips (200 kN)}$$

UNCRACKED FLEXURAL STIFFNESS OF BEAM: $E_c I_{cUNCR}$

$E_c I_{cUNCR}$ is the same for both positive and negative moment

Transformed area



$$A_{TOT} = 9(16) + 17.0 + 8.8 = 169.8 \text{ in.}^2$$

$$\text{Centroid: } \bar{x} = \frac{9(16)(8) + 17.0(14) + 8.8(1.31)}{169.8} = 8.3 \text{ in.}$$

$$I_{UNCR} = \frac{9(16)^3}{12} + 9(16)(8.3 - 8)^2 + 17(14 - 8.3)^2 + 8.8(8.3 - 1.3)^2 = 4068 \text{ in.}^4$$

$$E_c I_{cUNCR} = 2690(4068) = (1.09 \times 10^7 \text{ kips/in.}^2)(3.14 \times 10^4 \text{ kN-m}^2)$$

CRACKED FLEXURAL STIFFNESS: $\frac{EI}{c} CR$

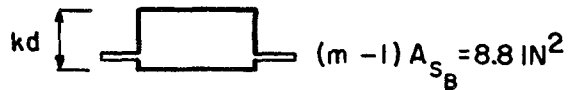
Postive moment direction



$$mA_{S_B} = 9.7 \text{ IN}^2$$

$$kd = 0.236(14.7) = 3.47 \text{ in.}$$

Negative moment direction



$$kd = 0.329(14) = 4.61 \text{ in.}$$

$$I_{CR} = \frac{9(4.61)^3}{3} + 8.8(4.51 - 1.3)^2 + 18.8(14 - 4.61)^2 = 2048 \text{ in.}^4$$

$$E_C I_{CR} = 2690(2098) = 5.51 \times 10^6 \text{ kips/in.}^2 \quad (15.8 \times 10^3 \text{ kN-m}^2)$$

INITIAL STIFFNESS OF SUBASSEMBLAGE

Use cracked flexural stiffness since working load moments exceed cracking moments.

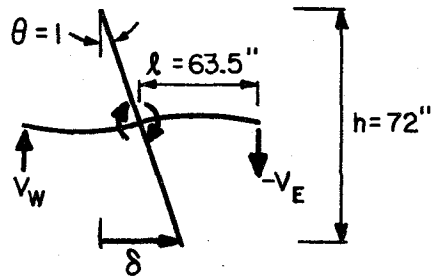
Rotational stiffness at joint:

$$k'_{ROT} = \frac{3E_C I_{CR}^+}{\ell} + \frac{3E_C I_{CR}^-}{\ell}$$

$$H_{EQ} = \frac{k_{ROT} \theta}{\ell}$$

$$S = h\theta$$

$$k = \frac{H_{EQ}}{\delta} = \frac{k_{ROT}}{\ell h}$$



$$K = \frac{1}{63.5(7.2)} \left[\frac{3(3.73 \times 10^6)}{63.5} + \frac{3(5.51 \times 10^6)}{63.5} \right]$$

$$= 95 \text{ k/in (16.6 kN/mm)}$$

FLEXURAL DEFLECTIONS

$$I_e = \left(\frac{M_{cr}}{M_{max}} \right) I_g + \left[1 - \frac{M_{cr}}{M_{max}} \right]^3 I_{cr} \quad \text{ACI 9-4}$$

$$M_{cr} = \frac{F_r I_g}{y_t} \quad (\text{ACI 9-5})$$

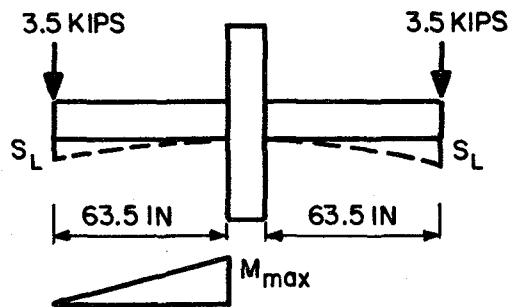
$F_r = 0.248 \text{ ksi (Experimental Data)}$

$$I_g = \frac{bh^3}{12} = \frac{9(16)^3}{12} = 3072 \text{ in.}^4$$

$$y_t = \frac{16}{2} = 8 \text{ in.}$$

$$M_{cr} = \frac{0.248(3072)}{8} = 95 \text{ kip-in.}$$

DEFLECTION OF BEAMS DUE TO INITIAL GRAVITY LOAD MOMENT



$$M_{max} = 3.5(63.5) = 222 \text{ kip-in.}$$

$$\frac{M_{cr}}{M_{max}} = \frac{95}{222} = 0.427$$

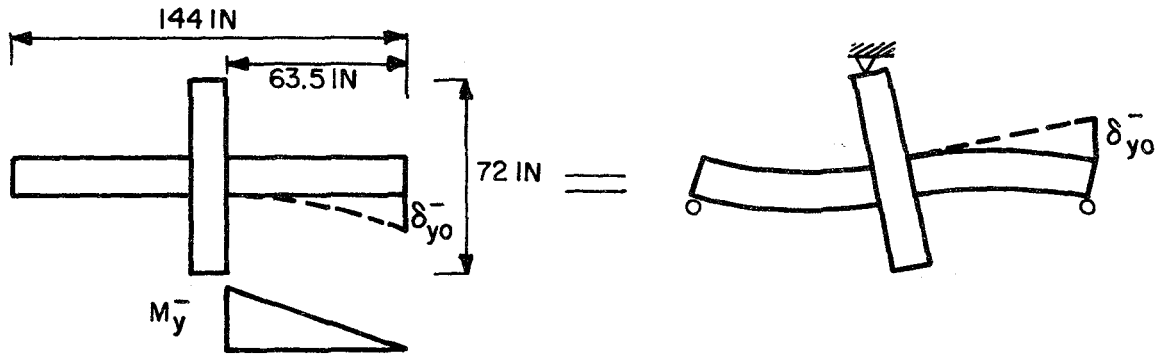
$$I_{ce}^- = 2048 \text{ in.}^4$$

$$I_e = (0.427)^3 3072 + [1 - (0.427)^3] 2048 = 2128 \text{ in.}^4$$

$$E_c I_e = 2.69 \times 10^3 (2128) = 5.72 \times 10^6 \text{ k-in.}^2$$

$$\delta_i = \frac{1}{5.72 \times 10^6} (63.5) (222) \frac{1}{2} \frac{2}{3} (63.5) = 0.052 \text{ in.}$$

DEFECTION DUE TO M_y^- (= 1439 kip-in.)



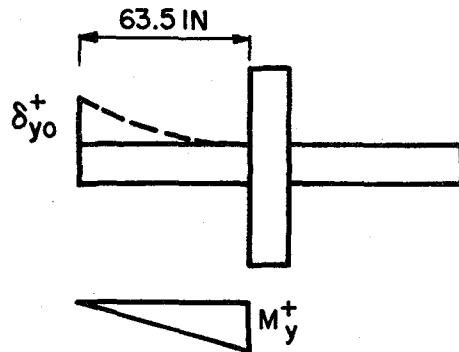
Due to geometry of specimen, deflection of end of beam relative to tangent drawn from column equals horizontal displacement δ at base of column using (ACI 9-4)

$$I_e = 2084 \text{ in.}^4 (= I_{cr})$$

$$E_c I_e = 2.69 \times 10^3 (2084) = 5.51 \times 10^6 \text{ kip-in.}^2$$

$$\delta_{yo} = \frac{1}{5.51 \times 10^6} (63.5) (1439) \frac{1}{2} \frac{2}{3} (63.5) = 0.351 \text{ in.}$$

DEFLECTION DUE TO M_y^+ (= 821 kip-in)

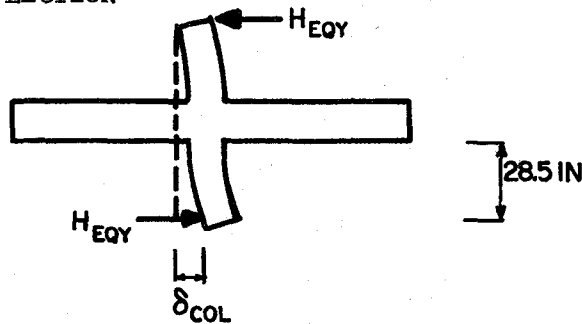


Using (ACI 9-4) $I_e = 1385 \text{ in}^4 (= I_{cr})$

$$E_c I_e = 2.69 \times 10^3 (1385) = 3.73 \times 10^6 \text{ k-in.}^2$$

$$\delta_{yo}^+ = \frac{1}{3.73 \times 10^6} (63.5) (821) \frac{1}{2} \frac{2}{3} (63.5) = 0.296 \text{ in.}$$

COLUMN DEFLECTION



$$H_{EQY} = 35.6 \text{ kips}$$

$$I = I_g = \frac{(17)^4}{12} = 6960 \text{ in.}^4$$

$$\delta_{COL} = \frac{2 H_{EQ} (28.5)^3}{3 E I} = \frac{2 (35.6) (28.5)^3}{3 (2.67 \times 10^3) (6960)} = 0.029 \text{ in.}$$

Must adjust δ_y^- and δ_y^+ for column deflection and deflection of beam due to gravity load moment.

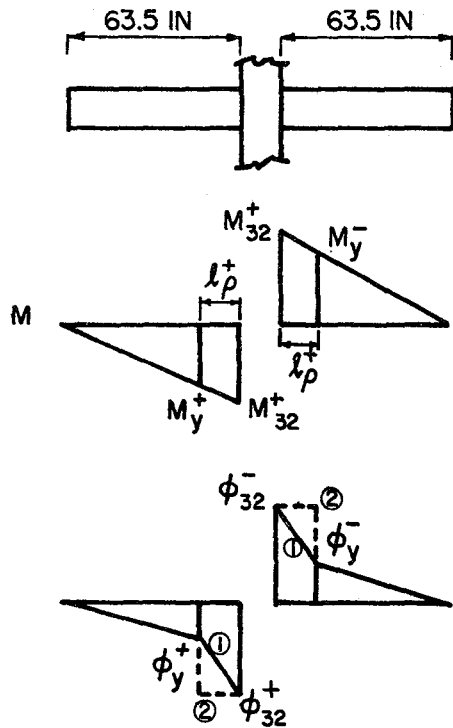
$$\delta_y^- = \delta_{yo}^- - \delta_i + \delta_{COL} = 0.351 - 0.052 + 0.029 = 0.328 \text{ in.}$$

$$= 0.33 \text{ in. (8.4mm.)}$$

$$\delta_y^+ = \delta_{y0}^+ + \delta_i + \delta_{COL} = 0.296 + 0.052 + 0.029 = 0.377 \text{ in.}$$

$$= 0.38 \text{ in. (9.7mm.)}$$

DEFLECTION AT LP32



$$M_{32}^- = 1791 \text{ kip-in}$$

$$M_{32}^+ = 1063$$

$$M_y^- = 1439 \text{ kip-in}$$

$$M_y^+ = 821$$

$$l_{\rho}^- = \left(1 - \frac{1439}{1791}\right) 63.5 = 13.2 \text{ in.}$$

$$l_{\rho}^+ = \left(1 - \frac{821}{1063}\right) 63.5 = 14.7 \text{ in.}$$

$$\phi_{32}^- = 2.47 \times 10^{-3} \text{ rad.}$$

$$\phi_y^- = 2.43 \times 10^{-4} \text{ rad.}$$

$$\phi_{32}^+ = 2.95 \times 10^{-3} \text{ rad.}$$

Assuming that the distribution of ϕ over l_{ρ} is given by profile (1)

$$\delta_{32}^- = \frac{1}{2} (\phi_{32}^- - \phi_y^-) l_{\rho}^- (63.5 - \frac{2}{3} l_{\rho}^-) + \phi_y^- l_{\rho} (63.5 - \frac{l_{\rho}}{2}) +$$

$$\frac{1}{3} \phi_y^- (63.5 - l_{\rho}^-)^2$$

$$= \frac{1}{2} (2.47 \times 10^{-3} - 2.43 \times 10^{-4}) (13.2) (63.5 - \frac{2}{3}(13.2)) +$$

$$2.43 \times 10^{-4} (13.2) (63.5 - \frac{13.2}{2}) + \frac{1}{3} (2.43 \times 10^{-4}) (63.5 - 13.2)^2$$

$$\delta_{32}^{-} = 1.19 \text{ in. (30.3mm)}$$

Similarly

$$\delta_{32}^{+} = 1.42 \text{ in. (36.1mm.)}$$

Assuming that the distribution of ϕ over l_{ρ} is given by profile (2)

(Attempt to account for additional ϕ due to diagonal tension cracking)

$$\begin{aligned}\delta_{32}^{-} &= \phi_{32}^{-} l_{\rho}^{-} (63.5 - \frac{1}{2} l_{\rho}^{-}) + \frac{1}{3} \phi_Y^{-} (63.5 - l_{\rho}^{-})^2 \\ &= 2.47 \times 10^{-3} (13.2) (63.5 - \frac{1}{2}(13.2)) + \frac{1}{3} (2.43 \times 10^{-4}) (63.5 - 13.2)^2\end{aligned}$$

$$\delta_{32}^{-} = 2.06 \text{ in. (52.3mm.)}$$

Similarly

$$\delta_{32}^{+} = 2.28 \text{ in. (57.9mm.)}$$

EARTHQUAKE ENGINEERING RESEARCH CENTER REPORTS



EARTHQUAKE ENGINEERING RESEARCH CENTER REPORTS

NOTE: Numbers in parenthesis are Accession Numbers assigned by the National Technical Information Service; these are followed by a price code. Copies of the reports may be ordered from the National Technical Information Service, 5285 Port Royal Road, Springfield, Virginia, 22161. Accession Numbers should be quoted on orders for reports (PB --- ---) and remittance must accompany each order. Reports without this information were not available at time of printing. Upon request, EERC will mail inquirers this information when it becomes available.

- EERC 67-1 "Feasibility Study Large-Scale Earthquake Simulator Facility," by J. Penzien, J.G. Bouwkamp, R.W. Clough and D. Rea - 1967 (PB 187 905)A07
- EERC 68-1 Unassigned
- EERC 68-2 "Inelastic Behavior of Beam-to-Column Subassemblages Under Repeated Loading," by V.V. Bertero - 1968 (PB 184 888)A05
- EERC 68-3 "A Graphical Method for Solving the Wave Reflection-Refraction Problem," by H.D. McNiven and Y. Mengi - 1968 (PB 187 943)A03
- EERC 68-4 "Dynamic Properties of McKinley School Buildings," by D. Rea, J.G. Bouwkamp and R.W. Clough - 1968 (PB 187 902)A07
- EERC 68-5 "Characteristics of Rock Motions During Earthquakes," by H.B. Seed, I.M. Idriss and F.W. Kiefer - 1968 (PB 188 338)A03
- EERC 69-1 "Earthquake Engineering Research at Berkeley," - 1969 (PB 187 906)All
- EERC 69-2 "Nonlinear Seismic Response of Earth Structures," by M. Dibaj and J. Penzien - 1969 (PB 187 904)A08
- EERC 69-3 "Probabilistic Study of the Behavior of Structures During Earthquakes," by R. Ruiz and J. Penzien - 1969 (PB 187 886)A06
- EERC 69-4 "Numerical Solution of Boundary Value Problems in Structural Mechanics by Reduction to an Initial Value Formulation," by N. Distefano and J. Schujman - 1969 (PB 187 942)A02
- EERC 69-5 "Dynamic Programming and the Solution of the Biharmonic Equation," by N. Distefano - 1969 (PB 187 941)A03
- EERC 69-6 "Stochastic Analysis of Offshore Tower Structures," by A.K. Malhotra and J. Penzien - 1969 (PB 187 903)A09
- EERC 69-7 "Rock Motion Accelerograms for High Magnitude Earthquakes," by H.B. Seed and I.M. Idriss - 1969 (PB 187 940)A02
- EERC 69-8 "Structural Dynamics Testing Facilities at the University of California, Berkeley," by R.M. Stephen, J.G. Bouwkamp, R.W. Clough and J. Penzien - 1969 (PB 189 111)A04
- EERC 69-9 "Seismic Response of Soil Deposits Underlain by Sloping Rock Boundaries," by H. Dezfulian and H.B. Seed - 1969 (PB 189 114)A03
- EERC 69-10 "Dynamic Stress Analysis of Axisymmetric Structures Under Arbitrary Loading," by S. Ghosh and E.L. Wilson - 1969 (PB 189 026)A10
- EERC 69-11 "Seismic Behavior of Multistory Frames Designed by Different Philosophies," by J.C. Anderson and V. V. Bertero - 1969 (PB 190 662)A10
- EERC 69-12 "Stiffness Degradation of Reinforcing Concrete Members Subjected to Cyclic Flexural Moments," by V.V. Bertero, B. Bresler and H. Ming Liao - 1969 (PB 202 942)A07
- EERC 69-13 "Response of Non-Uniform Soil Deposits to Travelling Seismic Waves," by H. Dezfulian and H.B. Seed - 1969 (PB 191 023)A03
- EERC 69-14 "Damping Capacity of a Model Steel Structure," by D. Rea, R.W. Clough and J.G. Bouwkamp - 1969 (PB 190 663)A06
- EERC 69-15 "Influence of Local Soil Conditions on Building Damage Potential during Earthquakes," by H.B. Seed and I.M. Idriss - 1969 (PB 191 036)A03
- EERC 69-16 "The Behavior of Sands Under Seismic Loading Conditions," by M.L. Silver and H.B. Seed - 1969 (AD 714 982)A07
- EERC 70-1 "Earthquake Response of Gravity Dams," by A.K. Chopra - 1970 (AD 709 640)A03
- EERC 70-2 "Relationships between Soil Conditions and Building Damage in the Caracas Earthquake of July 29, 1967," by H.B. Seed, I.M. Idriss and H. Dezfulian - 1970 (PB 195 762)A05
- EERC 70-3 "Cyclic Loading of Full Size Steel Connections," by E.P. Popov and R.M. Stephen - 1970 (PB 213 545)A04
- EERC 70-4 "Seismic Analysis of the Charaima Building, Caraballeda, Venezuela," by Subcommittee of the SEAONC Research Committee: V.V. Bertero, P.F. Fratessa, S.A. Mahin, J.H. Sexton, A.C. Scordelis, E.L. Wilson, L.A. Wyllie, H.B. Seed and J. Penzien, Chairman - 1970 (PB 201 455)A06

- EERC 70-5 "A Computer Program for Earthquake Analysis of Dams," by A.K. Chopra and P. Chakrabarti - 1970 (AD 723 994)A05
- EERC 70-6 "The Propagation of Love Waves Across Non-Horizontally Layered Structures," by J. Lysmer and L.A. Drake 1970 (PB 197 896)A03
- EERC 70-7 "Influence of Base Rock Characteristics on Ground Response," by J. Lysmer, H.B. Seed and P.B. Schnabel 1970 (PB 197 897)A03
- EERC 70-8 "Applicability of Laboratory Test Procedures for Measuring Soil Liquefaction Characteristics under Cyclic Loading," by H.B. Seed and W.H. Peacock - 1970 (PB 198 016)A03
- EERC 70-9 "A Simplified Procedure for Evaluating Soil Liquefaction Potential," by H.B. Seed and I.M. Idriss - 1970 (PB 198 009)A03
- EERC 70-10 "Soil Moduli and Damping Factors for Dynamic Response Analysis," by H.B. Seed and I.M. Idriss - 1970 (PB 197 869)A03
- EERC 71-1 "Koyna Earthquake of December 11, 1967 and the Performance of Koyna Dam," by A.K. Chopra and P. Chakrabarti 1971 (AD 731 496)A06
- EERC 71-2 "Preliminary In-Situ Measurements of Anelastic Absorption in Soils Using a Prototype Earthquake Simulator," by R.D. Borcherdt and P.W. Rodgers - 1971 (PB 201 454)A03
- EERC 71-3 "Static and Dynamic Analysis of Inelastic Frame Structures," by F.L. Porter and G.H. Powell - 1971 (PB 210 135)A06
- EERC 71-4 "Research Needs in Limit Design of Reinforced Concrete Structures," by V.V. Bertero - 1971 (PB 202 943)A04
- EERC 71-5 "Dynamic Behavior of a High-Rise Diagonally Braced Steel Building," by D. Rea, A.A. Shah and J.G. Bouwkamp 1971 (PB 203 584)A06
- EERC 71-6 "Dynamic Stress Analysis of Porous Elastic Solids Saturated with Compressible Fluids," by J. Ghaboussi and E. L. Wilson - 1971 (PB 211 396)A06
- EERC 71-7 "Inelastic Behavior of Steel Beam-to-Column Subassemblages," by H. Krawinkler, V.V. Bertero and E.P. Popov 1971 (PB 211 335)A14
- EERC 71-8 "Modification of Seismograph Records for Effects of Local Soil Conditions," by P. Schnabel, H.B. Seed and J. Lysmer - 1971 (PB 214 450)A03
- EERC 72-1 "Static and Earthquake Analysis of Three Dimensional Frame and Shear Wall Buildings," by E.L. Wilson and H.H. Dovey - 1972 (PB 212 904)A05
- EERC 72-2 "Accelerations in Rock for Earthquakes in the Western United States," by P.B. Schnabel and H.B. Seed - 1972 (PB 213 100)A03
- EERC 72-3 "Elastic-Plastic Earthquake Response of Soil-Building Systems," by T. Minami - 1972 (PB 214 868)A08
- EERC 72-4 "Stochastic Inelastic Response of Offshore Towers to Strong Motion Earthquakes," by M.K. Kaul - 1972 (PB 215 713)A05
- EERC 72-5 "Cyclic Behavior of Three Reinforced Concrete Flexural Members with High Shear," by E.P. Popov, V.V. Bertero and H. Krawinkler - 1972 (PB 214 555)A05
- EERC 72-6 "Earthquake Response of Gravity Dams Including Reservoir Interaction Effects," by P. Chakrabarti and A.K. Chopra - 1972 (AD 762 330)A08
- EERC 72-7 "Dynamic Properties of Pine Flat Dam," by D. Rea, C.Y. Liaw and A.K. Chopra - 1972 (AD 763 928)A05
- EERC 72-8 "Three Dimensional Analysis of Building Systems," by E.L. Wilson and H.H. Dovey - 1972 (PB 222 438)A06
- EERC 72-9 "Rate of Loading Effects on Uncracked and Repaired Reinforced Concrete Members," by S. Mahin, V.V. Bertero, D. Rea and M. Atalay - 1972 (PB 224 520)A08
- EERC 72-10 "Computer Program for Static and Dynamic Analysis of Linear Structural Systems," by E.L. Wilson, K.-J. Bathe, J.E. Peterson and H.H. Dovey - 1972 (PB 220 437)A04
- EERC 72-11 "Literature Survey - Seismic Effects on Highway Bridges," by T. Iwasaki, J. Penzien and R.W. Clough - 1972 (PB 215 613)A19
- EERC 72-12 "SHAKE-A Computer Program for Earthquake Response Analysis of Horizontally Layered Sites," by P.B. Schnabel and J. Lysmer - 1972 (PB 220 207)A06
- EERC 73-1 "Optimal Seismic Design of Multistory Frames," by V.V. Bertero and H. Kamil - 1973
- EERC 73-2 "Analysis of the Slides in the San Fernando Dams During the Earthquake of February 9, 1971," by H.B. Seed, K.L. Lee, I.M. Idriss and F. Makdisi - 1973 (PB 223 402)A14

- EERC 73-3 "Computer Aided Ultimate Load Design of Unbraced Multistory Steel Frames," by M.B. El-Hafez and G.H. Powell 1973 (PB 248 315)A09
- EERC 73-4 "Experimental Investigation into the Seismic Behavior of Critical Regions of Reinforced Concrete Components as Influenced by Moment and Shear," by M. Celebi and J. Penzien - 1973 (PB 215 884)A09
- EERC 73-5 "Hysteretic Behavior of Epoxy-Repaired Reinforced Concrete Beams," by M. Celebi and J. Penzien - 1973 (PB 239 568)A03
- EERC 73-6 "General Purpose Computer Program for Inelastic Dynamic Response of Plane Structures," by A. Kanaan and G.H. Powell - 1973 (PB 221 260)A08
- EERC 73-7 "A Computer Program for Earthquake Analysis of Gravity Dams Including Reservoir Interaction," by P. Chakrabarti and A.K. Chopra - 1973 (AD 766 271)A04
- EERC 73-8 "Behavior of Reinforced Concrete Deep Beam-Column Subassemblages Under Cyclic Loads," by O. Küstü and J.G. Bouwkamp - 1973 (PB 246 117)A12
- EERC 73-9 "Earthquake Analysis of Structure-Foundation Systems," by A.K. Vaish and A.K. Chopra - 1973 (AD 766 272)A07
- EERC 73-10 "Deconvolution of Seismic Response for Linear Systems," by R.B. Reimer - 1973 (PB 227 179)A08
- EERC 73-11 "SAP IV: A Structural Analysis Program for Static and Dynamic Response of Linear Systems," by K.-J. Bathe, E.L. Wilson and F.E. Peterson - 1973 (PB 221 967)A09
- EERC 73-12 "Analytical Investigations of the Seismic Response of Long, Multiple Span Highway Bridges," by W.S. Tseng and J. Penzien - 1973 (PB 227 816)A10
- EERC 73-13 "Earthquake Analysis of Multi-Story Buildings Including Foundation Interaction," by A.K. Chopra and J.A. Gutierrez - 1973 (PB 222 970)A03
- EERC 73-14 "ADAP: A Computer Program for Static and Dynamic Analysis of Arch Dams," by R.W. Clough, J.M. Raphael and S. Mojtahedi - 1973 (PB 223 763)A09
- EERC 73-15 "Cyclic Plastic Analysis of Structural Steel Joints," by R.B. Pinkney and R.W. Clough - 1973 (PB 226 843)A08
- EERC 73-16 "QUAD-4: A Computer Program for Evaluating the Seismic Response of Soil Structures by Variable Damping Finite Element Procedures," by I.M. Idriss, J. Lysmer, R. Hwang and H.B. Seed - 1973 (PB 229 424)A05
- EERC 73-17 "Dynamic Behavior of a Multi-Story Pyramid Shaped Building," by R.M. Stephen, J.P. Hollings and J.G. Bouwkamp - 1973 (PB 240 718)A06
- EERC 73-18 "Effect of Different Types of Reinforcing on Seismic Behavior of Short Concrete Columns," by V.V. Bertero, J. Hollings, O. Küstü, R.M. Stephen and J.G. Bouwkamp - 1973
- EERC 73-19 "Olive View Medical Center Materials Studies, Phase I," by B. Bresler and V.V. Bertero - 1973 (PB 235 986)A06
- EERC 73-20 "Linear and Nonlinear Seismic Analysis Computer Programs for Long Multiple-Span Highway Bridges," by W.S. Tseng and J. Penzien - 1973
- EERC 73-21 "Constitutive Models for Cyclic Plastic Deformation of Engineering Materials," by J.M. Kelly and P.P. Gillis 1973 (PB 226 024)A03
- EERC 73-22 "DRAIN - 2D User's Guide," by G.H. Powell - 1973 (PB 227 016)A05
- EERC 73-23 "Earthquake Engineering at Berkeley - 1973," (PB 226 033)A11
- EERC 73-24 Unassigned
- EERC 73-25 "Earthquake Response of Axisymmetric Tower Structures Surrounded by Water," by C.Y. Liaw and A.K. Chopra 1973 (AD 773 052)A09
- EERC 73-26 "Investigation of the Failures of the Olive View Stairtowers During the San Fernando Earthquake and Their Implications on Seismic Design," by V.V. Bertero and R.G. Collins - 1973 (PB 235 106)A13
- EERC 73-27 "Further Studies on Seismic Behavior of Steel Beam-Column Subassemblages," by V.V. Bertero, H. Krawinkler and E.P. Popov - 1973 (PB 234 172)A06
- EERC 74-1 "Seismic Risk Analysis," by C.S. Oliveira - 1974 (PB 235 920)A06
- EERC 74-2 "Settlement and Liquefaction of Sands Under Multi-Directional Shaking," by R. Pyke, C.K. Chan and H.B. Seed 1974
- EERC 74-3 "Optimum Design of Earthquake Resistant Shear Buildings," by D. Ray, K.S. Pister and A.K. Chopra - 1974 (PB 231 172)A06
- EERC 74-4 "LUSH - A Computer Program for Complex Response Analysis of Soil-Structure Systems," by J. Lysmer, T. Udaka, H.B. Seed and R. Hwang - 1974 (PB 236 796)A05

- EERC 74-5 "Sensitivity Analysis for Hysteretic Dynamic Systems: Applications to Earthquake Engineering," by D. Ray 1974 (PB 233 213)A06
- EERC 74-6 "Soil Structure Interaction Analyses for Evaluating Seismic Response," by H.B. Seed, J. Lysmer and R. Hwang 1974 (PB 236 519)A04
- EERC 74-7 Unassigned
- EERC 74-8 "Shaking Table Tests of a Steel Frame - A Progress Report," by R.W. Clough and D. Tang - 1974 (PB 240 869)A03
- EERC 74-9 "Hysteretic Behavior of Reinforced Concrete Flexural Members with Special Web Reinforcement," by V.V. Bertero, E.P. Popov and T.Y. Wang - 1974 (PB 236 797)A07
- EERC 74-10 "Applications of Reliability-Based, Global Cost Optimization to Design of Earthquake Resistant Structures," by E. Vitiello and K.S. Pister - 1974 (PB 237 231)A06
- EERC 74-11 "Liquefaction of Gravelly Soils Under Cyclic Loading Conditions," by R.T. Wong, H.B. Seed and C.K. Chan 1974 (PB 242 042)A03
- EERC 74-12 "Site-Dependent Spectra for Earthquake-Resistant Design," by H.B. Seed, C. Ugas and J. Lysmer - 1974 (PB 240 953)A03
- EERC 74-13 "Earthquake Simulator Study of a Reinforced Concrete Frame," by P. Hidalgo and R.W. Clough - 1974 (PB 241 944)A13
- EERC 74-14 "Nonlinear Earthquake Response of Concrete Gravity Dams," by N. Pal - 1974 (AD/A 006 583)A06
- EERC 74-15 "Modeling and Identification in Nonlinear Structural Dynamics - I. One Degree of Freedom Models," by N. Distefano and A. Rath - 1974 (PB 241 548)A06
- EERC 75-1 "Determination of Seismic Design Criteria for the Dumbarton Bridge Replacement Structure, Vol. I: Description, Theory and Analytical Modeling of Bridge and Parameters," by F. Baron and S.-H. Pang - 1975 (PB 259 407)A15
- EERC 75-2 "Determination of Seismic Design Criteria for the Dumbarton Bridge Replacement Structure, Vol. II: Numerical Studies and Establishment of Seismic Design Criteria," by F. Baron and S.-H. Pang - 1975 (PB 259 408)A11 (For set of EERC 75-1 and 75-2 (PB 259 406))
- EERC 75-3 "Seismic Risk Analysis for a Site and a Metropolitan Area," by C.S. Oliveira - 1975 (PB 248 134)A09
- EERC 75-4 "Analytical Investigations of Seismic Response of Short, Single or Multiple-Span Highway Bridges," by M.-C. Chen and J. Penzien - 1975 (PB 241 454)A09
- EERC 75-5 "An Evaluation of Some Methods for Predicting Seismic Behavior of Reinforced Concrete Buildings," by S.A. Mahin and V.V. Bertero - 1975 (PB 246 306)A16
- EERC 75-6 "Earthquake Simulator Study of a Steel Frame Structure, Vol. I: Experimental Results," by R.W. Clough and D.T. Tang - 1975 (PB 243 981)A13
- EERC 75-7 "Dynamic Properties of San Bernardino Intake Tower," by D. Rea, C.-Y. Liaw and A.K. Chopra - 1975 (AD/A008 406) A05
- EERC 75-8 "Seismic Studies of the Articulation for the Dumbarton Bridge Replacement Structure, Vol. I: Description, Theory and Analytical Modeling of Bridge Components," by F. Baron and R.E. Hamati - 1975 (PB 251 539)A07
- EERC 75-9 "Seismic Studies of the Articulation for the Dumbarton Bridge Replacement Structure, Vol. 2: Numerical Studies of Steel and Concrete Girder Alternates," by F. Baron and R.E. Hamati - 1975 (PB 251 540)A10
- EERC 75-10 "Static and Dynamic Analysis of Nonlinear Structures," by D.P. Mondkar and G.H. Powell - 1975 (PB 242 434)A08
- EERC 75-11 "Hysteretic Behavior of Steel Columns," by E.P. Popov, V.V. Bertero and S. Chandramouli - 1975 (PB 252 365)A11
- EERC 75-12 "Earthquake Engineering Research Center Library Printed Catalog," - 1975 (PB 243 711)A26
- EERC 75-13 "Three Dimensional Analysis of Building Systems (Extended Version)," by E.L. Wilson, J.P. Hollings and H.H. Dovey - 1975 (PB 243 989)A07
- EERC 75-14 "Determination of Soil Liquefaction Characteristics by Large-Scale Laboratory Tests," by P. De Alba, C.K. Chan and H.B. Seed - 1975 (NUREG 0027)A08
- EERC 75-15 "A Literature Survey - Compressive, Tensile, Bond and Shear Strength of Masonry," by R.L. Mayes and R.W. Clough - 1975 (PB 246 292)A10
- EERC 75-16 "Hysteretic Behavior of Ductile Moment Resisting Reinforced Concrete Frame Components," by V.V. Bertero and E.P. Popov - 1975 (PB 246 388)A05
- EERC 75-17 "Relationships Between Maximum Acceleration, Maximum Velocity, Distance from Source, Local Site Conditions for Moderately Strong Earthquakes," by H.B. Seed, R. Murarka, J. Lysmer and I.M. Idriss - 1975 (PB 248 172)A03
- EERC 75-18 "The Effects of Method of Sample Preparation on the Cyclic Stress-Strain Behavior of Sands," by J. Mulilis, C.K. Chan and H.B. Seed - 1975 (Summarized in EERC 75-28)

- EERC 75-19 "The Seismic Behavior of Critical Regions of Reinforced Concrete Components as Influenced by Moment, Shear and Axial Force," by M.B. Atalay and J. Penzien - 1975 (PB 258 842)A11
- EERC 75-20 "Dynamic Properties of an Eleven Story Masonry Building," by R.M. Stephen, J.P. Hollings, J.G. Bouwkamp and D. Jurukovski - 1975 (PB 246 945)A04
- EERC 75-21 "State-of-the-Art in Seismic Strength of Masonry - An Evaluation and Review," by R.L. Mayes and R.W. Clough 1975 (PB 249 040)A07
- EERC 75-22 "Frequency Dependent Stiffness Matrices for Viscoelastic Half-Plane Foundations," by A.K. Chopra, P. Chakrabarti and G. Dasgupta - 1975 (PB 248 121)A07
- EERC 75-23 "Hysteretic Behavior of Reinforced Concrete Framed Walls," by T.Y. Wong, V.V. Bertero and E.P. Popov - 1975
- EERC 75-24 "Testing Facility for Subassemblages of Frame-Wall Structural Systems," by V.V. Bertero, E.P. Popov and T. Endo - 1975
- EERC 75-25 "Influence of Seismic History on the Liquefaction Characteristics of Sands," by H.B. Seed, K. Mori and C.K. Chan - 1975 (Summarized in EERC 75-28)
- EERC 75-26 "The Generation and Dissipation of Pore Water Pressures during Soil Liquefaction," by H.B. Seed, P.P. Martin and J. Lysmer - 1975 (PB 252 648)A03
- EERC 75-27 "Identification of Research Needs for Improving Aseismic Design of Building Structures," by V.V. Bertero 1975 (PB 248 136)A05
- EERC 75-28 "Evaluation of Soil Liquefaction Potential during Earthquakes," by H.B. Seed, I. Arango and C.K. Chan - 1975 (NUREG 0026)A13
- EERC 75-29 "Representation of Irregular Stress Time Histories by Equivalent Uniform Stress Series in Liquefaction Analyses," by H.B. Seed, I.M. Idriss, F. Makdissi and N. Banerjee - 1975 (PB 252 635)A03
- EERC 75-30 "FLUSH - A Computer Program for Approximate 3-D Analysis of Soil-Structure Interaction Problems," by J. Lysmer, T. Udaka, C.-F. Tsai and H.B. Seed - 1975 (PB 259 332)A07
- EERC 75-31 "ALUSH - A Computer Program for Seismic Response Analysis of Axisymmetric Soil-Structure Systems," by E. Berger, J. Lysmer and H.B. Seed - 1975
- EERC 75-32 "TRIP and TRAVEL - Computer Programs for Soil-Structure Interaction Analysis with Horizontally Travelling Waves," by T. Udaka, J. Lysmer and H.B. Seed - 1975
- EERC 75-33 "Predicting the Performance of Structures in Regions of High Seismicity," by J. Penzien - 1975 (PB 248 130)A03
- EERC 75-34 "Efficient Finite Element Analysis of Seismic Structure - Soil - Direction," by J. Lysmer, H.B. Seed, T. Udaka, R.N. Hwang and C.-F. Tsai - 1975 (PB 253 570)A03
- EERC 75-35 "The Dynamic Behavior of a First Story Girder of a Three-Story Steel Frame Subjected to Earthquake Loading," by R.W. Clough and L.-Y. Li - 1975 (PB 248 841)A05
- EERC 75-36 "Earthquake Simulator Study of a Steel Frame Structure, Volume II - Analytical Results," by D.T. Tang - 1975 (PB 252 926)A10
- EERC 75-37 "ANSR-I General Purpose Computer Program for Analysis of Non-Linear Structural Response," by D.P. Mondkar and G.H. Powell - 1975 (PB 252 386)A08
- EERC 75-38 "Nonlinear Response Spectra for Probabilistic Seismic Design and Damage Assessment of Reinforced Concrete Structures," by M. Murakami and J. Penzien - 1975 (PB 259 530)A05
- EERC 75-39 "Study of a Method of Feasible Directions for Optimal Elastic Design of Frame Structures Subjected to Earthquake Loading," by N.D. Walker and K.S. Pister - 1975 (PB 257 781)A06
- EERC 75-40 "An Alternative Representation of the Elastic-Viscoelastic Analogy," by G. Dasgupta and J.L. Sackman - 1975 (PB 252 173)A03
- EERC 75-41 "Effect of Multi-Directional Shaking on Liquefaction of Sands," by H.B. Seed, R. Pyke and G.R. Martin - 1975 (PB 258 781)A03
- EERC 76-1 "Strength and Ductility Evaluation of Existing Low-Rise Reinforced Concrete Buildings - Screening Method," by T. Okada and B. Bresler - 1976 (PB 257 906)A11
- EERC 76-2 "Experimental and Analytical Studies on the Hysteretic Behavior of Reinforced Concrete Rectangular and T-Beams," by S.-Y.M. Ma, E.P. Popov and V.V. Bertero - 1976 (PB 260 843)A12
- EERC 76-3 "Dynamic Behavior of a Multistory Triangular-Shaped Building," by J. Petrovski, R.M. Stephen, E. Gartenbaum and J.G. Bouwkamp - 1976
- EERC 76-4 "Earthquake Induced Deformations of Earth Dams," by N. Serff and H.B. Seed - 1976

- EERC 76-5 "Analysis and Design of Tube-Type Tall Building Structures," by H. de Clercq and G.H. Powell - 1976 (PB 252 220) A10
- EERC 76-6 "Time and Frequency Domain Analysis of Three-Dimensional Ground Motions, San Fernando Earthquake," by T. Kubo and J. Penzien (PB 260 556)A11
- EERC 76-7 "Expected Performance of Uniform Building Code Design Masonry Structures," by R.L. Mayes, Y. Omote, S.W. Chen and R.W. Clough - 1976
- EERC 76-8 "Cyclic Shear Tests on Concrete Masonry Piers," Part I - Test Results," by R.L. Mayes, Y. Omote and R.W. Clough - 1976 (PB 264 424)A06
- EERC 76-9 "A Substructure Method for Earthquake Analysis of Structure - Soil Interaction," by J.A. Gutierrez and A.K. Chopra - 1976 (PB 257 783)A08
- EERC 76-10 "Stabilization of Potentially Liquefiable Sand Deposits using Gravel Drain Systems," by H.B. Seed and J.R. Booker - 1976 (PB 258 820)A04
- EERC 76-11 "Influence of Design and Analysis Assumptions on Computed Inelastic Response of Moderately Tall Frames," by G.H. Powell and D.G. Row - 1976
- EERC 76-12 "Sensitivity Analysis for Hysteretic Dynamic Systems: Theory and Applications," by D. Ray, K.S. Pister and E. Polak - 1976 (PB 262 859)A04
- EERC 76-13 "Coupled Lateral Torsional Response of Buildings to Ground Shaking," by C.L. Kan and A.K. Chopra - 1976 (PB 257 907)A09
- EERC 76-14 "Seismic Analyses of the Banco de America," by V.V. Bertero, S.A. Mahin and J.A. Hollings - 1976
- EERC 76-15 "Reinforced Concrete Frame 2: Seismic Testing and Analytical Correlation," by R.W. Clough and J. Gidwani - 1976 (PB 261 323)A08
- EERC 76-16 "Cyclic Shear Tests on Masonry Piers, Part II - Analysis of Test Results," by R.L. Mayes, Y. Omote and R.W. Clough - 1976
- EERC 76-17 "Structural Steel Bracing Systems: Behavior Under Cyclic Loading," by E.P. Popov, K. Takanashi and C.W. Roeder - 1976 (PB 260 715)A05
- EERC 76-18 "Experimental Model Studies on Seismic Response of High Curved Overcrossings," by D. Williams and W.G. Godden - 1976
- EERC 76-19 "Effects of Non-Uniform Seismic Disturbances on the Dumbarton Bridge Replacement Structure," by F. Baron and R.E. Hamati - 1976
- EERC 76-20 "Investigation of the Inelastic Characteristics of a Single Story Steel Structure Using System Identification and Shaking Table Experiments," by V.C. Matzen and H.D. McNiven - 1976 (PB 258 453)A07
- EERC 76-21 "Capacity of Columns with Splice Imperfections," by E.P. Popov, R.M. Stephen and R. Philbrick - 1976 (PB 260 378)A04
- EERC 76-22 "Response of the Olive View Hospital Main Building during the San Fernando Earthquake," by S. A. Mahin, R. Collins, A.K. Chopra and V.V. Bertero - 1976
- EERC 76-23 "A Study on the Major Factors Influencing the Strength of Masonry Prisms," by N.M. Mostaghel, R.L. Mayes, R. W. Clough and S.W. Chen - 1976
- EERC 76-24 "GADFLEA - A Computer Program for the Analysis of Pore Pressure Generation and Dissipation during Cyclic or Earthquake Loading," by J.R. Booker, M.S. Rahman and H.B. Seed - 1976 (PB 263 947)A04
- EERC 76-25 "Rehabilitation of an Existing Building: A Case Study," by B. Bresler and J. Axley - 1976
- EERC 76-26 "Correlative Investigations on Theoretical and Experimental Dynamic Behavior of a Model Bridge Structure," by K. Kawashima and J. Penzien - 1976 (PB 263 388)A11
- EERC 76-27 "Earthquake Response of Coupled Shear Wall Buildings," by T. Srichatrapimuk - 1976 (PB 265 157)A07
- EERC 76-28 "Tensile Capacity of Partial Penetration Welds," by E.P. Popov and R.M. Stephen - 1976 (PB 262 899)A03
- EERC 76-29 "Analysis and Design of Numerical Integration Methods in Structural Dynamics," by H.M. Hilber - 1976 (PB 264 410)A06
- EERC 76-30 "Contribution of a Floor System to the Dynamic Characteristics of Reinforced Concrete Buildings," by L.J. Edgar and V.V. Bertero - 1976
- EERC 76-31 "The Effects of Seismic Disturbances on the Golden Gate Bridge," by F. Baron, M. Arikan and R.E. Hamati - 1976
- EERC 76-32 "Infilled Frames in Earthquake Resistant Construction," by R.E. Klingner and V.V. Bertero - 1976 (PB 265 892)A13

- UCB/EERC-77/01 "FLUSH - A Computer Program for Probabilistic Finite Element Analysis of Seismic Soil-Structure Interaction," by M.P. Romo Organista, J. Lysmer and H.B. Seed - 1977
- UCB/EERC-77/02 "Soil-Structure Interaction Effects at the Humboldt Bay Power Plant in the Ferndale Earthquake of June 7, 1975," by J.E. Valera, H.B. Seed, C.F. Tsai and J. Lysmer - 1977 (PB 265 795)A04
- UCB/EERC-77/03 "Influence of Sample Disturbance on Sand Response to Cyclic Loading," by K. Mori, H.B. Seed and C.K. Chan - 1977 (PB 267 352)A04
- UCB/EERC-77/04 "Seismological Studies of Strong Motion Records," by J. Shoja-Taheri - 1977 (PB 269 655)A10
- UCB/EERC-77/05 "Testing Facility for Coupled-Shear Walls," by L. Li-Hyung, V.V. Bertero and E.P. Popov - 1977
- UCB/EERC-77/06 "Developing Methodologies for Evaluating the Earthquake Safety of Existing Buildings," by No. 1 - B. Bresler; No. 2 - B. Bresler, T. Okada and D. Zisling; No. 3 - T. Okada and B. Bresler; No. 4 - V.V. Bertero and B. Bresler - 1977 (PB 267 354)A08
- UCB/EERC-77/07 "A Literature Survey - Transverse Strength of Masonry Walls," by Y. Omote, R.L. Mayes, S.W. Chen and R.W. Clough - 1977 (PB 277 933)A07
- UCB/EERC-77/08 "DRAIN-TABS: A Computer Program for Inelastic Earthquake Response of Three Dimensional Buildings," by R. Guendelman-Israel and G.H. Powell - 1977 (PB 270 693)A07
- UCB/EERC-77/09 "SUBWALL: A Special Purpose Finite Element Computer Program for Practical Elastic Analysis and Design of Structural Walls with Substructure Option," by D.Q. Le, H. Peterson and E.P. Popov - 1977 (PB 270 567)A05
- UCB/EERC-77/10 "Experimental Evaluation of Seismic Design Methods for Broad Cylindrical Tanks," by D.P. Clough (PB 272 280)A13
- UCB/EERC-77/11 "Earthquake Engineering Research at Berkeley - 1976," - 1977 (PB 273 507)A09
- UCB/EERC-77/12 "Automated Design of Earthquake Resistant Multistory Steel Building Frames," by N.D. Walker, Jr. - 1977 (PB 276 526)A09
- UCB/EERC-77/13 "Concrete Confined by Rectangular Hoops Subjected to Axial Loads," by J. Vallenias, V.V. Bertero and E.P. Popov - 1977 (PB 275 165)A06
- UCB/EERC-77/14 "Seismic Strain Induced in the Ground During Earthquakes," by Y. Sugimura - 1977 (PB 284 201)A04
- UCB/EERC-77/15 "Bond Deterioration under Generalized Loading," by V.V. Bertero, E.P. Popov and S. Viwathanatepa - 1977
- UCB/EERC-77/16 "Computer Aided Optimum Design of Ductile Reinforced Concrete Moment Resisting Frames," by S.W. Zagajeski and V.V. Bertero - 1977 (PB 280 137)A07
- UCB/EERC-77/17 "Earthquake Simulation Testing of a Stepping Frame with Energy-Absorbing Devices," by J.M. Kelly and D.F. Tsztso - 1977 (PB 273 506)A04
- UCB/EERC-77/18 "Inelastic Behavior of Eccentrically Braced Steel Frames under Cyclic Loadings," by C.W. Roeder and E.P. Popov - 1977 (PB 275 526)A15
- UCB/EERC-77/19 "A Symplified Procedure for Estimating Earthquake-Induced Deformations in Dams and Embankments," by F.I. Makdisi and H.B. Seed - 1977 (PB 276 820) A04
- UCB/EERC-77/20 "The Performance of Earth Dams during Earthquakes," by H.B. Seed, F.I. Makdisi and P. de Alba - 1977 (PB 276 821)A04
- UCB/EERC-77/21 "Dynamic Plastic Analysis Using Stress Resultant Finite Element Formulation," by P. Lukkunapvasit and J.M. Kelly - 1977 (PB 275 453)A04
- UCB/EERC-77/22 "Preliminary Experimental Study of Seismic Uplift of a Steel Frame," by R.W. Clough and A.A. Huckelbridge 1977 (PB 278 769)A08
- UCB/EERC-77/23 "Earthquake Simulator Tests of a Nine-Story Steel Frame with Columns Allowed to Uplift," by A.A. Huckelbridge - 1977 (PB 277 944)A09
- UCB/EERC-77/24 "Nonlinear Soil-Structure Interaction of Skew Highway Bridges," by M.-C. Chen and J. Penzien - 1977 (PB 276 176)A07
- UCB/EERC-77/25 "Seismic Analysis of an Offshore Structure Supported on Pile Foundations," by D.D.-N. Liou and J. Penzien 1977 (PB 283 180)A06
- UCB/EERC-77/26 "Dynamic Stiffness Matrices for Homogeneous Viscoelastic Half-Planes," by G. Dasgupta and A.K. Chopra - 1977 (PB 279 654)A06
- UCB/EERC-77/27 "A Practical Soft Story Earthquake Isolation System," by J.M. Kelly and J.M. Eidingner - 1977 (PB 276 814)A07
- UCB/EERC-77/28 "Seismic Safety of Existing Buildings and Incentives for Hazard Mitigation in San Francisco: An Exploratory Study," by A.J. Meltner - 1977 (PB 281 970)A05
- UCB/EERC-77/29 "Dynamic Analysis of Electrohydraulic Shaking Tables," by D. Rea, S. Abedi-Hayati and Y. Takahashi 1977 (PB 282 569)A04
- UCB/EERC-77/30 "An Approach for Improving Seismic - Resistant Behavior of Reinforced Concrete Interior Joints," by E. Galunic, V.V. Bertero and E.P. Popov - 1977

- UCB/EERC-78/01 "The Development of Energy-Absorbing Devices for Aseismic Base Isolation Systems," by J.M. Kelly and D.F. Tsztoo 1978 (PB 284 978)A04
- UCB/EERC-78/02 "Effect of Tensile Prestrain on the Cyclic Response of Structural Steel Connections," by J.G. Bouwkamp and A. Mukhopadhyay - 1978
- UCB/EERC-78/03 "Experimental Results of an Earthquake Isolation System using Natural Rubber Bearings," by J.M. Eidingger and J.M. Kelly - 1978
- UCB/EERC-78/04 "Seismic Behavior of Tall Liquid Storage Tanks," by A. Niwa 1978
- UCB/EERC-78/05 "Hysteretic Behavior of Reinforced Concrete Columns Subjected to High Axial and Cyclic Shear Forces," by S.W. Zagajeski, V.V. Bertero and J.G. Bouwkamp - 1978
- UCB/EERC-78/06 "Inelastic Beam-Column Elements for the ANSR-I Program," by A. Riahi, D.G. Row and G.H. Powell - 1978
- UCB/EERC-78/07 "Studies of Structural Response to Earthquake Ground Motion," by O.A. Lopez and A.K. Chopra - 1978
- UCB/EERC-78/08 "A Laboratory Study of the Fluid-Structure Interaction of Submerged Tanks and Caissons in Earthquakes," by R.C. Byrd - 1978 (PB 284 957)A08
- UCB/EERC-78/09 "Models for Evaluating Damageability of Structures," by I. Sakamoto and B. Bresler - 1978
- UCB/EERC-78/10 "Seismic Performance of Secondary Structural Elements," by I. Sakamoto - 1978
- UCB/EERC-78/11 Case Study--Seismic Safety Evaluation of a Reinforced Concrete School Building," by J. Axley and B. Bresler 1978
- UCB/EERC-78/12 "Potential Damageability in Existing Buildings," by T. Blejwas and B. Bresler - 1978
- UCB/EERC-78/13 "Dynamic Behavior of a Pedestal Base Multistory Building," by R. M. Stephen, E. L. Wilson, J. G. Bouwkamp and M. Button - 1978
- UCB/EERC-78/14 "Seismic Response of Bridges - Case Studies," by R.A. Imbsen, V. Nutt and J. Penzien - 1978
- UCB/EERC-78/15 "A Substructure Technique for Nonlinear Static and Dynamic Analysis," by D.G. Row and G.H. Powell - 1978
- UCB/EERC-78/16 "Seismic Performance of Nonstructural and Secondary Structural Elements," by Isao Sakamoto - 1978

- UCB/EERC-78/17 "Model for Evaluating Damageability of Structures," by Isao Sakamoto and B. Bresler - 1978
- UCB/EERC-78/18 "Response of K-Braced Steel Frame Models to Lateral Loads," by J.G. Bouwkamp, R.M. Stephen and E.P. Popov - 1978
- UCB/EERC-78/19 "Rational Design Methods for Light Equipment in Structures Subjected to Ground Motion," by Jerome L. Sackman and James M. Kelly - 1978
- UCB/EERC-78/20 "Testing of a Wind Restraint for Aseismic Base Isolation," by James M. Kelly and Daniel E. Chitty - 1978
- UCB/EERC-78/21 "APOLLO A Computer Program for the Analysis of Pore Pressure Generation and Dissipation in Horizontal Sand Layers During Cyclic or Earthquake Loading," by Philippe P. Martin and H. Bolton Seed - 1978
- UCB/EERC-78/22 "Optimal Design of an Earthquake Isolation System," by M.A. Bhatti, K.S. Pister and E. Polak - 1978
- UCB/EERC-78/23 "MASH A Computer Program for the Non-Linear Analysis of Vertically Propagating Shear Waves in Horizontally Layered Deposits," by Philippe P. Martin and H. Bolton Seed - 1978
- UCB/EERC-78/24 "Investigation of the Elastic Characteristics of a Three Story Steel Frame Using System Identification," by Izak Kaya and Hugh D. McNiven - 1978
- UCB/EERC-78/25 "Investigation of the Nonlinear Characteristics of a Three-Story Steel Frame Using System Identification," by I. Kaya and H.D. McNiven - 1978
- UCB/EERC-78/26 "Studies of Strong Ground Motion in Taiwan," by Y.M. Hsiung, B.A. Bolt and J. Penzien - 1978
- UCB/EERC-78/27 "Cyclic Loading Tests of Masonry Single Piers Volume 1 - Height to Width Ratio of 2," by P.A. Hidalgo, R.L. Mayes, H.D. McNiven & R.W. Clough - 1978
- UCB/EERC-78/28 "Cyclic Loading Tests of Masonry Single Piers Volume 2 - Height to Width Ratio of 1," by S.-W.J.Chen, P.A. Hidalgo, R.L. Mayes, R.W. Clough & H.D. McNiven - 1978
- UCB/EERC-78/29 "Analytical Procedures in Soil Dynamics," by J. Lysmer - 1978
- UCB/EERC-79/01 "Hysteretic Behavior of Lightweight Reinforced Concrete Beam-Column Subassemblages," by B. Forzani, E.P. Popov, and V.V. Bertero - 1979

B53
2

For sale by the National Technical Information Service, U. S. Department of Commerce, Springfield, Virginia 22161.

See back of report for up to date listing of EERC reports.